University College of Southeast Norway

Evaluation of Phosphor Materials for 4K Laser Projector

Master of Micro and Nano Systems Technology

Submission date: May 2017

Supervisor: Xuyuan Chen, Mustafa Balci, M. Nadeem Akram

University College of Southeast Norway
Department of Micro Systems

Evaluation of Phosphor Materials for 4K Laser Projector

Fan Chen

IMS, HSN

Fan.Chen@student.hbv.no

Abstract

Phosphor converted warm white light with high luminous efficacy and color rendering index is crucial for the future of blue diode laser driven lightning and display technologies. Particularly in projection displays where the high power (over 150 W) blue laser source is focused on the phosphor, the ideal phosphor candidate should provide better conversion efficiency, longer lifetime (20000 hours) and lower thermal overheat. We have characterized Ce doped single crystals as stationary phosphor candidates for blue laser driven solid lighting without heatsink. The luminous properties of the single crystals are improved when compared to the commercial phosphor wheels (Ce^{3+}: $Y_3Al_5O_{12}$) and luminous efficacy over 250 lm/W was achieved. The high-power blue diode laser driven temperature increase versus quantum efficiency change is discussed. The specific effect of temperature on quantum efficiency: when the temperature is less than a special value, the quantum efficiency increases with increasing temperature; when the temperature is greater than this special value, the quantum efficiency decreases with increasing temperature. This special value is called “Quenching Temperature”, and the increase in quantum efficiency is very gentle, but the reduction in quantum efficiency is very rapid. The experimental results show that the existence of Gd element greatly reduces the quenching temperature. This means that the phosphor containing the Gd element cannot be used under high power lasers. In Ce doped single crystals phosphor, the quenching temperature is increased when compared to the polycrystalline crystal phosphor. The ideal geometry and design of these Ce doped single crystals can serve as potential phosphors candidates for high-power blue diode laser driven projectors

Acknowledgements

First and foremost, I am most grateful to my supervisor, Professor Xuyuan Chen, Professor M. Nadeem Akram and Postdoctoral Mustafa Balci, whose useful suggestions, incisive comments and constructive criticism have contributed greatly to the completion of this thesis. They tremendous assistance in developing the framework for analysis and in having gone through the draft versions of this thesis several times as well as her great care in life deserve more thanks than I can find words to express.

Special thanks to Mr. Kang Du for improving the scientific writing of my thesis and for helping me with experiment and all the problems I met during my measurements. I am grateful for your enthusiasm and patience every time

Last but not least, I owe much to my friends and classmates for their valuable suggestions and critiques which are of help and importance in making the thesis a reality.

List of Contents:

Abstract ····· *i*

Acknowledgements ····· *iii*

List of Contents: ····· *v*

List of Figures ····· *viii*

List of Tables ····· *xii*

Chapter 1 Introduction ····· **1**

1.1 Overview of projection displays ····· 2

1.1.1 Liquid crystal display projector ····· 4

1.1.2 Digital light processing projector ····· 4

1.2 Laser display technology projector ····· 5

1.2.1 RGB laser projector ····· 5

1.2.2 Phosphor + blue laser projector ····· 6

1.2.3 LED + laser + phosphor projector ····· 8

1.3 Introduction of luminescence material ····· 9

1.3.1 Classification of luminescence ····· 9

1.3.2 Photoluminescence ····· 10

1.3.3 Phosphors and lamps ····· 11

1.4 Purposes and organization of this thesis ····· 12

Chapter 2 Basic theoretical knowledge ····· **14**

2.1 Excitation and emission spectrums ····· 14

2.2 Features of rare earth (RE) ions with respect to luminescence ····· 15

2.3 Rare earths energy levels and transitions ····· 16

2.3.1 Electronic transitions ····· 17

2.3.2 Energy level and luminescence of Ce^{3+} ····· 18

2.4 Energy transfer ····· 18

2.5 Basic concepts of fluorescence lifetime ····· 20

2.6 Basic concepts of quantum efficiency ····· 22

Chapter 3 Experimental preparations ····· **24**

3.1 Sample morphology and composition ····· 24

3.2 Exitation and emission spectrums and Lifetime ····· 24

3.2.1 Introduction of FS5 fluorescence spectrophotometer ····· 25

3.2.2 Measurement methods of fluorescence lifetime ····· 26

3.3 Quantum efficiency ····· 27

3.3.1 Measurement methods of quantum efficiency ····· 27

3.3.2 The experimental process of measuring quantum efficiency ····· 30
3.4 Temperature change control ····· 31

Chapter 4 SEM and EDS results and discussions ····· 32

4.1 Single crystal LuAG: Ce^{3+} ····· 32
4.2 Single crystal and polycrystalline YAG: Ce^{3+} ····· 33
4.3 Single crystal of GGAG: Ce^{3+} and GDYAG: Ce^{3+} ····· 35

Chapter 5 Excitation and emission spectrums results and discussions ····· 37

5.1 Single crystal LuAG: Ce^{3+} ····· 37
5.1.1 Excitation spectrum of single crystal LuAG: Ce^{3+} ····· 37
5.1.2 Emission spectrum of single crystal LuAG: Ce^{3+} ····· 38
5.1.3 CIE (Commission International de l'Éclairage) chromaticity of LuAG: Ce^{3+} ····· 39
5.1.4 Luminescence mechanism of LuAG: Ce^{3+} ····· 40
5.2 Single crystal and polycrystalline YAG: Ce^{3+} ····· 41
5.2.1 Polycrystalline YAG: Ce^{3+} ····· 41
5.2.2 Excitation and emission spectrums of YAG: Ce^{3+} single crystal ····· 42
5.2.3 Comparison of polycrystalline YAG: Ce^{3+} and single crystal YAG: Ce^{3+} ····· 43
5.2.4 Energy level diagram of Ce^{3+} in YAG host material ····· 44
5.3 Single crystal GGAG: Ce^{3+} and GDYAG: Ce^{3+} ····· 45
5.3.1 Excitation and emission spectrums of GGAG: Ce^{3+} ····· 46
5.3.2 Excitation and emission spectrums of GDYAG: Ce^{3+} ····· 47
5.3.3 Electronic transition and energy transfer of Ce^{3+} and Gd^{3+} ions ····· 47
5.4 Comparison of the five samples ····· 48

Chapter 6 Fluorescence lifetime and quantum efficiency results and discussions ·· 50

6.1 Fluoresence liftime ····· 50
6.2 Quantum efficiency ····· 52

Chapter 7 Temperature change results and discussions ····· 55

7.1 Excitation and emission spectrums ····· 55
7.1.1 Single crystal LuAG: Ce^{3+} ····· 55
7.1.2 Single crystal GGAG: Ce^{3+} ····· 57
7.1.3 Single crystal GDYAG: Ce^{3+} ····· 58
7.1.4 Single crystal YAG: Ce^{3+} ····· 59
7.1.5 Polycrystalline YAG: Ce^{3+} ····· 61
7.1.6 Comparison the five samples ····· 62
7.2 Fluorescence lifetime ····· 63
7.2.1 Single crystal LuAG: Ce^{3+} ····· 63
7.2.2 Polycrystalline YAG: Ce^{3+} ····· 64
7.2.3 Single crystal YAG: Ce^{3+} ····· 64
7.2.4 Single crystal GDYAG: Ce^{3+} ····· 65

7.2.5 Single crystal GGAG: Ce^{3+} ····· 66
7.2.6 Comparison of fluorescence lifetime of the five samples at different temperatures · 66
7.3 Theoritical analysis based on Mott–Seitz mechanism ····· 67

Chapter 8 Conclusion ····· 69

Bibliography ····· 70

Appendix ····· I

List of Figures

Figure 1-1: Schematic architecture of the projection display, shows that a projector consists of illumination source, a light engine, a projection lens, and the screen. 3
Figure 1-2: Single-Chip projector working principle [9] 3
Figure 1-3: Three-Chip projector working principle [10] 3
Figure 1-4: schematic configuration and working principle of LCD display chip [3] 4
Figure 1-5: Schematic configuration and working principle of DLP display chip 5
Figure 1-6: Christie cinema projector [11] 6
Figure 1-7: Working principle of laser phosphor projector [12] 7
Figure 1-8: Working principle of ViewSonic Pro9000 LED/Laser Hybrid Projector [13] 8
Figure 1-9: Working principle of CASIO'S laser and LED hybrid light source projector (SLIM) [14] (left), and Hisense Laser TV (right). 8
Figure 1-10: Photoluminescence process [16] 11
Figure 2-1: Generic Excitation and emission spectrums for a fluorescent dye 14
Figure 2-2: Energy level of Ce^{3+} luminescence center [25] 18
Figure 2-3: Fluorescence lifetime 21
Figure 2-4: Graphic representation of IQE and EQE 22
Figure 3-1: SU3500: Hitachi Scanning Electron Microscope 24
Figure 3-2: FS5 fluorescence spectrophotometer 25
Figure 3-3: Work principle of TCSPC technique (single cycle) 26
Figure 3-4: Step 1 of measuring quantum efficiency. 27
Figure 3-5: Step 2 of measuring quantum efficiency (measure emission spectrum) 28
Figure 3-6: Step 3 of measuring quantum efficiency (measure re-excited emission spectrum) 29
Figure 3-7: The relationship of absorbed, re-absorbed and emitted. 29
Figure 3-8: Actual measuring quantum efficiency process. 30
Figure 3-9: Experimental setup for quantum efficiency measurement (A: integrating sphere; B: laser device; C: control device) 30
Figure 3-10: Temperature control experimental setup 31
Figure 3-11: Characteristic of HT24S heater. 31
Figure 4-1: LuAG surface morphology ((a) is LuAG polished surface sample micro photos, (b) ais LuAG polished surface sample micro photos.) 32

Figure 4-2: LuAG EDS results plot (left one is polished and right one is grounded) . 33
Figure 4-3: EDS results of YAG single crystal (a) and YAG wheel (b). 34
Figure 4-4: YAG wheel structure (a), and re-absorb process (b). 34
Figure 4-5: (a) is EDS result of GGAG; (b) is EDS result of GdYAG. 36
Figure 5-1: Excitation spectrum (λ_{em} = 510nm) of LuAG: Ce^{3+} phosphor 38
Figure 5-2: Emission spectrum of LuAG: Ce^{3+} phosphors and deconvoluted emission spectrum (solid line—measured; dash line—Gaussian fitted) 38
Figure 5-3: CIE chromaticity coordinates of the LuAG: Ce^{3+} 39
Figure 5-4: Luminescence mechanism of LuAG: Ce^{3+} 40
Figure 5-5: Excitation and emission spectrums of YAG: Ce^{3+} polycrystalline 42
Figure 5-6: Excitation and emission spectrums of YAG: Ce^{3+} single crystal 42
Figure 5-7: Comparison of YAG: Ce^{3+} single crystal and polycrystalline 43
Figure 5-8: CIE chromaticity coordinates of the YAG: Ce^{3+} polycrystalline and single crystal 44
Figure 5-9: Energy level diagram of Ce^{3+} in YAG host material` 45
Figure 5-10: Excitation and emission spectrums of GGAG: Ce^{3+} 46
Figure 5-11: Excitation and emission spectrums of GDYAG: Ce^{3+} 47
Figure 5-12: Electronic transition of Ce^{3+} and Gd^{3+} in GGAG and GDYAG host materials 48
Figure 5-13: Comparison of emission spectrums of five samples 48
Figure 5-14: Comparison of CIE chromaticity of five samples 49
Figure 6-1: Fitting result of the LuAG: Ce^{3+} single crystal 50
Figure 6-2: Fluorescence lifetime of the LuAG: Ce^{3+} at room temperature. Excitation wavelength, 450 nm; emission wavelength, 550 nm. 51
Figure 6-3: Quantum efficiency measurement of LuAG: Ce^{3+} single crystal phosphor. 52
Figure 6-4: The relationship between quantum efficiency and laser power of LuAG: Ce^{3+} 53
Figure 7-1: Excitation and emission spectrums of LuAG: Ce^{3+} at different temperatures 56
Figure 7-2: CIE chromaticity coordinates and relative emission intensity of LuAG: Ce^{3+} 56

Figure 7-3: Excitation and emission spectrums of GGAG: Ce^{3+} at different temperature 57
Figure 7-4: CIE chromaticity coordinates and relative emission intensity of GGAG: Ce^{3+} 57
Figure 7-5: Excitation and emission spectrums of GDYAG: Ce^{3+} at different temperature 58
Figure 7-6: CIE chromaticity coordinates and relative emission intensity of GDYAG: Ce^{3+} 59
Figure 7-7: Excitation and emission spectrums of YAG: Ce^{3+} single crystal at different temperature 60
Figure 7-8: CIE chromaticity coordinates and relative emission intensity of YAG: Ce^{3+} single crystal 60
Figure 7-9: Excitation and emission spectrums of YAG: Ce^{3+} polycrystalline at different temperature 61
Figure 7-10: CIE chromaticity coordinates and relative emission intensity of YAG: Ce^{3+} polycrystalline 62
Figure 7-11: Comparison of relative emission intensity of five samples at different temperature 62
Figure 7-12: (a), Fluorescence lifetime measurement results of LuAG: Ce^{3+} single crystal at different temperature. (b), Comparison of relative emission intensity and fluorescence lifetime at same temperature. 63
Figure 7-13: (a), Fluorescence lifetime measurement results of YAG: Ce^{3+} polycrystalline at different temperature. (b), Comparison of relative emission intensity and fluorescence lifetime at same temperature. 64
Figure 7-14: (a), Fluorescence lifetime measurement results of YAG: Ce^{3+} single crystal at different temperature. (b), Comparison of relative emission intensity and fluorescence lifetime at same temperature. 65
Figure 7-15: (a), Fluorescence lifetime measurement results of GDYAG: Ce^{3+} single crystal at different temperature. (b), Comparison of relative emission intensity and fluorescence lifetime at same temperature. 65
Figure 7-16: (a), Fluorescence lifetime measurement results of GGAG: Ce^{3+} single crystal at different temperature. (b), Comparison of relative emission intensity and fluorescence lifetime at same temperature. 66

Figure 7-17: Comparison of fluorescence lifetime of five samples at different temperature 67
Figure 7-18: Configuration coordinate diagram of Ce^{3+} center. The influence of increased temperature and Gd element addition on the position of $5d_1$ excited state parabolas and that of conduction band is marked. 67

List of Tables

Table 4-1 LuAG EDS results of composition ratio of elements 33
Table 4-2 YAG EDS results of composition ratio of elements 35
Table 4-3 GGAG and GdYAG EDS results of composition ratio of elements 36
Table 6-1 Fluorescence lifetime of five samples 52
Table 6-2 Quantum efficiency measurement results 53

Chapter 1 Introduction

Studies show that people's perceptual organs obtain information from the outside world 83% by sight, 11% by hearing, 3.5% by smell ,1.5% by touch and 1% by taste, approaching 2/3 of the information is obtained through the eyes [1]. Therefore, the image display technology has become the most important technology for visualization study, information display, and video entertainment. The state of the arts in display technology enclose direct-view, projection or virtual. Direct view displays produce their images on the surface being viewed. The images from projection displays are formed on auxiliary surfaces, which are physically separated from the image-generating component. With a virtual display (VR), there is no real image in space; the optical signal is brought to a focus only on the retina. As the immerging technology, there is a long way for VR to go for satisfied performance, for example, high resolution and fast speed. The direct-view technology has been advanced from cathode ray tube (CRT) [2], liquid crystal display (LCD) [3], plasma display (PD) [4], light-emitting diode (LED) [5], to reach organic light emitting diode (OLED) [6] and with size of 120 inch. Due to the display applications extended from indoor to outdoor, from small screen to large screen, and from low brightness to high brightness, the projection display becomes the future demanded display technology. The projectors display the images on the screen by projecting images formed on DLP (digital light processor from Texas Instrument), LCD, and LCoS (liquid crystal on silicon), with lamp in use 1) xenon lamps, on very high end and extremely bright projectors, 2) UHP (ultra-high pressure) that use mercury vapor, 3) LED lights, and the last 4) Laser lights. Due to the short lamp life (xenon lamps 500 to 1500 hours), low brightness (UHP lamps < 3000 lm/single lamp, LED <1500 lm), and poor color display (xenon, UHP, and LED) source, laser lights become extremely attractive illumination source for projectors. Although laser lights are expensive, the application in cinema, large screen home-theater, and the super-brightness 60000lm applications lead the birth of so-called laser display technique (LDT) [7]. LDT is an emerging technology, which has developed rapidly and matured in recent years. The laser projectors make breakthrough improvements. Compared with traditional projectors, laser projectors have a longer lifetime, it can last beyond 20000 hours [8], which is four times the average lifetime of UHP lamp projectors. The color range is 2 times of NTSC standard. The power consumption is about 30 to 25% of lamp

projectors. The number of optics in the system is greatly reduced. The LDT technology can have the laser modular configuration and enables super-brightness projectors of 60000lm.

1.1 Overview of projection displays

Projection displays consist of an image generation light engine and a display screen which is physically separated from the image-generating engine. Projection displays bring out larger images from electronic signals by modulating the light from an illumination system with a device called a light valve. Nowadays, the technology is also applied to portable systems such as Pico-projectors.

Projectors can be classified accord to the different working principle of the light valves, typically, LCD projectors, DLP projectors, and LCoS projectors. With the revolution development of using laser lights as the illumination source, laser projectors become the latest generation projectors.

As example shown in figures 1-1 to 1-3, we schematically present the architectures and working principles of 3-chip and 1-chip projectors. Figure 1-1 presenting the framework of the projector configuration, shows that a projector consists of illumination source, a light engine, a projection lens, and the screen. The illumination is a broadband white lamp. The light engine generates the image which the projection lens projects on the screen with certain roughness. The image will be observable in a wide view angle for large number of viewers. Figure 1-2 presents the single-chip projector in which the light engine is built up with only one light valve device or image generation chip (any of LCD, DLP or LCoS). The illumination will be separated to three colors with filters on a wheel, e.g., color wheel. Basic color wheels support red, blue, and green, whereas more advanced color wheels support cyan, magenta, and yellow. Different color beams reach the light valve device in the time sequence to form a colorful image. Figure 1-3 presents the three-chip projector in which the light engine is built up with three light valve devices (three-chip). The three-chip projector in general for high-end performance. No color wheel will be involved in such a configuration. The white light is passed through a series of dichroic mirrors. Dichroic mirrors work by only allowing certain colors in the light spectrum to be reflected, while others pass through. The dichroic mirrors in the projectors separate the light into the three primary colors, green, red, and blue. These three colors are then sent to a separate chip to generate red, green, and blue images and the engine overlaps the images to display the final colorful

picture. Three-panel design requires each panel to be in perfect position to combine the image at the proper angle.

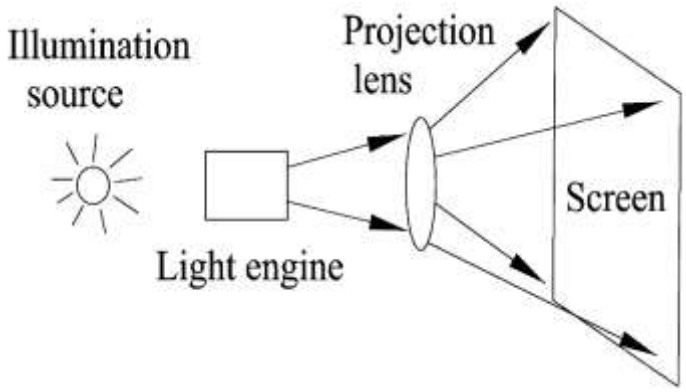

Figure 1-1: Schematic architecture of the projection display, shows that a projector consists of illumination source, a light engine, a projection lens, and the screen.

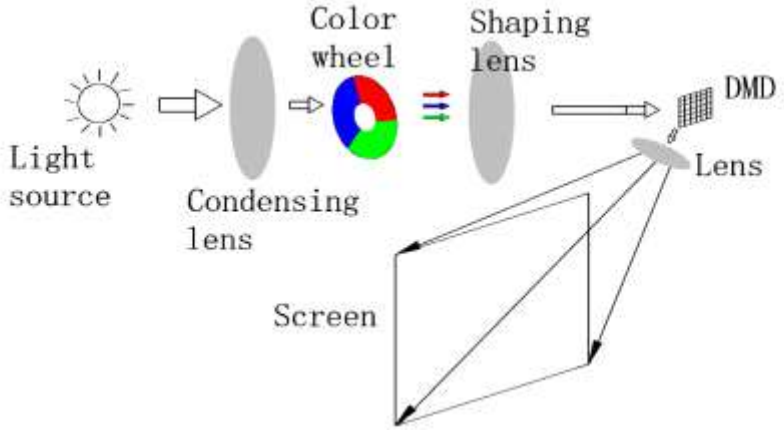

Figure 1-2: Single-Chip projector working principle [9]

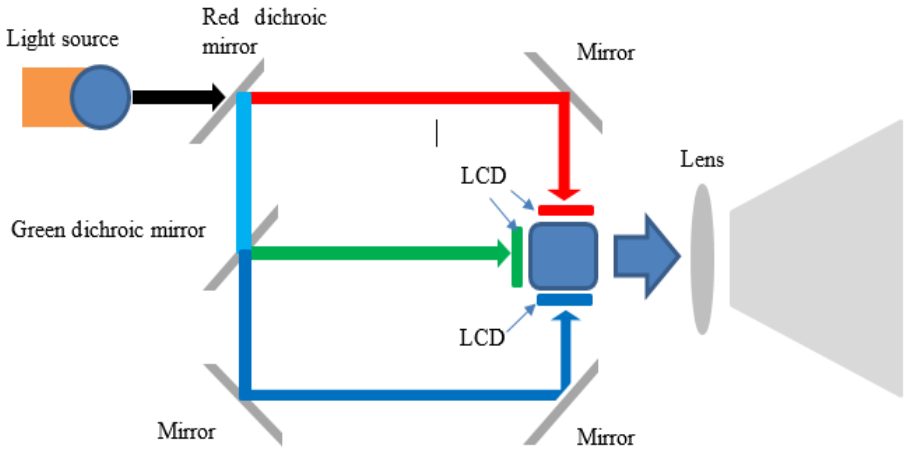

Figure 1-3: Three-Chip projector working principle [10]

1.1.1 **Liquid crystal display projector**

LCD panel in LCD projectors has many cells which are defined as the pixels of the LCD panel (see figure 1-4). Each pixel works by allowing or stopping the polarized light to travel through, which consists of a pair of polarizing filter glasses filled with liquid crystal. The pair of polarizing filter glasses are vertically aligned to each other. The liquid crystal can be electrically controlled to make the polarized light propagate through it by rotating light waves by 90° or 0°. In such a configuration, the liquid crystal can effectively block/let all light from passing through the panel. Each pixel in LCD panel has a separate electrical control system to allow individual independent action. The resolution of each LCD or the clarity of the image is determined by the total number of the pixels.

The technology in LCD projectors is more established and reliable than film projectors. However, they may still require maintenance, as pixels can burn out and dust particles can interfere with image quality [3].

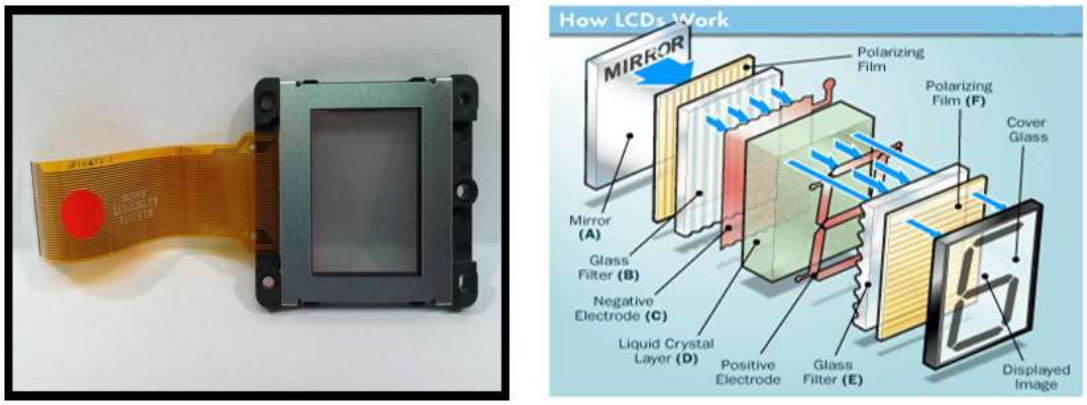

Figure 1-4: schematic configuration and working principle of LCD display chip [3]

1.1.2 **Digital light processing projector**

DLP consists an array of millions of tiny mirrors which can reflect light toward the screen (an "on" pixel) or away (an "off" pixel), see figure 1-5. Each mirror, not more than 5um x 5 um in dimension, is subjected to independent adjustment, moving toward or away from the light source to create a dark or light pixel. DLP projectors require less maintenance than LCD projectors because they have a sealed chip design, which means dust cannot settle on the chip and cause an image spot. They are effectively immune to color decay. On the other hand, LCD projectors have no moving parts, differing from DLP projectors design, they are generally less expensive than their DLP counterparts.

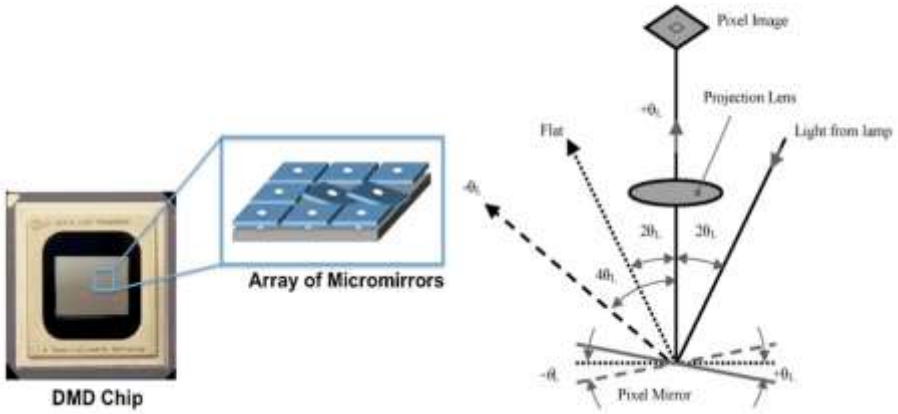

Figure 1-5: Schematic configuration and working principle of DLP display chip

1.2 Laser display technology projector

Light source as important part of the projector optical engine, whatever for film projectors at the time when the projector was born or for the digital projectors in nowadays, are also constantly changing, such as from the initial halogen, high-pressure mercury lamp, xenon lamp, to the latest LED. Currently, RGB laser sources such as semiconductor laser diodes and frequency doubling laser sources have become extremely attractive because laser sources can delivery wide color gamut for vivid image, long life, high brightness, low energy consumption. So far, using the laser light as the illumination source has formed a display technology platform for high brightness, which can be cataloged as pure RGB laser projector with three primary colors, projectors with blue laser plus phosphor light source, and projectors with blue laser plus phosphor plus LED. Each light source has its own advantages and disadvantages, and been used to different applications.

1.2.1 RGB laser projector

Laser is a coherent light beam; coherent, in this context, means that it is of single wavelength or extremely narrow bandwidth, unlike ordinary light which showers on us with a wide bandwidth spectrum. Using of laser as a light source for projectors is a hot topic in the field of projectors in recent years. For laser projector, the best solution is RGB pure laser projector from the point views of rich color image, long lifetime, as well as low energy consumption. In principle, there is no highest limitation for the brightness when laser is used as the light source because they can be easily integrated as high power source modular. The brightness of the laser projector can be promoted

upto 60000lm which is limited by the display chip capability. Up to now, the projection equipment with three primary colors of pure laser technology has been "infiltrated" into the fields of simulation, exhibition, conference center, outdoor curtain wall, digital cinema and home theater, and has great development space and broad market application prospect. Figure 1-6 shows a Christie cinema projector with laser source modular in rack.

Figure 1-6: Christie cinema projector [11]

For RGB laser light sources, the choice is very limited, only two types e.g., solid-state laser sources and semiconductor laser diodes are available in the market. The semiconductor pumped frequency doubled laser is also a solid-state laser source. It is composed of a semiconductor laser (pump source), a frequency-doubling crystal and an oscillation cavity. The solid-state laser source including the pumped frequency doubled laser source has sub-nm bandwidth spectrum and thus high-level coherence property. Such laser sources have the highest speckle contrast, which can be seen by the viewers if there are no active speckle reduction methods. Semiconductor laser diodes have become available recently. Comparing the solid-state laser source, they have several nm bandwidth spectrums, which form less laser speckle contrast. In addition to the technology challenge in laser speckle reduction, all laser sources are expensive for making projectors in consuming market.

1.2.2 **Phosphor + blue laser projector**

Due to the laser speckle issue in the pure RGB laser projectors, as well as the high cost of the laser sources, a mixture of laser diodes plus phosphor material has been an

attractive solution in the consuming market, such as educational projectors, home theaters, as well as low lumens (<12000lm) professional applications. Motived by available high power blue laser diodes, such as, 3.5W blue laser diodes produced by Nichia, laser phosphor technology has been advanced significantly in last two years. The red laser diode and green laser diodes are still very expensive. The laser phosphor technology uses blue laser diodes with red and green variety of phosphors to generate the white light source. Due to the Stokes effect, the thermal management of the phosphor material is a bottleneck issue. Therefore, for a large lumens projector, rotating phosphor wheel, which distributes the thermal energy in time sequence, has to be applied to produce red and green colors, as shown in Figure 1-7. Recently, the use of multicolor fluorescent pink wheel rotation effectively solves the thermal quenching and heat dissipation of the phosphor [12]. In addition to stand with the high-intensity excitation light irradiation, the use of multi-color fluorescent pink wheel can achieve different colors of light output for composing the final white light.

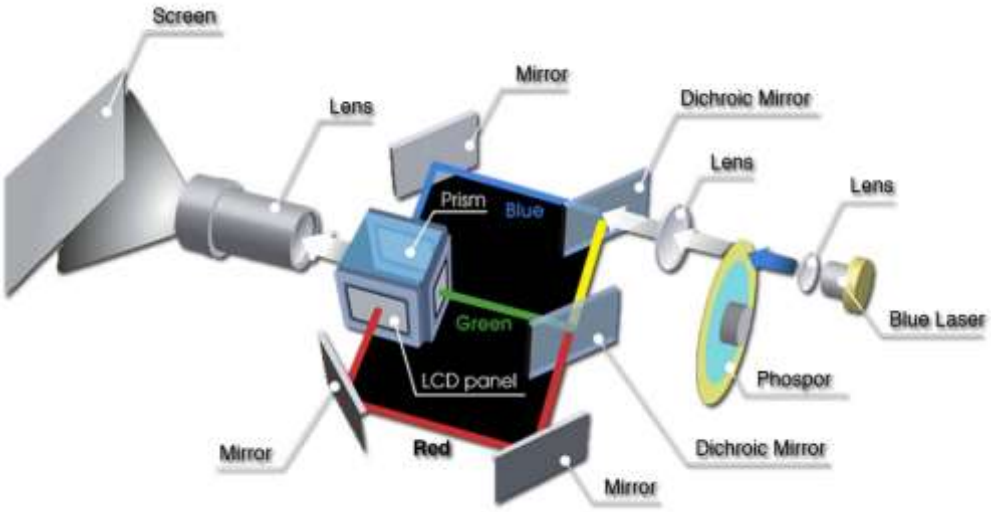

Figure 1-7: Working principle of laser phosphor projector [12]

The application of laser phosphor for display technology can provide cheap projectors in the market with inherent weakness of poor color gamut comparing the RGB laser projectors. In addition, the laser phosphor projector also has limited brightness, which is critical for 3D large screen cinema. With fast developing pace of semiconductor laser diodes of red and green, the cost will become acceptable in many projection market sections in some years. However, as current market demands, about 80% of laser projectors are based on the laser phosphor solution.

1.2.3 **LED + laser + phosphor projector**

LED + laser + phosphor display technology is based on the laser phosphor display technology to add the RED LED source. The main reason for such a hybrid design is the red phosphor has very low efficiency, which results in a significant waste of blue laser source and large loss of wall plug efficiency. To improve the total wall plug efficiency, there are two different designs. First, the blue laser and green phosphor wheel is used to get the green color, blue and red color is provided by LEDs. As shown in figure 1-8, this technology has been applied in ViewSonic Pro9000 LED/Laser Hybrid Projector [13].

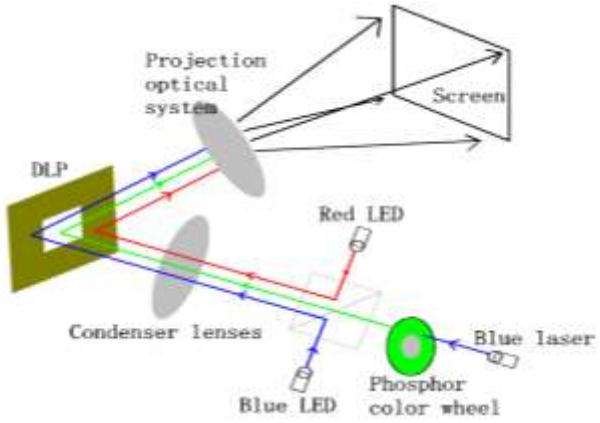

Figure 1-8: Working principle of ViewSonic Pro9000 LED/Laser Hybrid Projector [13]

Second, blue laser, phosphor wheel, and red LED are applied to provide three primary colors. The schematic design is shown in figure 1-9, which is the design from CASIO projector (SLIM). Such a design gives designer the opportunity to increasing the brightness upto 15000lm. Therefore, more and more projector products are equipped with such hybrid technology.

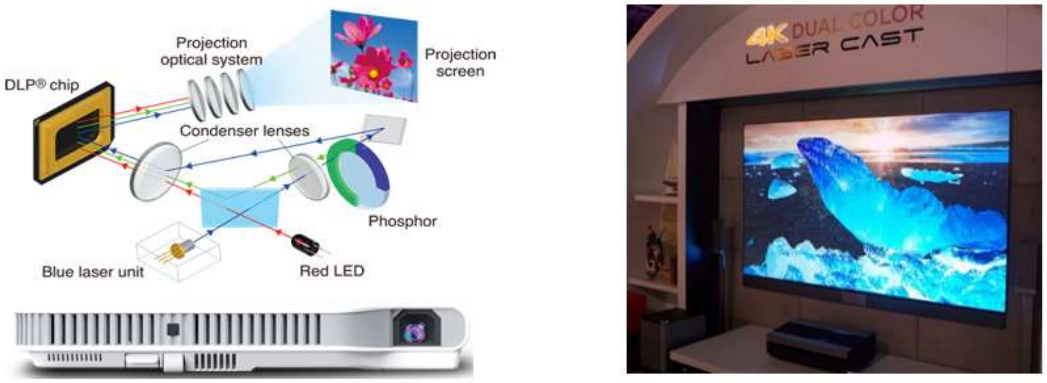

Figure 1-9: Working principle of CASIO'S laser and LED hybrid light source projector (SLIM) [14] (left), and Hisense Laser TV (right).

1.3 Introduction of luminescence material

Light as a form of energy, is created either by incandescence or by luminescence. Incandescence is light from heat energy. If we heat something to a high enough temperature, it will begin to glow, that is incandescence, such as, the tungsten filament in an ordinary light bulb, is heated by pass electricity, which glows brightly "white hot". The sun glows by incandescence. Luminescence is "cold light" that can be emitted at normal and lower temperatures. In luminescence, some energy source kicks an electron of an atom out of its lowest energy "ground" state into a higher energy "excited" state, then the electron returns the energy in the form of light when it falls back to its "ground" state. With few exceptions, the excitation energy is always greater than the energy of the emitted light.

1.3.1 Classification of luminescence

Luminescence is traditionally classified as fluorescence and phosphorescence. The word Phosphorescence was derived from the word phosphor, which means light emission from a substance after the exciting radiation, has ceased. The word fluorescence was introduced to denote the imperceptible short afterglow of material after the excitation. In 1888, a German physicist Eilhardt Wiedemann first used the word “luminescence” which includes both fluorescence and phosphorescence. This word originates from the Latin word “lumen” which means light. Historically, luminescence characterized by temperature-independent decay was called fluorescence, while that exhibiting temperature-dependent decay was called phosphorescence. However, in accordance with the modern conventions, fluorescence refers to emission of relatively short persistence (10^{-6} –10^{-12} s), whereas phosphorescence persists considerably longer. The line of demarcation is rather arbitrary. In short, fluorescence is the emission of visible light by a material under the stimulus of visible or invisible radiation of shorter wavelength. If the fluorescent glow persists for an appreciable time after the stimulating rays have been cut-off, this after-glow is termed as phosphorescence.

The various categories of the luminescence can be established depending on the mode of excitation:

1. Photoluminescence, when the excitation is by electromagnetic radiation/photons.

2. Cathodoluminescence, when the excitation is by energetic electrons or cathode rays.
3. Electroluminescence, when light emission is triggered by electric influences.
4. Radioluminescence, when the excitation is by high-energy X-rays or γ rays.
5. Sonoluminescence, when the excitation is by ultrasonic waves.
6. Triboluminescence, when a material is mechanical treated.
7. Chemiluminescence is light emitted during chemical reactions.
8. Ionoluminescence is light emitted by energetic ions interacting with solid matter.
9. Thermoluminescence is light emitted by temperatures above a certain point.
10. Bioluminescence is the form of chemiluminescence from living organisms.

For high lumens display applications, photoluminescence wins out from the above list. In this thesis, we focus on the photoluminescence of the phosphor materials [15, 16].

1.3.2 **Photoluminescence**

Photoluminescence (PL) refers to the luminescence of a solid material (phosphor) excited by light of another wavelength, typically ultraviolet (UV), visible or infrared light, as shown in figure 1-10 for band-to-band luminescence. PL has two major types, namely, intrinsic photoluminescence and extrinsic photoluminescence. Intrinsic photoluminescence is displayed by materials which contain no impurity atoms. Extrinsic photoluminescence results from intentionally incorporated impurities, in most cases metallic impurities or intrinsic defects. There are three kinds of intrinsic photoluminescence, include band-to-band luminescence, excitons luminescence and cross-luminescence. Band-to-band luminescence results from the recombination of an electron in the conduction band with a hole in the valence band and can only be observed in a very pure crystal at relatively high temperatures. An exciton is a composite particle resulting from the coupling of an electron and a hole, which then travels in a crystal and produces luminescence by releasing its energy at luminescent centers. Cross-luminescence is produced by the recombination of an electron in the valence band with a hole in the outermost core band. It can only take place when the energy difference between the top of the valence band and that of the outermost core band is smaller than the band-gap energy; otherwise, an Auger process occurs.

Most of the observed types of luminescence that have practical applications belong to extrinsic photoluminescence. Extrinsic photoluminescence is classified into two types, namely localized and delocalized luminescence. In a delocalized luminescence,

the excited electrons and holes of the host lattice participate in the luminescence process, while in a case of the localized luminescence the excitation and emission processes are confined in a localized luminescence center, the host lattice does not contribute to luminescence process. Laser technology is a kind of photoluminescence in which the emission is stimulated and the laser beam is coherent. The most prevalent use of photoluminescent in nowadays is the phosphors in fluorescent lamps and LED lamps.

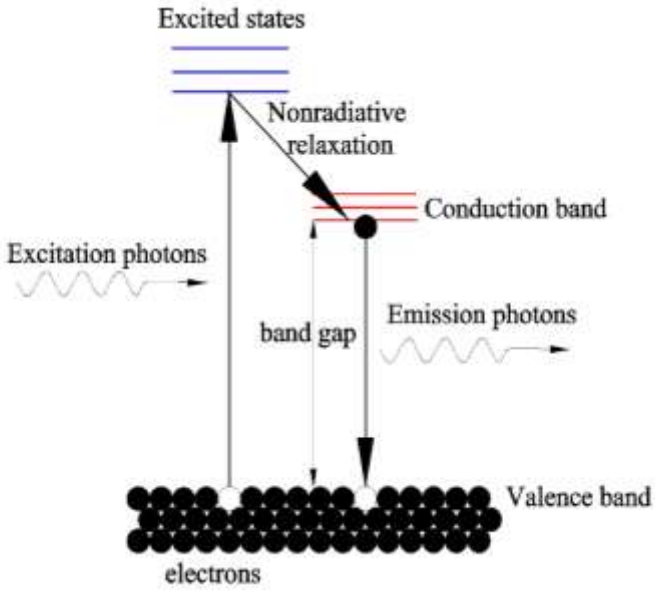

Figure 1-10: Photoluminescence process [16]

1.3.3 **Phosphors and lamps**

The luminescent materials known as phosphors convert energy into electromagnetic radiation, usually in the visible frequency range. The word “Phosphor” was invented in the early 17th century with the discovery of the “Bolognian stone” in Italy. This sintered stone was observed emitting red light in the dark after exposure of sun light. Similar finding was reported from many places in Europe and these lights emitting stones were named phosphors, means, “light bearer” in Greek. Therefore, phosphors are solid luminescent materials that emit photons when excited by an external energy source, such as an electron beam (cathodoluminescence) or a light beam (photoluminescence). Phosphors are composed of an inert host lattice that is transparent to the excitation radiation, and an activator, typically a 3d or 4f electron metal that is excited under energy bombardment. The process of luminescence occurs by absorption of energy at the activator site, relaxation, and subsequent emission of a photon and a return to the ground state. The efficiency of a phosphor depends on the amount of relaxation that occurs during activation and emission. Relaxation is the process in which

energy is lost to the lattice as heat, and it needs to be minimized in order to extract the highest luminous efficiency, defined as the ratio of the energy emitted to the energy absorbed.

Since the birth of the incandescent lamps more than a century ago, several new lamps have been developed. Many of them are discharge lamps with far higher efficacies (lumen per watt) than the incandescent lamps. Different lamps have different possibility about wattage, efficacy size, performance and colour temperature.

1.4 Purposes and organization of this thesis

In recent years, laser projection has become the world's projection market upstart. However, a disadvantage of the laser projector is that the production cost of the green and red laser is too high. In addition, it is still a challenge that the laser speckle is created by using coherent laser sources, which damages the quality of the displayed image. In order to reduce the cost, the research of the phosphorescent material with the laser as the excitation light source is inevitable. Especially, in the low-end consumer market and educational applications, the laser phosphor solution exhibits an obvious attraction, compact, low speckle noise, and low cost. In the NFR financed HiLase project, our group works closely with multinational company Barco for developing next generation projectors, in which laser phosphor is an important research topic. My master thesis work will contribute to the project by thoroughly characterizing different phosphorescent materials including ceramic and crystal ones. Working together with a post-doc, I have involved in the following works such as designing the measurement strategy, building in-house measurement facility, configuring the measurement setup, performing the measurements, analyzing the results. The thesis will present all the achieved results and consists of six chapters. The following are the brief summary of each chapter.

The first chapter mainly introduces the background of the projector, the motivations and significance of this research. A brief description of the phosphorescent material is given.

Chapter two is the theoretical knowledge, focusing on the luminescence mechanism of rare earth ions. Including the luminescence properties of rare earth ions, electronic transition, energy transfer and conservation, etc.

Chapter three describes the experimental setup and instruments, including their working principle and parameter settings. These instruments mainly include FS5

fluorescence spectrometer, laser array, SEM and EDS, etc. as well as temperature control system.

Chapter four is about experiment procedures for characterization, such as, surface topography, elemental composition, excitation and emission spectrum, life time, quantum efficiency.

Chapter five deals with the experimental results and discussions.

Chapter six presents the conclusions and discuss the future studies.

Material selection. The objects we studied included several samples: Ce^{3+}: YAG($Y_3Al_5O_{12}$), Ce^{3+}: LuAG($Lu_3Al_5O_{12}$), Ce^{3+}: GGAG($Gd_3Al_5O_{12}$), Ce^{3+}: GDYAG ($(Gd,Y)_3Al_5O_{12}$)

Chapter 2 Basic theoretical knowledge

Basic theoretical knowledge is very important for research work. Therefore, in this chapter, I will focus on the basic theoretical knowledge about this work. It should include Excitation and emission spectrums, features of rare earth (RE) ions with respect to luminescence, rare earths energy levels and transitions, energy transfer, basic concepts of fluorescence lifetime and basic concepts of quantum efficiency.

2.1 Excitation and emission spectrums

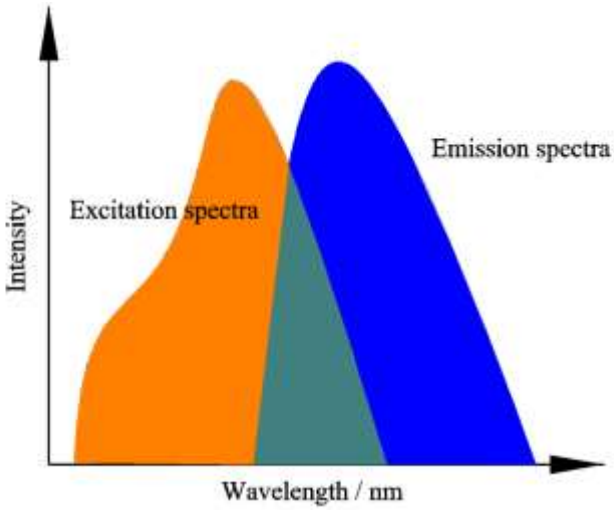

Figure 2-1: Generic Excitation and emission spectrums for a fluorescent dye

Figure 2-1 shows a typical spectrum of the excitation and emission of a fluorochrome. These spectrums are generated by an instrument called a spectrofluorimeter, which comprised two spectrometers: an illuminating spectrometer and an analyzing spectrometer. First, the dye sample is strongly illuminated by a color of light that is found to cause some fluorescence. A spectrum of the fluorescent emission is obtained by scanning with the analyzing spectrometer using this fixed illumination color. The analyzer is then fixed at the brightest emission color, and a spectrum of the excitation is obtained by scanning with the illuminating spectrometer and measuring the variation in emission intensity at this fixed wavelength. For the purpose of designing filters, these spectrums are normalized to a scale of relative intensity.

These color spectrums are described quantitatively by wavelength of light. The most common wavelength unit for describing fluorescence spectrum is the nanometer

(nm). The colors of the visible spectrum can be broken up into the approximate wavelength values [17]:

Violet and indigo	400−450 nm
Blue and aqua	450−500 nm
Green	500−570 nm
Yellow and orange	570−610 nm
Red	610 nm to approximately 750nm

On the short-wavelength end of the visible spectrum is the near-ultraviolet (near-UV) band from 320 to 400nm, and on the long-wavelength end is the near-infrared (near-IR) band from 750 to approximately 2,500nm. The broad band of light from 320 to 2,500nm marks the limits of transparency of crown glass and window glass, and this is the band most often used in fluorescence microscopy. Some applications, especially in organic chemistry, utilize excitation light in the mid-ultraviolet band (190–320nm), but special UV-transparent illumination optics must be used. There are several general characteristics of fluorescence spectrum that pertain to fluorescence microscopy and filter design. First, although some substances have very broad spectrum of excitation and emission, most fluorochromes have well-defined bands of excitation and emission. The spectrum of figure 2-1 are a typical example. The difference in wavelength between the peaks of these bands is referred to as the Stokes shift [17].

2.2 Features of rare earth (RE) ions with respect to luminescence

In display application of luminescence mostly inorganic solids doped with rare earth impurities are used. It is necessary to understand the mechanism of these display materials. Basically, there are four important parameters, viz. excitation type and spectrum, relaxation to emitting state and the decay time, and emission intensity and emission spectrum. RE spectrum were observed extremely sharp (line-spectrum). The above-mentioned four factors vary from one-host materials to another.

The characteristic properties of the RE ions are attributable to the presence in the ion of a deep-lying 4f shell, which is not entirely filled. The electrons of this shell are screened by those in the outer shells (except for La^{3+} and Lu^{3+}), and as a result they give rise to number of discrete energy levels. Since the presence of crystal lattice scarcely affects the position of these levels, there is a resemblance between the energy level diagram of a free ion and that of the incorporated ion. In case of the latter, usually the

terms are shifted to lower wave numbers. Some empirical laws have been formulated regarding the magnitude of this effect [18–21].

In spite of the resemblance of the energy levels of free RE ions and the RE ions in solids, there is an important difference in the emission properties. In solids, the emission of RE ions is observed at different spectrum position than the absorption. The difference between the absorption and emission wavelength is described as 'Stokes Shift'. The shift for the transition within 4f shell results from the fact that the absorption and emission takes place between different levels. Usually, absorption corresponds to the transition from ground state to higher excited states. Electron in the higher excited state then loses energy to lattice till the states lying just below the previous excited states are available. When the difference between the adjacent states is large, then the energy corresponding to this transition cannot be transferred to lattice and it is given out in the form of emission. The emission thus corresponds to the transition from the intermediate state to the ground state.

RE ions are usually trivalent. Ions corresponding to configurations $4f^0$ (La^{3+}), $4f^7$ (Gd^{3+}) and 4f 14 (Lu^{3+}) are stable. The RE element next to these three tends to exchange electron and acquire this stable configuration. For understanding the luminescent properties of rare earth ions, it is necessary to know their key energy levels. The energy level may be divided into three categories, those corresponding to $4f^n$ configuration,$4f^{n-1}5d$ configuration, and those corresponding to charge transfer involving the neighboring ions.

$4f^{n-1}5d$ levels may be understood as formed by the electron in the 5d orbital interacting with $4f^{n-1}$ core. As a consequence of this strong crystal field effect on the 5d electron, $4f^{n-1}5d$ configurations of RE ions in solids are very different from those of free ions. $4f^n \rightarrow 4f^{n-1}5d$ absorption of most of the RE^{3+} and RE^{2+} ions exhibit two features. First, they consist of strong bands corresponding to the components of 5d orbital split in the crystal field. Consequently, their spectrum is similar when ions are embedded in same type of host. Second, the structures of 5d bands can be fitted to energy differences in the ground multiples of the $4f^{n-1}$ configurations.

2.3 Rare earths energy levels and transitions

There are 14 rare earth elements and they lie between lanthanum (^{57}La) and hafnium (^{72}Hf). Their atomic configurations consist of partially filled 4f shells. It is important to note that ions with either filled 4f levels such as Lu^{3+} or ions that have no

4f electrons such as La^{3+}, will have no electronic energy levels to induce excitation in/or near the visible region. The azimuthal quantum number (*l*) of 4f orbitals is 3, which gives 2l + 1 = 7 orbital state (7 orbital orientation) and allows 14 electrons to stay. In the nonexcited state, these electrons will be distributed in such a way that they will have the maximum combined spin angular momentum (S). According to Hund's rule, the spin angular momentum S is added to the orbital angular momentum L to give the total angular momentum J. For the lowest ground state, J = L − S, when the number of 4f electrons is larger than 7.

2.3.1 **Electronic transitions**

An electronic state is indicated by notation $^{2S+1}L_J$, where L represents the letters S, P, D, F, G, H, I, K, L, M, N… corresponding to the resultant orbital quantum number of 4f electrons L=0,1,2,3,4,5,6,7,8..., respectively [20]. An electronic state is actually expressed as an intermediate coupling state and can be described as a mixed state of several $^{2S+1}L_J$ states and a spin–orbit interaction. This mixing due to spin–orbit is actually small for the levels near the ground states, and it is larger for the states that are neighbors with the same J numbers. The effect of the mixing is very large in the optical transition probabilities, although it is relatively small on the energy levels. Rare earth ions (doubly or triply charged) can be present in ionic solids. For the case of the triply charged, all 5d and 6s orbitals are empty and the 4f is partially occupied. The optically active 4f electrons are shielded from the crystalline electric field by the outer 5s and 5p shells. The resulting effect is that the neighboring ligands have very little affection on the 4f electrons. The energy levels of the 4f electrons are very similar to the free ion levels characterized by the L, S, and J values with allowance made for some term mixing [22] and this is because of the weak interaction with the lattice environment. The spectrum lines (either of emission or absorption) are sharp and the energy positions are not (usually) crystalline host dependent.

For the case of divalent rare earth ions, the energy separation between the $4f^n$ and $4f^{n-1}5d$ configurations will be large and the transitions between these two may be observed by normal spectroscopy. These transitions are dipole-allowed and are about 10^6 times stronger than the very frequently observed 4f → 4f transitions in trivalent (rare-earth) ions. The emission and excitation spectrum of the divalent europium ion are mainly composed of two types of electronic transitions: a strong 4f → 5d transition with a high energy and a weak 4f → 4f transition at low energies. The gross feature of

the spectrum of this type of rare earth ions is considered to arise from the T_{2g} and E_g components of the 5d electron in the cubic crystalline field. The strongest lines were actually assigned to pure electronic transitions from $4f^n$ to 4f n−1 5d which was assumed to be caused by the interaction between the $4f^{n-1}$ core and the 5d electron, the $4f^{n-1}$5d level being spaced with the energy gaps in the $4f^{n-1}$ ground multiples [23].

2.3.2 Energy level and luminescence of Ce^{3+}

The luminescence transition in Ce^{3+} is 5d(^{2}D)-4f(^{2}F). The transition energy is the lowest among the lanthanide ions, but the energy gap from the $5d_1$ states to the nearest 4f state is so large that the 5d level serves as an efficient light-emitting state. It is well-known that the 4f ground state of Ce^{3+} is split into two energy levels, $^2F_{5/2}$ and $^2F_{7/2}$, due to spin–orbit coupling, and lead to a double-peak structure due to the two terminating levels of the 4f configuration of Ce^{3+}. The decay time of the Ce^{3+} emission is 10-50 ns [24], the shortest one observed in lanthanide ions. Figure 1-12 shows a typical energy level of the Ce^{3+} luminescence center.

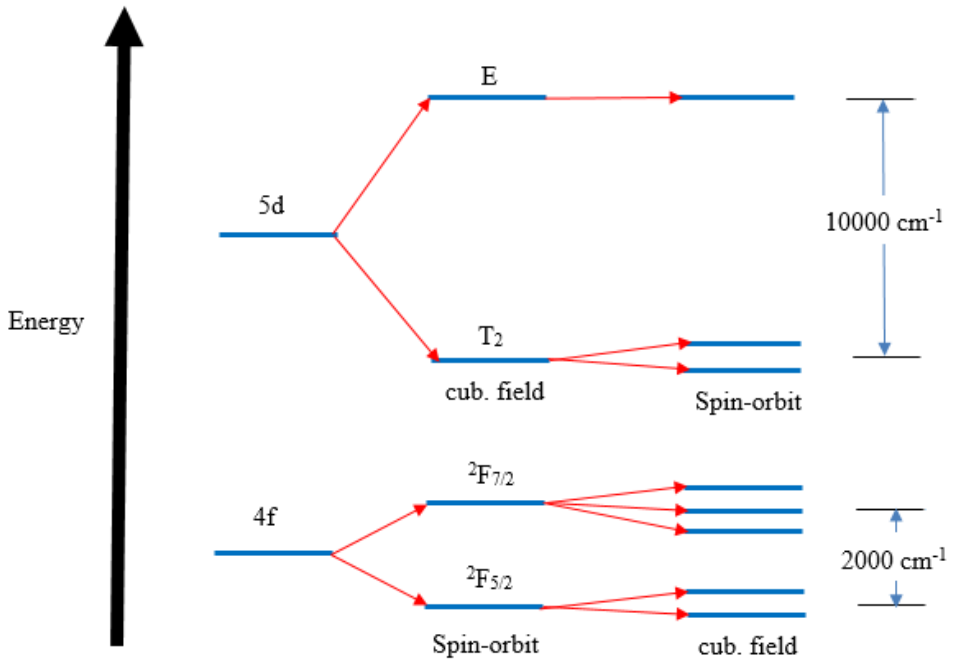

Figure 2-2: Energy level of Ce^{3+} luminescence center [25]

2.4 Energy transfer

The process in which the excitation of a certain ion migrates to another ion is called energy transfer. It is very important to understand this effect in order to develop

efficient luminescent materials. The luminescent materials had several types of energy transfer [26]:

i. Resonant energy transfer between ions of same energy level—for this case, the excitation energy of a certain ion migrates to another one of the same species that is in the ground state. This type of transfer is also divided into three categories: First, multipolar interaction, and this is both transitions are of electric dipole character; the second is the exchange interaction, and this is when the donor and the acceptor are both located so close that their electronic wave functions overlap and the transfer is due to a quantum mechanical interaction; and lastly, the phonon-assisted energy transfer, which occurs when there is a difference E between the transition energies of the donor and the acceptor, and is compensated by either a phonon emission or absorption.
ii. Spectrum diffusion—in this case, the excited ion can give its energy to other ions that are at different sites and/or lattice environment, due to the fact that the doping ions stay at a slightly different lattice environment. This will translate to a shift in the emission spectrum to longer wavelengths and an increment on the width of the emission peak.
iii. Energy donation—in this case, the energy transfer can occur between different ions, one of them is called adonor and the other an acceptor. An ion at an excited higher energy level can transfer most of its energy to other ions. The other ions stay at a lower energy levels and release the differential energy in the form of phonons.
iv. Sensitizer's transfer—a donor that usually has a strong absorption of external radiation and transfers it very efficiently to an acceptor is called a sensitizer; the caused emission is greatly enhanced. This process is also known as sensitization of the luminescence.
v. Quenching centers transfer—in this case, the acceptor kills the emission of the active center or the donating ions, and these ions neither emit at the required wavelength nor emit at all. Mostly, the phosphors that exhibit this type of luminescence are activated by sensitizers or co-activators.

It is important to determine the optimum concentration of dopant to be used, in order to obtain efficient luminescence with a minimum energy loss. For display application, the purity of color is the most important issue. For many ions emissions

can be from different upper excited states. The way to keep this emission from the upper states from occurring, and to purify the luminescence is to quench the emission via cross relaxation [27]. In this process, the excited ions from the upper states prefer to release part of their energy to the neighboring ions at the ground state, and then move to the lowest metastable state. Then these ions will return to the ground state and release the remaining energy at the desire wavelength. In order to be able to do this, the doping concentration should be sufficiently high, but it is important to note that in a heavily doped system the average distance between the ions becomes smaller, and therefore the excited ions can move around in the host causing resonant energy transfer.

2.5 Basic concepts of fluorescence lifetime

A fluorophore which is excited by a photon will relax to the ground state with a certain probability based on the decay rates through a number of different (radiative and/or nonradiative) decay pathways [28]. To observe fluorescence, one of these pathways must be by spontaneous emission of a photon. In the ensemble description, the fluorescence emitted will decay with time according to:

$$I(t) = I_0 e^{-t/\tau} \tag{2-1}$$

Where:

$$\frac{1}{\tau} = \sum K_i \tag{2-2}$$

In the above, t is time, τ is the fluorescence lifetime, I_0 is the initial fluorescence at $t = 0$, and K_i are the rates for each decay pathway, at least one of which must be the fluorescence decay rate K_f. More importantly, the lifetime τ is independent of the initial intensity and one of the emitted light. This can be utilized for making non-intensity based measurements in chemical sensing.

The fluorescence lifetime also can be description like this: absorption and emission processes are almost always studied on populations of molecules and the properties of the supposed typical members of the population are deduced from the macroscopic properties of the process. In general, the behavior of an excited population of fluorophores is described by a familiar rate equation:

$$\frac{dn(t)}{dt} = -k\, n(t) + f(t) \tag{2-3}$$

where n is the number of excited elements at time t, k is the rate constant of all deexcitation processes and $f(t)$ is an arbitrary function of the time, describing the time

course of the excitation. The dimensions of k are s^{-1} (transitions per molecule per unit time).

If excitation is switched off at $t = 0$, the last equation, takes the form:

$$\frac{dn(t)}{dt} = -k\, n(t) \tag{2-4}$$

and describes the decrease in excited molecules at all further times. Integration gives:

$$n(t) = n(0)\exp(-k * t) \tag{2-5}$$

The lifetime τ is equal to k^{-1}.

If a population of fluorophores are excited, the lifetime is the time it takes for the number of excited molecules to decay to 1/e or 36.8% of the original population according to:

$$\frac{dn(t)}{dn(0)} = e^{-t/\tau} \tag{2-6}$$

The deexcitation rate k is the sum of the rates of all possible deexcitation pathways:

$$K = k_f + k_i + k_x + k_{ET} + \ldots = k_f + k_{nr} \tag{2-7}$$

Here, k_f is the rate of fluorescence, k_i the rate of internal conversion and vibrational relaxation, k_x the rate of intersystem crossing, k_{ET} the rate of inter-molecular energy transfer and k_{nr} is the sum of rates of radiationless deexcitation pathways.

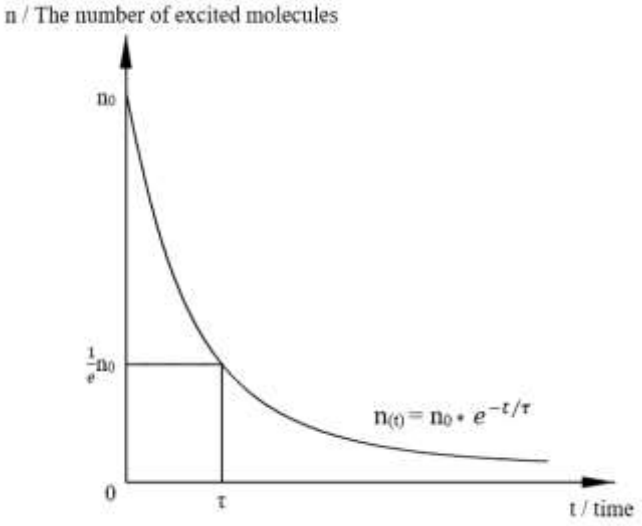

Figure 2-3: Fluorescence lifetime

Figure 2-3 shows the excited electronics attenuation process and the method od determine fluorescence lifetime. It is can be seen that the relationship between the number of excited molecules and time is:

$$n_{(t)} = n_{(0)} * e^{-t/\tau} \tag{2-8}$$

In this coordinate system, horizontal coordinate represent time, the vertical coordinate represents the number of excited molecules. The fluorescence lifetime is the time it takes for the number of excited molecules to decay to 1/e or 36.8% of the original excited molecules.

2.6 Basic concepts of quantum efficiency

In our project, two types of quantum efficiency should be considered internal quantum efficiency (IQE) and external quantum efficiency (EQE). Internal quantum efficiency (IQE) is defined as the proportion of the total number of photons emitted by the phosphor (fluorescence) vs the number of excitation photons (450 nm) that are absorbed and not reflected by the phosphor (equation 2-12). External quantum efficiency (EQE) is defined as the proportion of the total number of photons emitted by the phosphor (fluorescence) vs the number of excitation photons that are emitted by the excitation light source (equation 2-13). It is can be seen that the internal quantum efficiency (IQE) always bigger than the external quantum efficiency (EQE).

$$\mathrm{IQE} = \mathrm{Fluorescence}/(\mathrm{Excitation} - \mathrm{Reflection}) \quad (2\text{-}12)$$

$$\mathrm{EQE} = \mathrm{Fluorescence}/\mathrm{Excitation} \quad (2\text{-}13)$$

Here:

Fluorescence: total number of photons emitted by the phosphor.

Excitation: total number of photons emitted by the excitation laser source.

Reflection: total number of photons reflected and not absorbed by the phosphor.

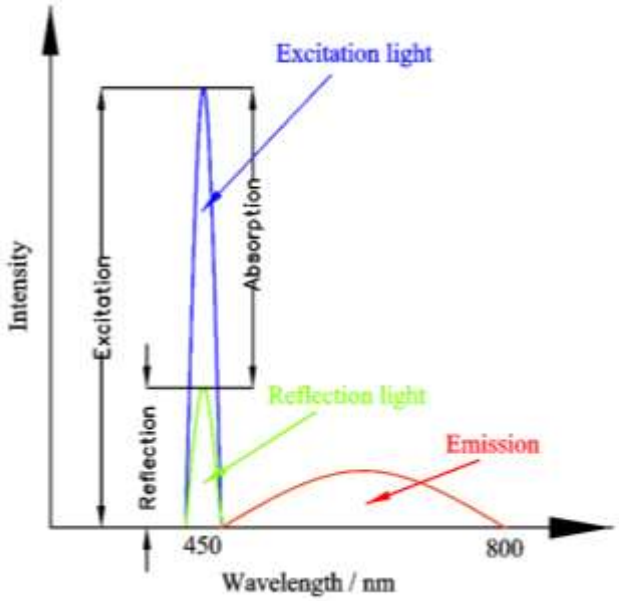

Figure 2-4: Graphic representation of IQE and EQE

The relationship between the total number of photons emitted by the excitation laser source and total number of photons reflected as shown in figure 2-4. As such, we see that the IQE measures the efficiency performance of the phosphor post-absorption and is not concerned with the amount of light that is reflected, while EQE measures the efficiency performance of the phosphor including absorption efficiency. IQE can be considered to be internal since it is concerned with the efficiency of the phosphor performance within the fluorescence process, while EQE can be considered to be external because it also considers the efficiency of the phosphor performance in absorbing an external excitation light.

This distinction is very useful for phosphor performance measurement because IQE provides information about the quality of the phosphor itself, while EQE provides further information about the absorption performance, which is typically concerned with the composition of the phosphor and possible changes that may be required. Together, these two metrics provide a standardized method of evaluation for any phosphorescent material, thus, it is very important.

Chapter 3 Experimental preparations

In this chapter, I will introduce the instruments and experimental setup which has been used in the experiment, such as, SU3500: Hitachi Scanning Electron Microscope (SEM) was be used to measure sample surface morphology; Energy Dispersive Spectrometry (EDS) was be used to measure the composition elements of each sample. FS5 fluorescence spectrophotometer was used in order to measure the Excitation and emission spectrums, and fluorescence lifetime, etc.

3.1 Sample morphology and composition

The SU3500 Scanning Electron Microscope (shown in figure 3-1) features innovative electron optics and signal detection systems to provide unparalleled imaging and analytical performance. Designed with intuitive logic, the new user-friendly GUI provides comprehensive image observation and display functions. Engineered for a wide range of applications including biological specimens and advanced materials, the SU3500 is sure to be the workhorse microscope in any laboratory.

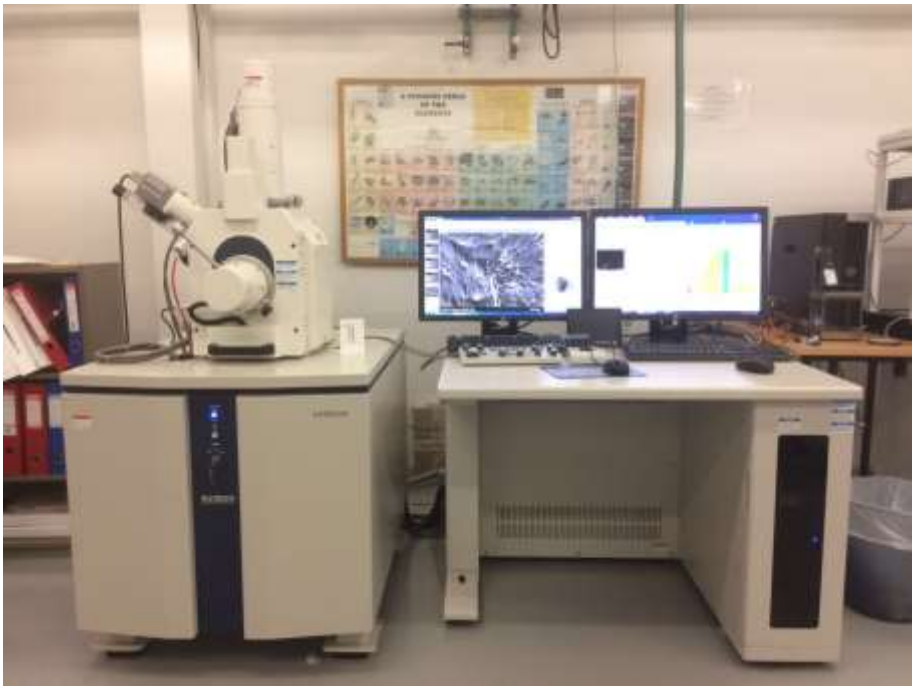

Figure 3-1: SU3500: Hitachi Scanning Electron Microscope

3.2 Exitation and emission spectrums and Lifetime

FS5 fluorescence spectrophotometer was used to measure the Excitation and emission spectrums, and fluorescence lifetime of each sample. These are very important properties for phosphor materials.

3.2.1 **Introduction of FS5 fluorescence spectrophotometer**

Figure 3-2 shows the FS5 fluorescence spectrophotometer, that is a fully integrated steady state fluorescence spectrometer designed to meet the highest specifications in the research and analytical markets. Ultimate sensitivity, coupled with high speed data acquisition and ease of use, makes the FS5 the ideal plug and play analytical tool. The optical design is the best in its class, utilizing specially selected optics to achieve the maximum in signal throughput.

Using single photon counting techniques for the highest detection sensitivity, the FS5 delivers data you can trust for a broad array of samples, from solutions and powders to films. The standard FS5 has a number of upgrade routes that are unique in its class, including:

- Extended wavelength coverage up to 1650 nm while maintaining the specified sensitivity in the UV and visible spectrum range.
- Computer-controlled polarizers to allow for automated anisotropy.
- Phosphorescence lifetime option with a lifetime range of microseconds to seconds.
- Fully integrated fluorescence lifetime option (TCSPC based) for the measurement of lifetimes from picoseconds to microseconds.

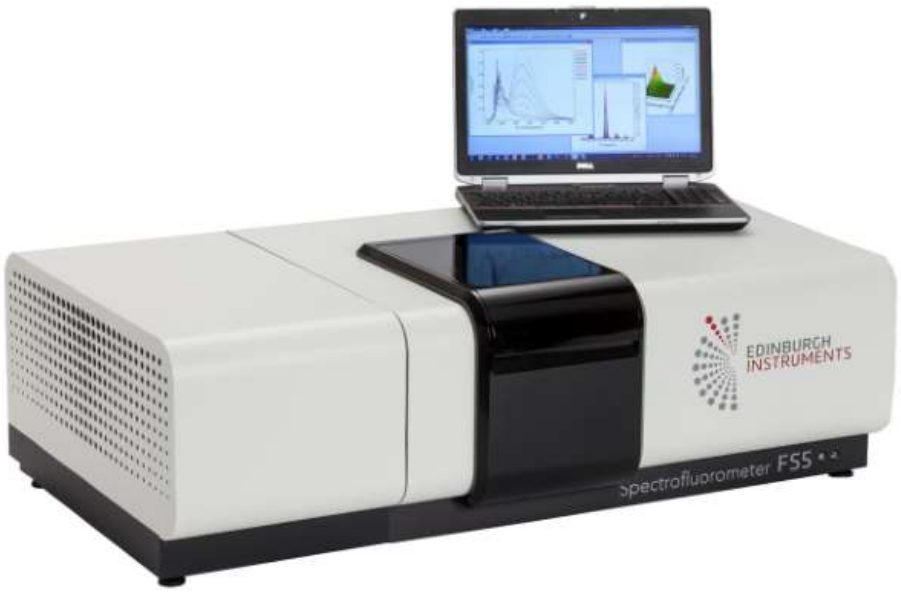

Figure 3-2: FS5 fluorescence spectrophotometer

3.2.2 **Measurement methods of fluorescence lifetime**

Absorption of light is followed by emission which has a distinct lifetime and can be used to characterise a process in a sample. In general, we have two ways to measure this fluorescence lifetime. One way to measure this lifetime is to use the Time Correlated Single Photon Counting (TCSPC) technique. The other way is use frequency (or harmonic) domain to deduced the fluorescence lifetime. In this work, we use the Time Correlated Single Photon Counting (TCSPC) technique to measure the fluorescence lifetime of our five samples.

The principle of measuring fluorescence lifetime with Correlated Single Photon Counting (TCSPC) technique is shown in figure 3-3. The light source is pulsed laser which wavelength is 450 nm. This discriminator is used to eliminates noise (dark counts of the photodetector) and generates pulses which are independent of the actual shape and amplitude of the detector pulse (which is generated when a photon hits the detector). The function of Time to Amplitude Converter (TAC) is to convert time to voltage signals by charging a capacitor.

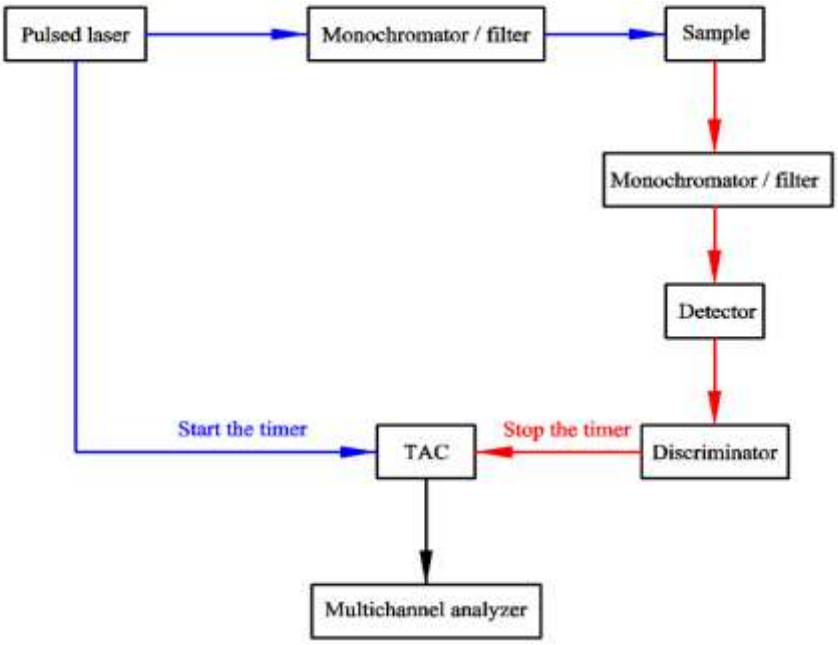

Figure 3-3: Work principle of TCSPC technique (single cycle)

The work process of the single cycle is like this: the pulsed laser emits an excitation pulse that can be splitting two signals, first one arrives directly to Time to Amplitude Converter (TAC) and start timer. The other one arrives to our sample and complete a photoluminescence (excitation and emission), and then, the emission photons should be detected by the detector (fixed wavelength, it is can be changed). When the detector

detects a photon, it immediately outputs a signal to TAC to stop the timer. Time to Amplitude Converter (TAC) convert the time to voltage signal and the voltage signal is stored by the multichannel analyzer.

Time to Amplitude Converter (TAC) however detects only one photon in each excitation cycle. If more photons arrive within a single time after excitation, only a single count is registered the discriminator does not take into account the size of the pulse from the detector once it is larger than the discrimination level. If no photon is detected Time to Amplitude Converter (TAC) is reset when reaching the maximum voltage. So, the average number of photons reaching the detector in each excitation cycle should be less than one.

3.3 Quantum efficiency

Quantum efficiency is one of the most important data for evaluating phosphor materials, in this part we use the integrating sphere and AvaSoft 8 enlightening spectroscopy (calibrated for wavelength and irradiance) to measure quantum efficiency.

3.3.1 Measurement methods of quantum efficiency

Quantum efficiency is measured using an integrating sphere, it can be divided into following three steps specifically.

1. Measure reference (Excitation).

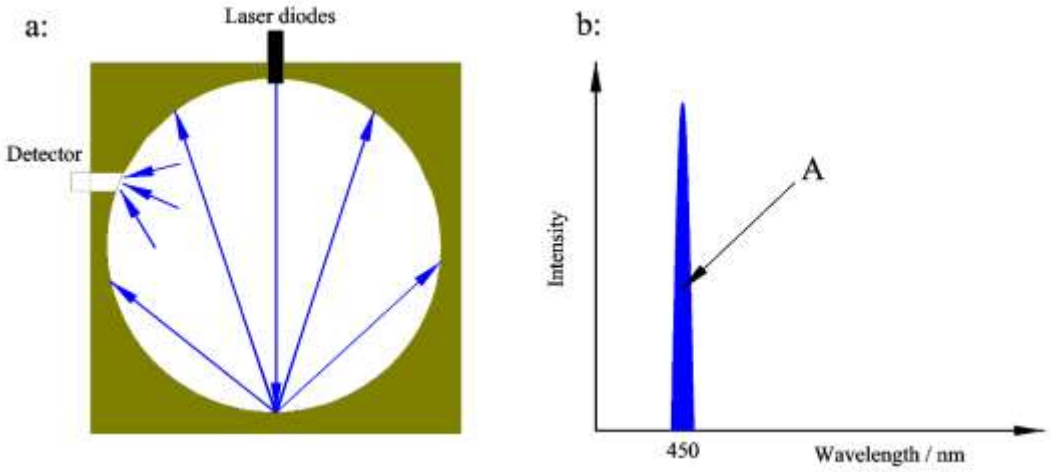

Figure 3-4: Step 1 of measuring quantum efficiency.

The first step is measure reference. The step1 is shown in figure 3-4, we just measure the intensity of the excitation light (blue laser with a wavelength of 450 nm). Note: no samples were placed in the integrating sphere. In the figure 3-4 (b), 'A' is the

integral value of the intensity versus wavelength, representing the number of photons from the excitation light source (450 nm laser).

2. Measure emission spectrum.

The second step is measure fluorescence spectrum. In this step, we put the sample on the bottom of the inner wall of the integrating sphere. The blue laser can be irradiated on sample directly, most of the light is absorbed by the sample, and a small portion of the light is reflected. A portion of the light that is not absorbed by the sample can be irradiated onto the sample again due to the diffuse reflection of the inner wall of the integrating sphere, that is named by re-excitation.

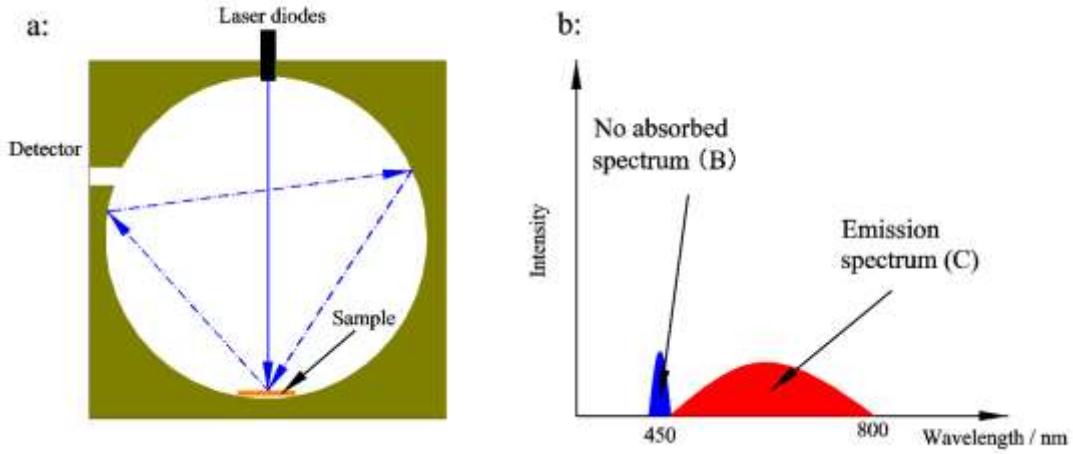

Figure 3-5: Step 2 of measuring quantum efficiency (measure emission spectrum)

Step 2 of measuring quantum efficiency is shown in figure 3-5. As shown in figure 3-5 (a), the solid line is laser (directly); dotted line is the re-excitation light. In the figure 3-5 (b), 'B' representing the number of photons not absorbed by sample, and 'C' representing the number of emission photons that consist of the emitted by laser (directly) and the emitted by re-excitation light.

3. Measure re-excited emission spectrum

The last step is measure re-excited emission spectrum. In this step, we just rotating the laser diodes makes the laser light cannot be irradiated on sample directly. At here, the sample is only work at re-excitation light. Figure 3-6 (a) shows this case, the solid line is laser (directly); dotted line is the re-excitation light. As shown in figure 3-6 (b), 'D' representing the number of photons that the photons from laser source minus the photons re-absorbed by sample; 'E' representing the number of emitted photons by re-excitation light.

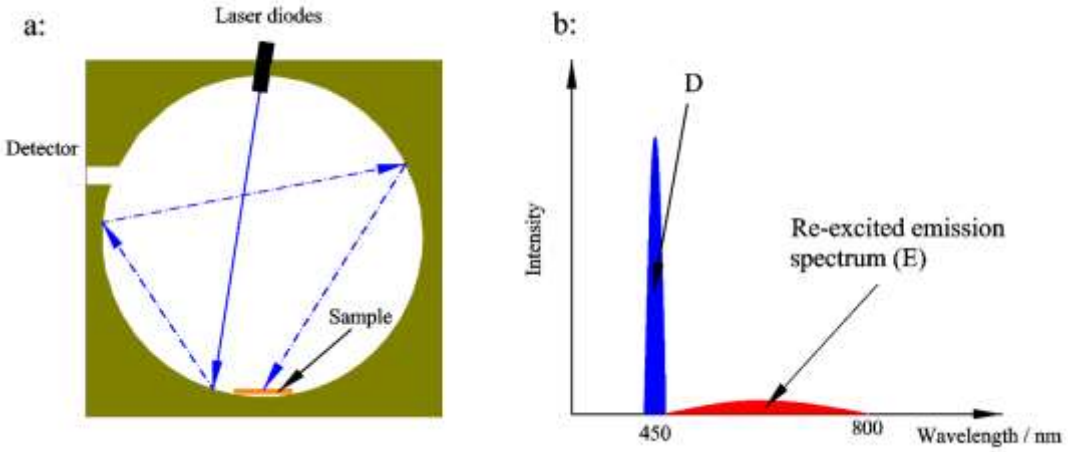

Figure 3-6: Step 3 of measuring quantum efficiency (measure re-excited emission spectrum)

The calculation method is as follows, internal quantum efficiency (IQE) use equation 3-1, and the external quantum efficiency (EQE) use equation 3-2.

$$IQE = (C - E)/(D - B) \tag{3-1}$$

$$EQE = (C - E)/A \tag{3-2}$$

Here, the meaning of each parameter is as follows:

A: is the number of photons from the excitation light source.

B: is the number of photons not absorbed by sample.

C: is the total of emission photons (directly and re-excited).

D: is the photons from laser source minus the photons re-absorbed by sample.

E: is the number of emitted photons by re-excitation light.

The relationship of the absorbed, re-absorbed and emitted is shown in figure 3-7. It is very clearly and easy to understand.

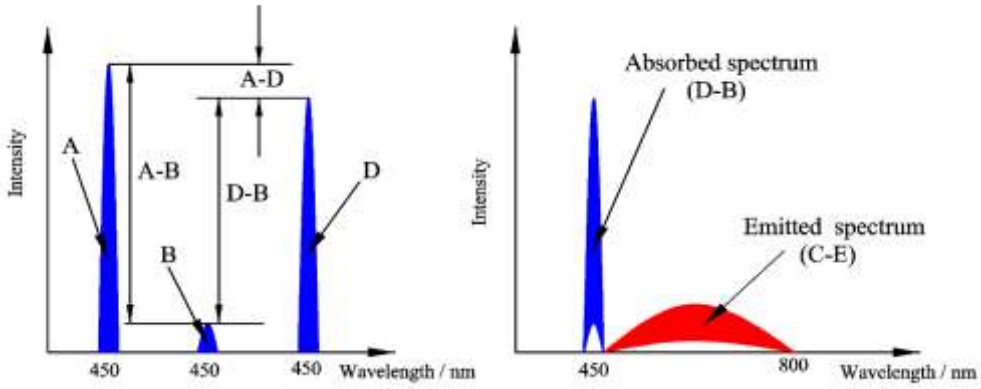

Figure 3-7: The relationship of absorbed, re-absorbed and emitted.

3.3.2 **The experimental process of measuring quantum efficiency**

In our work, we use 4 laser diodes as the excitation sources and focus on the sample surface, thus that is very difficult to rotate the laser device. Therefore, we use the method of changing the position of the sample take the place of the rotating laser device. This process is shown in figure 3-8.

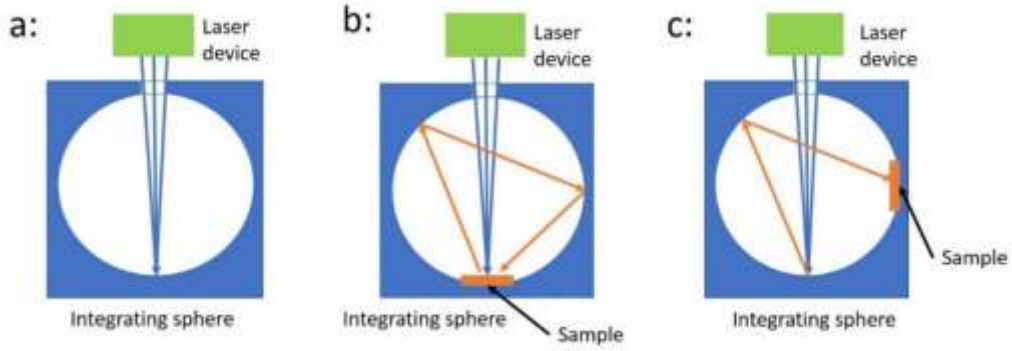

Figure 3-8: Actual measuring quantum efficiency process.

Figure 3-9 shows the experimental setup for quantum efficiency measurement in our lab room, that A is integrating sphere; B is laser device and C is control device. We put the sample on the bottom of the integrating sphere, the excitation light enters the integral sphere through the hole above the integrating sphere and focused on the surface of the sample.

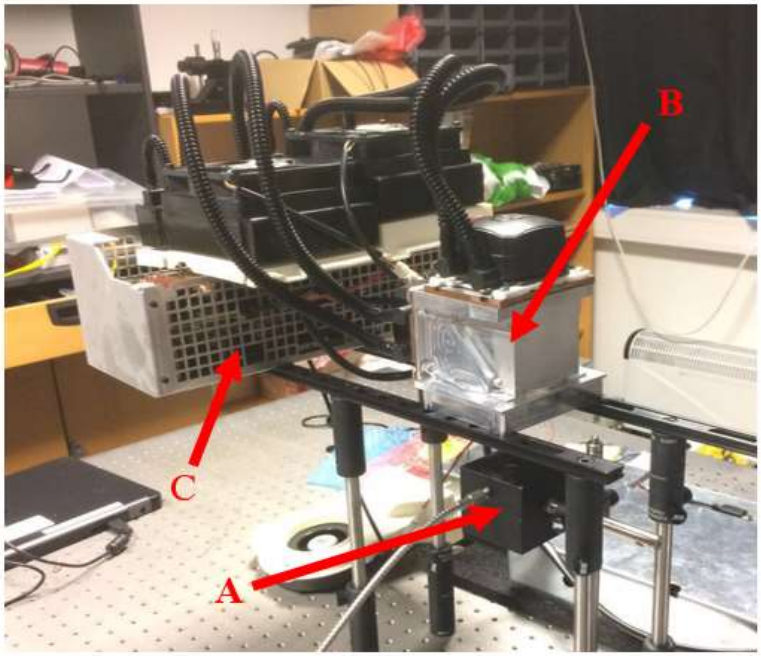

Figure 3-9: Experimental setup for quantum efficiency measurement (A: integrating sphere; B: laser device; C: control device)

3.4 Temperature change control

The experimental setup is shown in figure 3-10, in this setup, we use the HT24S heater to heating the samples (the temperature range is 25℃ - 350℃) and use the FS-5 fluorescence spectrophotometer to check the Excitation and emission spectrums at different temperature. The excitation light is 450 nm laser and the power of laser is very low that means the sample cannot heating by laser. Thus, the samples temperature just depended on the HT24S heater.

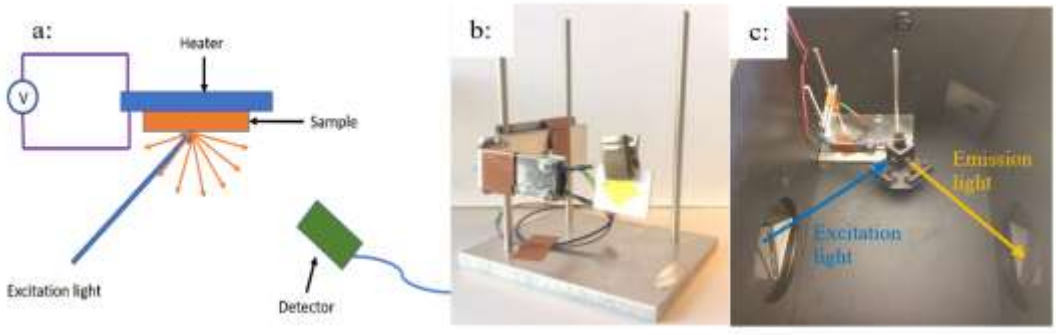

Figure 3-10: Temperature control experimental setup

The characteristic of HT24S heater is shown in table figure 3-11, that HT24S is a 20 mm x 20 mm heating element rod compatible with Thorlabs TC200 general-purpose heater controller. This 24 W heating element has 50 mm leads and is 1.7 mm thick, and the maximum temperature is 400℃.

Voltage (V)	Temperature (℃)
8.5	100
12.1	150
15.7	200
19.2	250
22.7	300
26.5	350

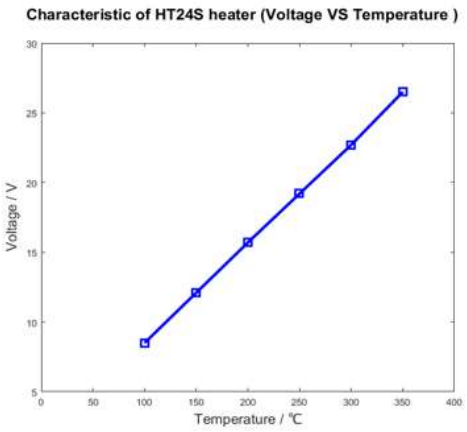

Figure 3-11: Characteristic of HT24S heater.

Chapter 4 SEM and EDS results and discussions

Two experiments were included the following part, sample surface morphology and composition elements. All of the samples were divided into two categories: polished surface and grounded surface based on the surface morphologies. The difference between two types of samples is roughness, the polished samples with small roughness and the grounded surface samples with the larger roughness, and the surface of these samples look like the muddy ground.

For the characterization of the sample, Scanning Electron Microscope (SEM) was used to obtain the surface morphologies of samples, and Energy Dispersive Spectrometer (EDS) was employed to check the composition elements.

4.1 Single crystal LuAG: Ce^{3+}

SEM picture and EDS results of Ce^{3+}: LuAG ($Lu_3AL_5O_{12}$) were shown in this section. The polished surface and grounded surface of LuAG sample were shown in figure 4-1, (a) is polished surface of LuAG sample, and (b) is polished surface of LuAG sample.

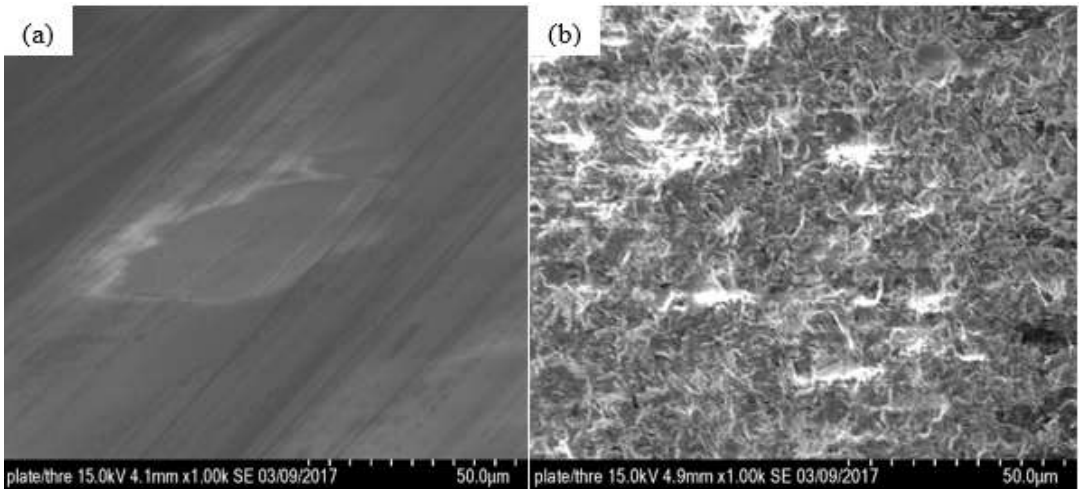

Figure 4-1: LuAG surface morphology ((a) is LuAG polished surface sample micro photos, (b) ais LuAG polished surface sample micro photos.)

From figure 4-1, it is noticed that the polished sample's surface is much smoother than grounded one. The surface morphology of the samples is very important in the optical system, especially material optics, because of the different surface could be caused different refractive indices and different reflectivity. The EDS results shown in

figure 4-2, and the corresponding composition ratio of elements is shown in table 4-1. In this EDS results plot, the X-axis represents the energy value of the X-ray and the Y-axis is the X-ray counts per second.

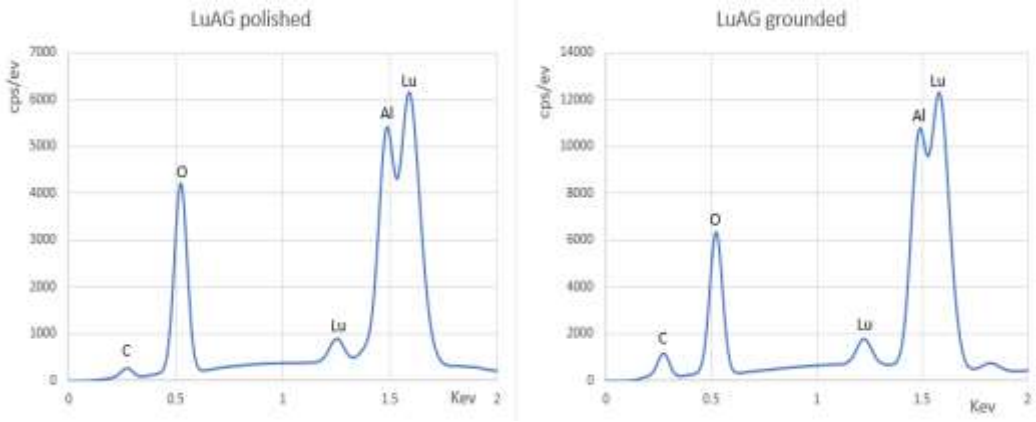

Figure 4-2: LuAG EDS results plot (left one is polished and right one is grounded)

Table 4-1 LuAG EDS results of composition ratio of elements

Sample	element	series	wt.%	norm. wt.%	norm. at.%	Error in wt.%
Polished	Carbon	K-series	0.7021	0.79481	2.69629	0.299884
	Oxygen	K-series	19.557	22.1391	56.3820	4.419759
	Aluminum	K-series	15.890	17.9874	27.1635	1.474028
	Lutetium	M-series	52.190	59.0786	13.7580	4.666988
		Sum:	88.341	100	100	
Grounded	Carbon	K-series	4.4772	10.4402	21.2578	1.254332
	Oxygen	K-series	14.420	33.6267	51.4009	3.321417
	Aluminum	K-series	10.921	25.4660	23.0826	1.062545
	Lutetium	L-series	13.065	30.4669	4.25856	0.928679
		Sum	42.884	100	100	

From the table 4-1, the oxygen and aluminum element in two samples are 56.4%, 27.2%, 51.4%, and 23.1%, respectively, which are close to each other. However, the carbon and lutetium elements are obvious distinct, 2.7%, 13.8% in polishes sample and 21.3%, 4.3% in ground sample, respectively. The carbon element in ground sample is clearly higher than the polishes one, the possible explain is that the grounded surface is much easily to allow some organic material adhered on the surface. Duo to the carbon concentration in grounded sample is much higher than the polished one, therefore, the lutetium content of the grounded sample should be less than the polished sample.

4.2 Single crystal and polycrystalline YAG: Ce^{3+}

Owing to the SEM image of YAG samples are similar as LuAG samples, just only shown the difference in composition elements. Therefore, the following test samples

only show the EDS results without SEM image. Figure 4-3 shows the EDS results of YAG single crystal and YAG wheel (powder).

In figure 4-3, (a) is YAG single crystal and (b) is YAG wheel (powder). The EDS result of YAG wheel (powder) shows two more peak than YAG single crystal, which means YAG wheel contains two more elements than that of YAG single crystal, silicon and niobium. Silicon and niobium element may originate from glass substrate, because the YAG wheel sample has coated on the top surface of glass. The schematic structure of YAG wheel is shown in figure 4-4(a).

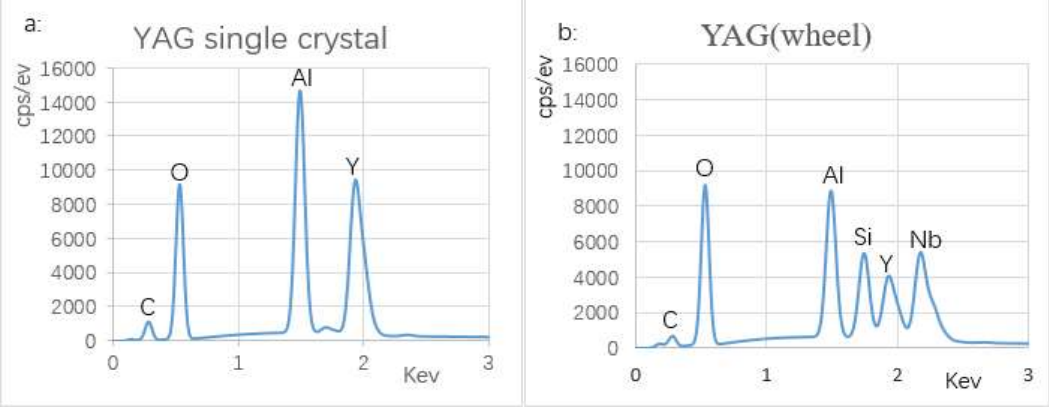

Figure 4-3: EDS results of YAG single crystal (a) and YAG wheel (b).

As figure 4-4(a) shown, the YAG wheel is displayed as “sandwich type” structure: a layer of YAG phosphor materials (powder) coated on the aluminum plate, and then a layer of glass protected on YAG phosphor materials (powder). The thickness of the aluminum plate is probably ~1 mm, which is much thicker than the YAG phosphors layer and glass layer. The aluminum plate was used to increase the absorption in the luminous process. Figure 4-4(b) shows the schematic of luminous process, when the excitation light is irradiated onto the sample, some part of light is reflected, and a part of the light is transmitted into the sample, then reflected by the mirror (aluminum plate) and re-absorbed by the sample.

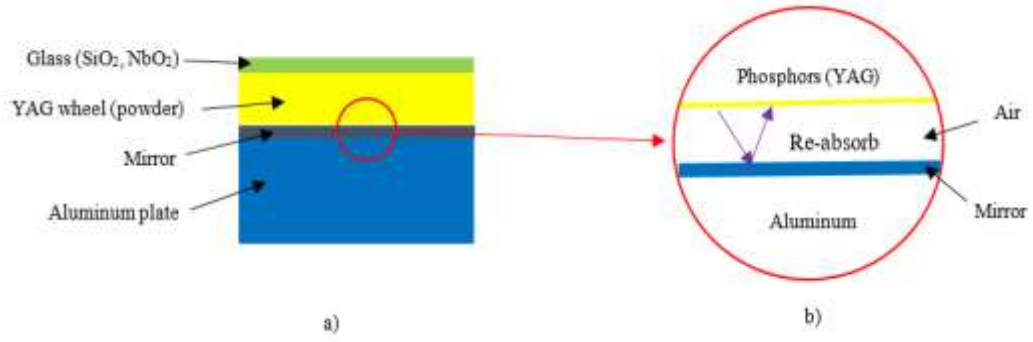

Figure 4-4: YAG wheel structure (a), and re-absorb process (b).

Table 4-2 shows the EDS results of composition elements of YAG single crystal and YAG wheel (powder). In this table, the oxygen content in YAG wheel sample is much higher than YAG single crystal. The reason maybe is that the thin layer of glass has coated on YAG wheel sample (SiO_2 and NbO_2), therefore which is abundant in oxygen.

Table 4-2 YAG EDS results of composition ratio of elements

Sample	element	series	wt.%	norm. wt.%	norm. at.%	Error in wt.%
YAG single crystal	Carbon	K-series	12.09899	11.02254	20.77345	3.267374
	Oxygen	K-series	43.76185	39.86833	56.40668	9.75731
	Aluminum	K-series	19.37836	17.65425	14.81115	1.844891
	Yttrium	M-series	34.52675	31.45488	8.00873	2.717617
		Sum:	109.766	100	100	
YAG wheel	Carbon	K-series	4.804414	5.406596	11.3077	1.439062
	Oxygen	K-series	32.51018	38.03266	60.73475	7.276927
	Aluminum	K-series	10.14812	11.34079	10.56891	0.991215
	Yttrium	L-series	13.0659	30.46699	4.258567	0.928679
	Silicon	K-series	6.34321	7.464694	6.785164	0.579219
	Niobium	L-series	20.1666	23.93481	6.603386	1.506105
		Sum	85.75522	100	100	

4.3 Single crystal of GGAG: Ce^{3+} and GDYAG: Ce^{3+}

Two samples contain gadolinium element in the tested samples. Due to the presence of gadolinium, the luminescent properties of the two samples are a little bit similar. Gadolinium gallium aluminum garnet (GGAG) is a new host material of rare earth doped phosphors, the element composition of GGAG and GDYAG were analyzed in this part. Figure 4-5 shows the EDS results of these two samples, (a) is the EDS result of GGAG and (b) is the EDS result of GDYAG.

The fourth peak in figure 4-5 (a) shows two elements which are gadolinium and gallium. The two peaks are almost overlapped, that can be explained by the energy of gadolinium element and gallium are close to each other. The corresponding energy of the characteristic X-ray of gadolinium element and gallium element are 1.181 Kev (Mα) and 1.098 Kev (Lα), respectively. In figure 4-5 (b), there has shown the cerium element. In fact, the trivalent cation of cerium (Ce^{3+}) is doped in the phosphor materials as a luminescent center, the concentration of cerium element is very less, around 0.4 at.%. Therefore, cerium element could be difficult to found by use of EDS technique.

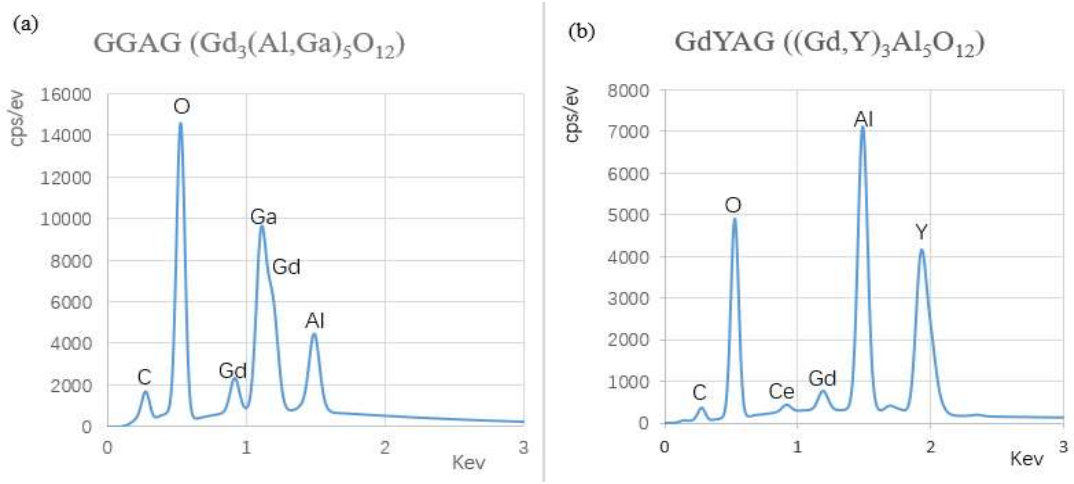

Figure 4-5: (a) is EDS result of GGAG; (b) is EDS result of GdYAG.

Table 4-3 GGAG and GdYAG EDS results of composition ratio of elements

Samples	element	series	wt.%	norm. wt.%	norm. at.%	Error in wt.%
GGAG	Carbon	K-series	9.1282764	9.7640708	13.9927055	2.481623709
	Oxygen	K-series	76.480244	74.050072	79.9569586	16.68019928
	Aluminum	K-series	2.5586169	7.9947197	4.99052198	0.28833388
	Gallium	K-series	0.3567612	1.0171140	0.24608591	0.179588975
	Gadolinium	L-series	14.187608	7.1740224	0.81372796	1.418053789
		Sum:	102.71150	100	100	
GdYAG	Carbon	K-series	3.362938	3.565629	8.713691	1.024589
	Oxygen	K-series	27.04646	28.6766	52.6101	6.039637
	Aluminum	K-series	21.07465	22.34486	24.30838	1.935495
	Yttrium	L-series	38.70305	41.03576	13.54806	3.020336
	Cerium	L-series	0.112734	0.119529	0.025039	0.072835
	Gadolinium	M-series	4.015595	4.257623	0.794734	0.490398
		Sum:	94.31542	100	100	

Table 4-3 shows the EDS composition element ratios of GGAG: Ce^{3+} and GdYAG: Ce^{3+}. Now, the investigation of gadolinium element was analyzed on GGAG: Ce^{3+} and GdYAG: Ce^{3+}. From the GGAG part in table 4-3, the characteristic X-ray of gadolinium element is L-series which is corresponding to the third peak shown in the figure 4-5 (a). The other gadolinium peak on figure 4-5 (a) is same as the gadolinium peak on the figure 4-5 (b), both are Mα characteristic X-ray and with the energy of 1.181 Kev.

Chapter 5 Excitation and emission spectrums results and discussions

Excitation and emission spectrums are very basic and important properties for phosphor materials. When the light is irradiated onto the sample surface, three cases can be occurred, reflection, transmission and absorption. The absorption spectrum is the ratio of the material to the absorption events of electromagnetic radiation at certain frequency. The excitation spectrum presents the relationship between the wavelength of the excitation light and the fluorescence intensity when the emission wavelength at a certain wavelength. The emission spectrum presents the relationship between the wavelength of the emission light and the fluorescence intensity when the excitation wavelength at a certain wavelength. Therefore, absorption spectrum always higher than excitation spectrum at same luminous process for the luminous mechanism of phosphor materials, due to only one part of absorbed photons are converted into another photon in the form of electron transitions, the other part of absorbed photons will be converted into heat and consumed. That could be a reason to explain the temperature of the tested sample will be increased when illuminated. The following tests were finished by use of FS5 fluorescence spectrophotometer.

5.1 Single crystal LuAG: Ce^{3+}

5.1.1 Excitation spectrum of single crystal LuAG: Ce^{3+}

The excitation spectrum of LuAG: Ce^{3+} phosphor is shown in figure 5-1, that emission wavelength is 510nm. Two excitation spectrum were observed at the wavelength of 349nm and a strong broad band ranging from 400nm to 500nm with a maximum wavelength of 450nm, respectively. These excitation bands are due to the absorption of the incident radiation by Ce^{3+} ions which leads to the excitation of electrons from the $4f^1$ ground state ($^2F_{5/2}$) to the excited state $5d^1$ ($^2D_{5/2}$, $^2D_{3/2}$). The electrons from the $4f^1$ ground state ($^2F_{5/2}$, $^2F_{7/2}$) transition to $5d^1$ excited state ($^2D_{5/2}$) is shown in the first excitation band (349nm); in addition, the electrons from the $4f^1$ ground ($^2F_{5/2}$) state transition to $5d^1$ excited state ($^2D_{3/2}$) is shown in the second excitation band (450nm).

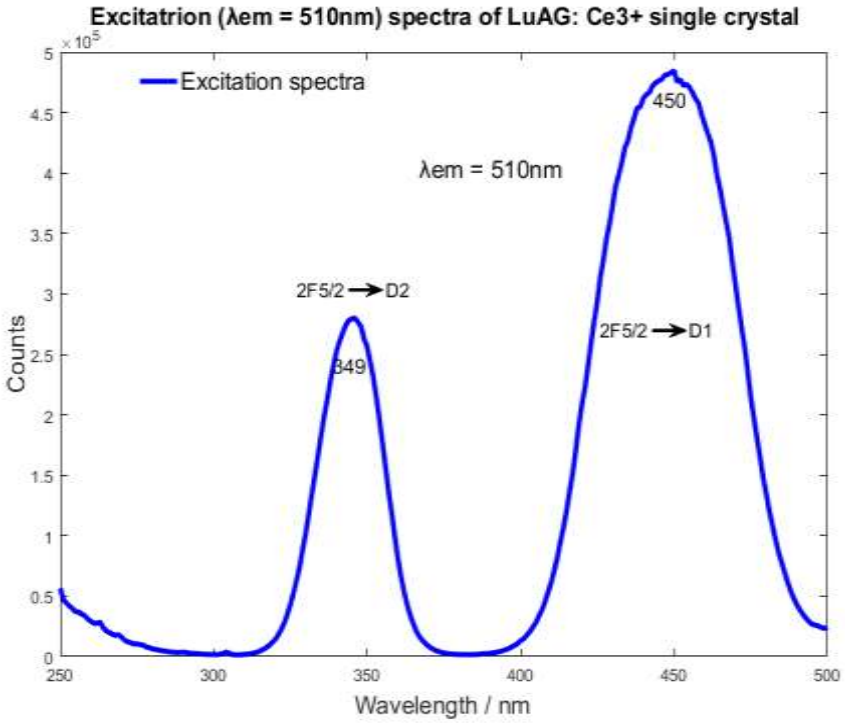

Figure 5-1: Excitation spectrum (λ_{em} = 510nm) of LuAG: Ce^{3+} phosphor

5.1.2 **Emission spectrum of single crystal LuAG: Ce^{3+}**

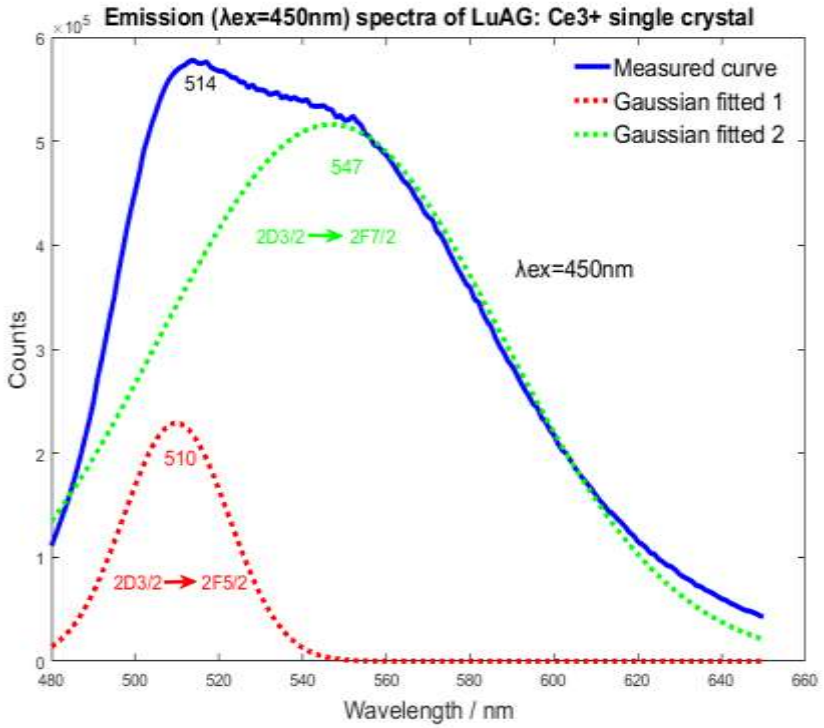

Figure 5-2: Emission spectrum of LuAG: Ce^{3+} phosphors and deconvoluted emission spectrum (solid line—measured; dash line—Gaussian fitted).

The figure 5-2 shows emission spectrum of LuAG: Ce^{3+} phosphor and the excitation wavelength is 450nm. Under 450 nm excitation, an asymmetrical emission spectrum (like shoulders) was obtained in the green region (515 nm); the result was the overlap of two emission bands. According to the Gaussian fitted results, shown in the figure 5-2 (dotted lines), it is observed that the emission spectrum can be superimposed by two bands with the center wavelength of 511nm and 548nm, which can be assigned to the $^2D \rightarrow {}^2F_{5/2}$ (510nm) and $^2D \rightarrow {}^2F_{7/2}$ (547nm) transitions of the Ce^{3+} ions, respectively.

5.1.3 CIE (Commission International de l'Éclairage) chromaticity of LuAG: Ce^{3+}

Corresponding CIE (Commission International de l'Éclairage) chromaticity coordinates of LuAG: Ce^{3+} are shown in figure 5-3. The point 1 (0.0580, 0.6882) is corresponding to the weak emission peak (510nm: $^2D_{3/2} \rightarrow {}^2F_{5/2}$) and point 3 (0.3598, 0.5857) is corresponding to the strong emission peak (547nm: $^2D_{3/2} \rightarrow {}^2F_{7/2}$). Point 2 (0.3379, 0.5943) is from our experimental (FS5 fluorescence spectrophotometer), that also is mixed by point 1 and point 3.

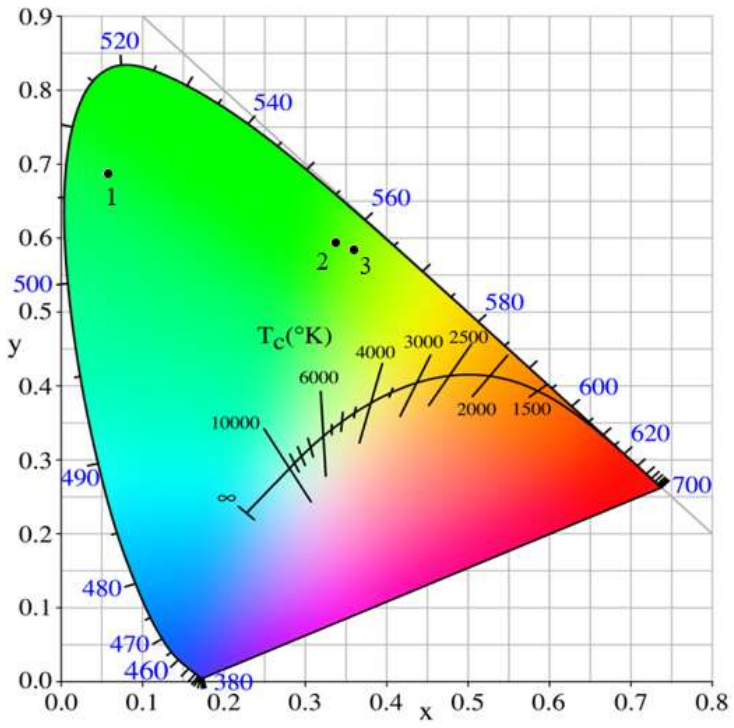

Figure 5-3: CIE chromaticity coordinates of the LuAG: Ce^{3+}

5.1.4 **Luminescence mechanism of LuAG: Ce^{3+}**

Figure 5-4 shows the energy level splitting of Ce^{3+} in LuAG host materials and mechanism of electronic transition. The excitation light is irradiated onto the sample, the energy of the photon of excitation lights be absorbed by outermost electronics of Ce^{3+} ions and transitions from ground state (4f) to excited state (5d), that is excitation process. Due to the spin of electrons, the ground state can be splitting into two different energy levels of $^2F_{7/2}$ and $^2F_{5/2}$, which are ground state. Due to the centroid shifting and crystal field effect, the excited state can be split into two excited state of $5d_1$ and $5d_2$, which are excited states. Due to the spin of electrons, excited state $5d_1$ can be split into two different energy levels of $^2D_{5/2}$ and $^2D_{3/2}$. Therefore, there have two different types of electron transition in the excitation process, one is from $^2F_{5/2}$ transition to $5d_2$, corresponding to 349nm excitation peak in the figure 5-1; the other is from $^2F_{5/2}$ transition to $5d_1$, corresponding to 450nm excitation peak in the figure 5-1.

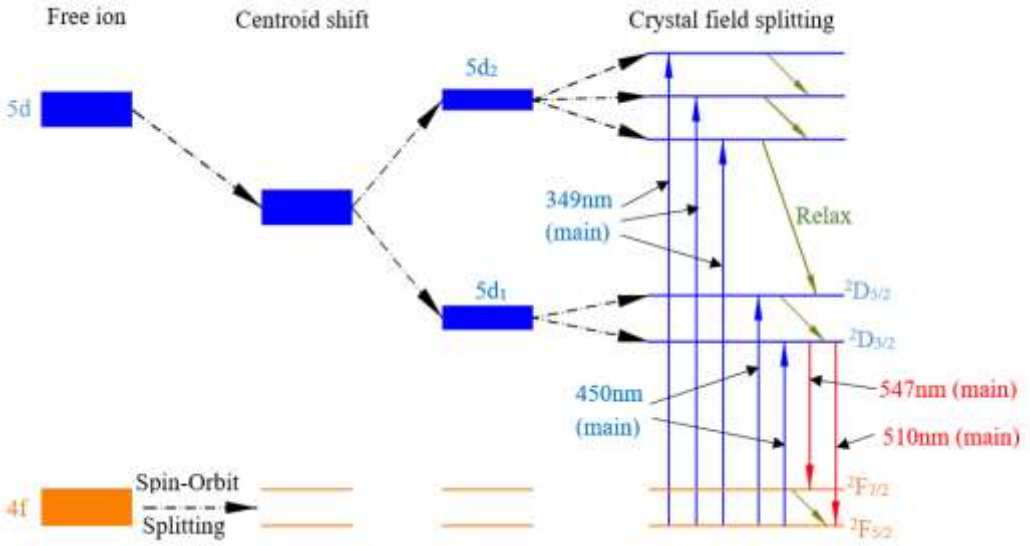

Figure 5-4: Luminescence mechanism of LuAG: Ce^{3+}

After excitation process, the electrons will return to the ground state because they could not stay at the high-energy level for a long time. For Ce^{3+} ions, the lowest level of excited state can be transition to ground state is $^2D_{3/2}$, thus, the electronics of $5d_2$ excited state should be transition to $5d_1$ excited state through the relaxation method, shown in figure 5-4. And then, the electronics will be transition from $^2D_{3/2}$ energy level to ground state ($^2F_{5/2}$ and $^2F_{7/2}$) and release the photon to consume the energy, that is emission process. Because of the ground state has two different energy levels of $^2F_{7/2}$ and $^2F_{5/2}$, and the band gap between $^2F_{7/2}$ energy level and $^2F_{5/2}$ energy level cannot be

ignored, so that the electronic transition of emission process should be show two different types. One is transition from $^2D_{3/2}$ to $^2F_{7/2}$, the other from $^2D_{3/2}$ to $^2F_{5/2}$, that is shown in figure 5-2.

5.2 Single crystal and polycrystalline YAG: Ce^{3+}

Yttrium aluminum garnet ($Y_3Al_5O_{12}$) doped with Ce^{3+} is a very important phosphor material because its scintillation properties [29, 30] it can efficiently convert the blue light-emitting diode radiation into a very broad yellow emission band [31, 32]. The comparison of the Excitation and emission spectrums of YAG: Ce^{3+} single crystal and YAG: Ce^{3+} wheel (powder) will presented in this part. YAG: Ce^{3+} single crystal and YAG: Ce^{3+} wheel have the same constituent elements and chemical formulas; however, those crystal structures are different. YAG: Ce^{3+} wheel is polycrystalline structure, but YAG: Ce^{3+} is single crystal. Therefore, the Excitation and emission spectrums should be a little bit difference at room temperature [33].

5.2.1 Polycrystalline YAG: Ce^{3+}

The D_2 site symmetry of the Ce^{3+} ion which substitutes for Y^{3+} in the YAG crystal splits the 5d excited state ^2D into five crystal-field levels [34]. Therefore, the electronic transition from 4f to 5d should be five different band energies and corresponding to five different excitation peaks at excitation spectrum. Those are approximate to 220 nm (45455 cm^{-1}), 261 nm (38314 cm^{-1}), 340 nm (29412 cm^{-1}), 372 nm (26882 cm^{-1}) and 460 nm (21739 cm^{-1}). In fact, the location of the 4f–5d bands (460 nm, 340 nm and 220 nm) can be observed by all studies, but for the other two (261 nm and 372 nm) could not observed in every study. In this work, the measured range of excitation spectrum was from 250 nm to 520 nm, thus only two peaks can be seen in excitation spectrum, shown in figure 5-5 (blue line). The excitation peaks of 343 nm and 454 nm can be attributed to electronic transition from ground state to excited state of different energy level, respectively. The broad emission band with a maximum wavelength of 541 nm and located in the range from 500 nm to700 nm (as shown in figure 5-5, red line), and this is ascribed to the electronic transition from 5d to 4f state of Ce^{3+} ions.

Figure 5-5 shows the Excitation and emission spectrums of YAG: Ce^{3+} polycrystalline that is normalized to maximum peak value, the blue line is corresponding to excitation spectrum and red line is corresponding to emission spectrum. The overlap is existed between excitation spectrum and emission spectrum,

the corresponding overlap range is approximately from 480nm to 530 nm. The overlap of excitation spectrum and emission spectrum is very important, owing to emission photons in this range can also excite electronics from ground state to excited state.

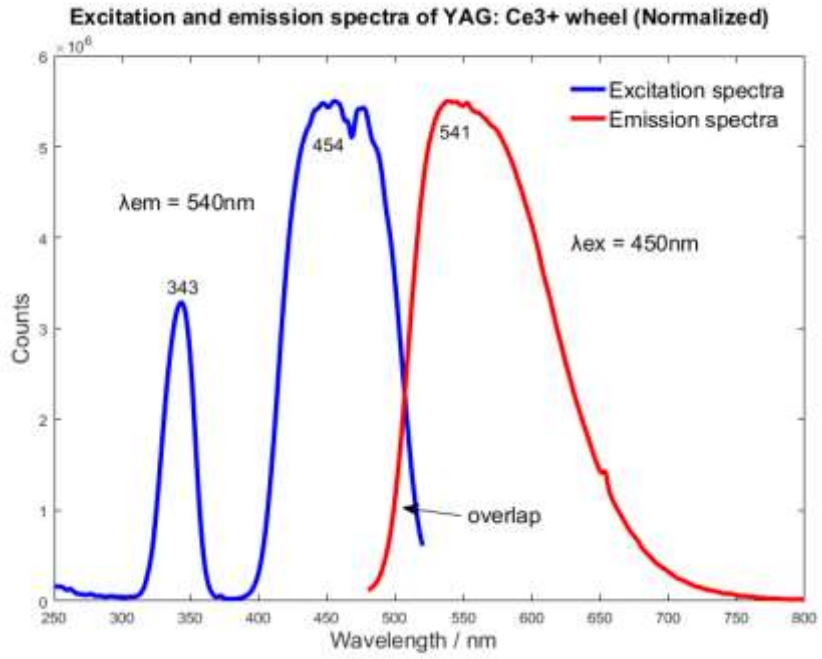

Figure 5-5: Excitation and emission spectrums of YAG: Ce^{3+} polycrystalline

5.2.2 **Excitation and emission spectrums of YAG: Ce^{3+} single crystal**

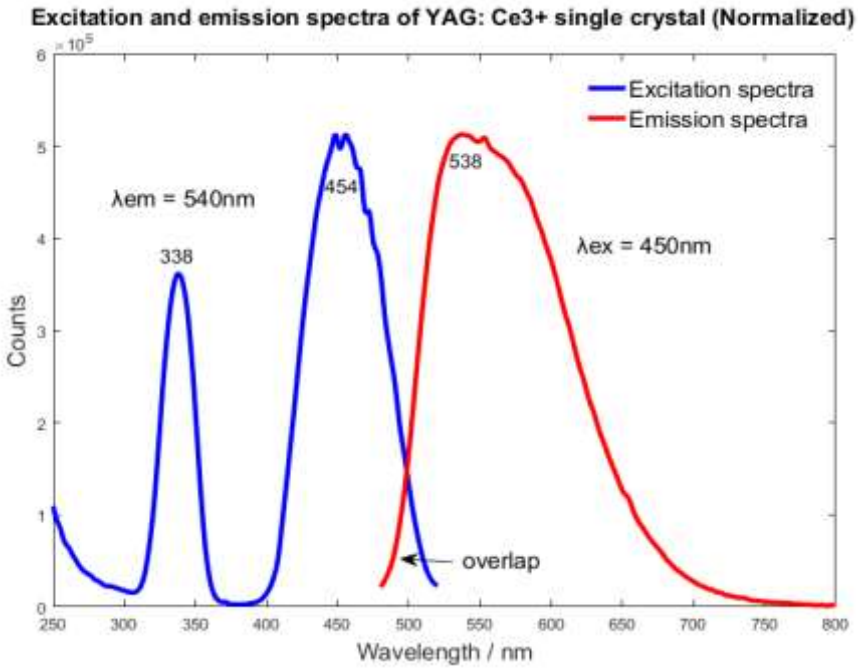

Figure 5-6: Excitation and emission spectrums of YAG: Ce^{3+} single crystal

Figure 5-6 shows the excitation and emission spectrums of YAG: Ce^{3+} single crystal, which is very similar as YAG: Ce^{3+} polycrystalline. Because of the phosphor materials is same only difference in crystal structure, thus the luminescence properties should be similar [35]. The differences between polycrystalline and single crystal are mainly reflected in the temperature characteristics, that will be discussed in the following part.

5.2.3 **Comparison of polycrystalline YAG: Ce^{3+} and single crystal YAG: Ce^{3+}**

The different of excitation and emission spectrums between the polycrystalline and single crystal of YAG: Ce^{3+} will be discussed in this part. Figure 5-7 shows the comparison of YAG: Ce^{3+} polycrystalline and YAG: Ce^{3+} single crystal, the blue line is corresponding to polycrystalline and red line is corresponding to single crystal; the dotted line is corresponding to excitation spectrum and solid line is corresponding to emission spectrum. The excitation peak of YAG: Ce^{3+} single crystal is higher than YAG: Ce^{3+} polycrystalline at the wavelength of ~340 nm, and sharper than that of YAG: Ce^{3+} polycrystalline at the wavelength of ~454 nm; The overlapped region between excitation spectrum and emission spectrum on YAG wheel is bigger than that of YAG single crystal.

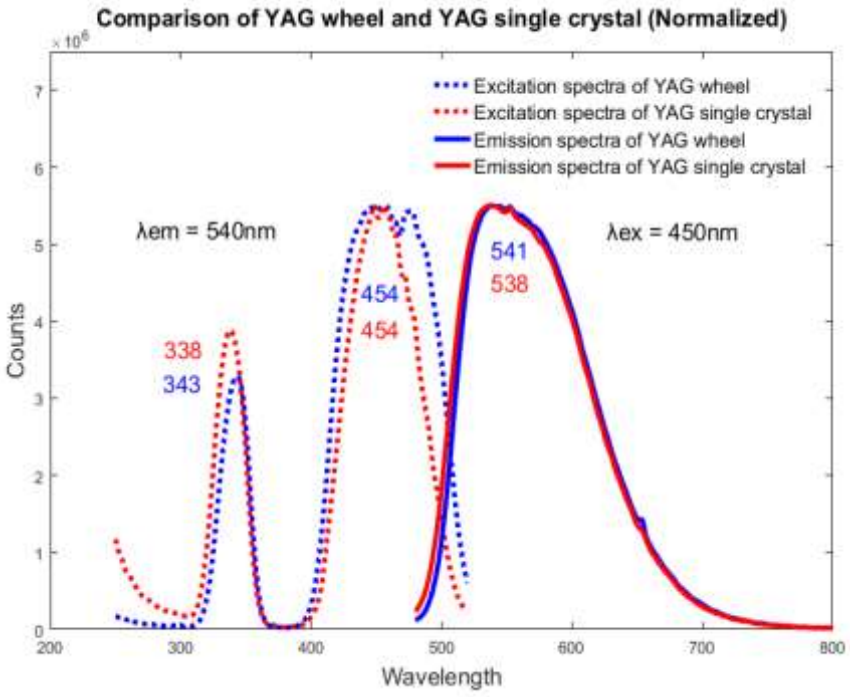

Figure 5-7: Comparison of YAG: Ce^{3+} single crystal and polycrystalline

The emission spectrum of YAG: Ce^{3+} polycrystalline and YAG: Ce^{3+} single crystal are similar, only 3 nm shift to upper wavelength on YAG: Ce^{3+} polycrystalline. This distinction can also be seen in the CIE (Commission International de l'Éclairage) chromaticity diagram, shown in figure 5-8. YAG: Ce^{3+} polycrystalline is closer to upper wavelength than YAG: Ce^{3+} single crystal. The CIE chromaticity coordinates value of YAG: Ce^{3+} single crystal is (0.4172, 0.5528) that is corresponding to point 2 at figure 5-8, The CIE chromaticity coordinates value of YAG: Ce^{3+} polycrystalline is (0.4271, 0.5508) that is corresponding to point 1 at figure 5-8 [36 - 42].

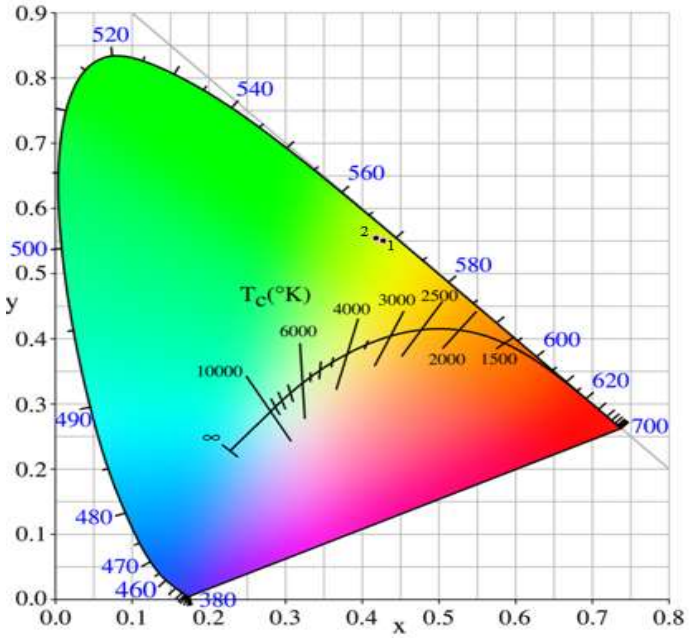

Figure 5-8: CIE chromaticity coordinates of the YAG: Ce^{3+} polycrystalline and single crystal

5.2.4 **Energy level diagram of Ce^{3+} in YAG host material**

Figure 5-9 shows the energy level splitting of Ce^{3+} in YAG host material. The Ce^{3+} free ions have a big band gap between the $4f^05d^1$ and $4f^15d^0$, when a Ce^{3+} ion is replaced in the YAG host crystal, two major effects result in the band gap: the centroid shift and crystal field splitting, overall these effects lead to a decrease in the energy difference between the $4f^05d^1$ and $4f^15d^0$ energy levels. Both of centroid shift and crystal field splitting processes greatly affect the $4f^05d^1$ electrons of the Ce^{3+} ion, whereas the well-shielded $4f^15d^0$ electrons are not strongly affected. Therefore, excitation state can be split into two main excited state, which are $5d_1$ and $5d_2$. Then, $5d_1$ excitation state can be split 2 different energy levels, that is $^2D_{5/2}$ and $^2D_{3/2}$ due to crystal field; and $5d_2$ excitation state also can be split into 3 different energy levels. The electronic transition

from 4f ground state to $5d_1$ excitation state is corresponding to 454 nm excitation peak shown in figure 5-7; the other electronic transition from 4f ground state to $5d_2$ excitation state is corresponding to 340 nm excitation peak shown in figure 5-7. The electronic cannot be stable in the excited state have the tendency to return to ground state. Electronic transition from $5d_2$ excited state to $5d_1$ excited state is nonradiative transition and the energy difference between $5d_2$ excited state and $5d_1$ excited state should as heat to transport surrounding the material. The electronic transition from $5d_1$ excited state to 4f ground state is radiative transition, releasing photons in this process. Because of the band gap between these two ground states $^2F_{7/2}$ and $^2F_{5/2}$ is very small, leading to only one emission peak in emission process.

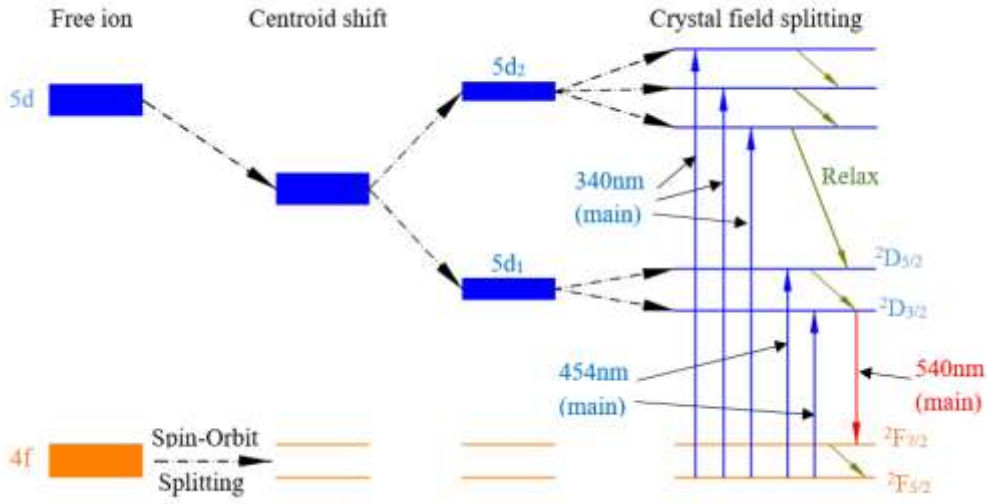

Figure 5-9: Energy level diagram of Ce^{3+} in YAG host material`

5.3 Single crystal GGAG: Ce^{3+} and GDYAG: Ce^{3+}

Two special samples contain gadolinium element which are GGAG: Ce^{3+} single crystal and GDYAG: Ce^{3+} single crystal. Due to the presence of gadolinium elements, the excitation and emission properties of the Ce^{3+} luminous center have changed significantly. The most obvious is that the excitation spectrum have three peaks at fixed emission wavelength. The new one excitation peak can be observed at around 275 nm, that is corresponding to electronic transition Gd^{3+} from ground state $^8S_{7/2}$ to excited state 6_I. Due to the participation of Gd^{3+}, the luminescence mechanism becomes more complicated.

5.3.1 **Excitation and emission spectrums of GGAG: Ce^{3+}**

Figure 5-10 shows the normalized Excitation and emission spectrums of GGAG: Ce^{3+}. The excitation spectrum was measured at the wavelength of 550 nm emission and the emission spectrum were measured at the wavelength of 450 nm excitation. The excitation spectrum has three peaks: 274 nm 341 nm and 441 nm, respectively. The weak peak around 274 nm are both observed on these samples. These are assigned to the electronic transition of Gd^{3+} ions from ground state $^8S_{7/2}$ to excited state 6_I which is in good agreement with the previous article, such as [43, 44]. 341 nm and 441 nm peaks should be assigned to the electronic transition of Ce^{3+} ions from ground state 4f to excited state $5d_1$ and $5d_2$, respectively.

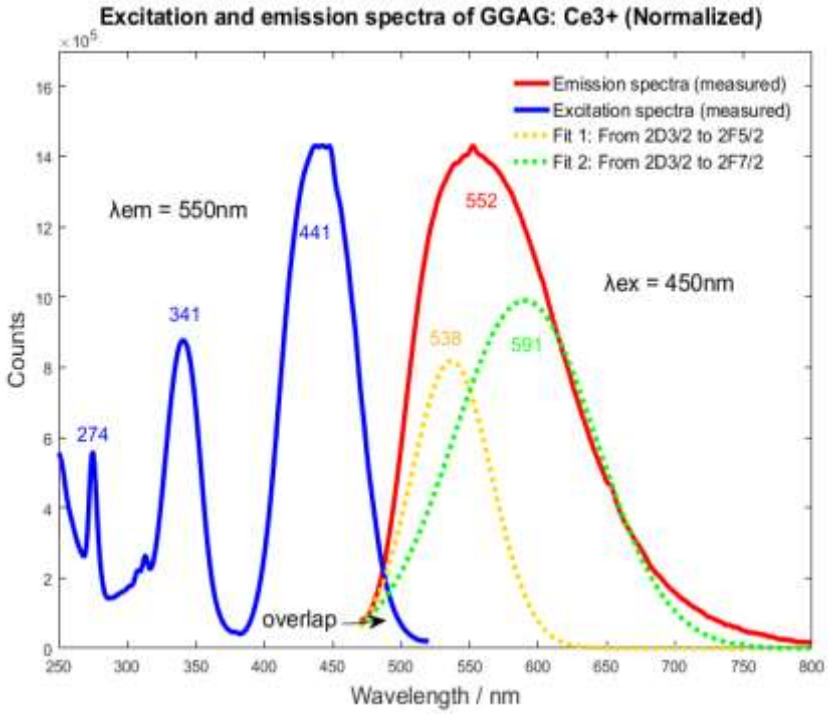

Figure 5-10: Excitation and emission spectrums of GGAG: Ce^{3+}

Because of the luminous center Ce^{3+} has two different ground states $^2F_{7/2}$ and $^2F_{5/2}$, leading to two different types of electronic transition in emission process. Therefore, the excitation spectrum of GGAG: Ce^{3+} can be split to two main emission peaks, which are in good agreement with the other articles [45]. In figure 5-10, the dotted line is corresponding to Gaussian fitting curve and the solid line is corresponding to measured curve. It is can be seen that the first fit curve (yellow dotted line) is correspond to transition from $^2D_{3/2}$ to $^2F_{7/2}$ (538 nm), the second fit curve (green dotted line) is correspond to transition from $^2D_{3/2}$ to $^2F_{5/2}$ (591 nm).

5.3.2 **Excitation and emission spectrums of GDYAG: Ce^{3+}**

Ce^{3+} doped $(Gd,Y)_3Al_5O_{12}$ single crystal phosphor is similar as Ce^{3+} doped $Gd_3Ga_3Al_2O_{12}$ single crystal phosphor at luminous properties. Figure 5-11 shows the normalized Excitation and emission spectrums of GDYAG: Ce^{3+} single crystal. The dotted line are Gaussian fitting results of GDYAG: Ce^{3+} emission spectrum, which is in good agreement with the GGAG: Ce^{3+} single crystal phosphor. Three excitation peak can be observed from 250 nm to 520 nm. A weak excitation around 275 nm peak was observed due to electronic transition of Gd^{3+} ions $^8S_{7/2} \rightarrow 6_I$, there have two excitation peaks around 339 nm and 457 nm, assigning to electronic transition of Ce^{3+} ions $4f \rightarrow 5d_1$ and $4f \rightarrow 5d_2$, respectively. Emission spectrum of GDYAG: Ce^{3+} also can be split into two mean emission bands, those are ~ 536 nm ($^2D_{3/2} \rightarrow {}^2F_{7/2}$) and ~ 586 nm ($^2D_{3/2} \rightarrow {}^2F_{5/2}$).

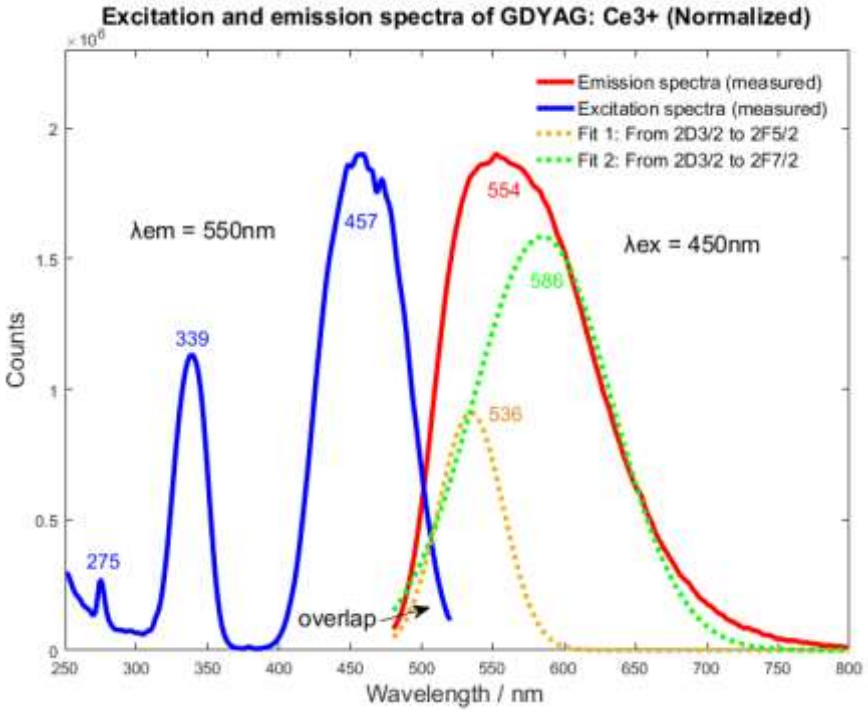

Figure 5-11: Excitation and emission spectrums of GDYAG: Ce^{3+}

5.3.3 **Electronic transition and energy transfer of Ce^{3+} and Gd^{3+} ions**

Gd^{3+} ions participate in the electronic transition during luminescence process of GGAG: Ce^{3+} and GDYAG: Ce^{3+} single crystal phosphor. Figure 5-12 shows the electronic transition of Ce^{3+} and Gd^{3+} ions in GGAG and GDYAG host materials. Gd^{3+} ions have three excited states, named 6_P, 6_I and 6_D, and one ground state on $^8S_{7/2}$. Because of the excited state 6_P of Gd^{3+} is very close to excited state $5d_2$ of Ce^{3+} ions,

thus the electronic transition from 6_P to $5d_2$ is prone to happen which belongs to relaxation phenomenon [46 - 50].

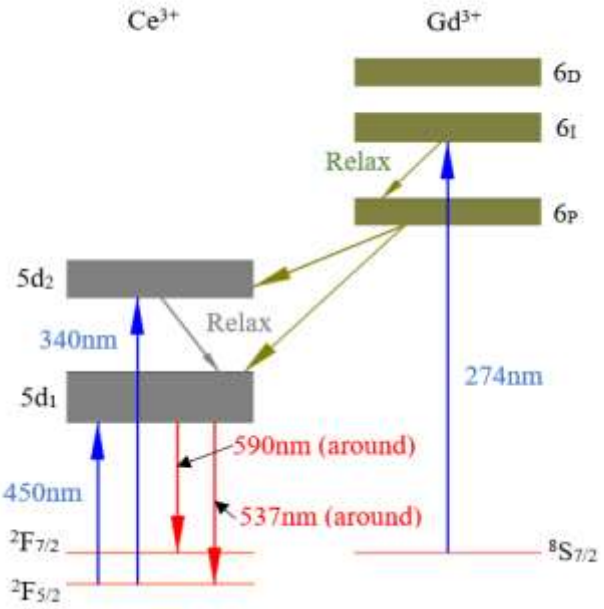

Figure 5-12: Electronic transition of Ce^{3+} and Gd^{3+} in GGAG and GDYAG host materials

5.4 Comparison of the five samples

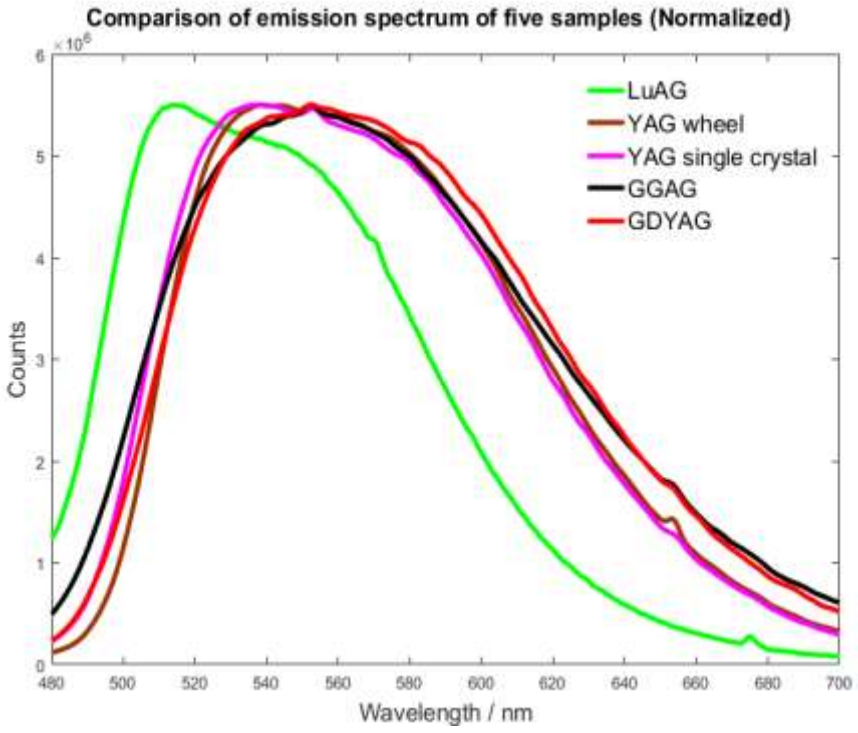

Figure 5-13: Comparison of emission spectrums of five samples

Figure 5-13 shows the comparison of emission spectrum of five samples. The emission band of LuAG: Ce^{3+} single crystal phosphor is much close to the shorter wavelength than the other four samples. It is mean that the LuAG: Ce^{3+} single crystal phosphor can be generated perfect green, and the other samples are very outstanding at orange and yellow regions. All the samples could not offer a good red part, but GDYAG: Ce^{3+} and GGAG: Ce^{3+} are better than YAG: Ce^{3+} single crystal and YAG: Ce^{3+} wheel at red part, LuAG: Ce^{3+} at red part is worst. Comparison of emission band of GGAG: Ce^{3+}, GDYAG: Ce^{3+}, YAG: Ce^{3+} single crystal and polycrystalline four samples, the emission peaks GGAG: Ce^{3+} and GDYAG: Ce^{3+} have a little bit shift (20 nm approximately) to upper wavelength when comparing with YAG: Ce^{3+} single crystal and polycrystalline [51].

Figure 5-14 shows the comparison of CIE chromaticity coordinates of five samples. The CIE chromaticity coordinates of these five samples are LuAG: Ce^{3+} (0.3379, 0.5943), YAG: Ce^{3+} single crystal (0.4172, 0.5528), YAG: Ce^{3+} polycrystalline (0.4271, 0.55), GGAG: Ce^{3+} (0.4232, 0.5408) and GDYAG: Ce^{3+} (0.4347, 0.5408), indicating that YAG: Ce^{3+} single crystal, YAG: Ce^{3+} polycrystalline, GGAG: Ce^{3+} and GDYAG: Ce^{3+} are much close to each other [52].

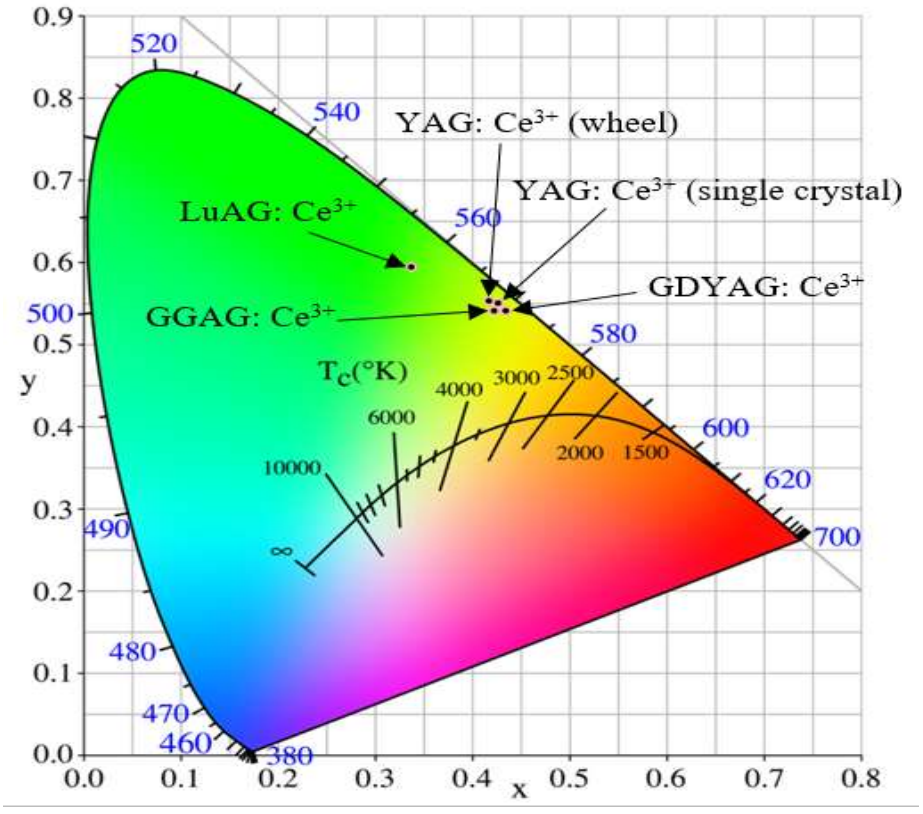

Figure 5-14: Comparison of CIE chromaticity of five samples

Chapter 6 Fluorescence lifetime and quantum efficiency results and discussions

Fluorescence lifetime is an important parameter to evaluate luminescence properties of luminescent materials. In this part, we use the FS-5 fluorescence spectrophotometer to measure the fluorescence lifetime of each samples, measurement method is called Time Correlated Single Photon Counting (TCSPC). This technique for fast single photon counting measurement can reach in the picosecond and nanosecond.

6.1 Fluoresence liftime

Figure 6-1 shows the fitting result of the LuAG: Ce^{3+} single crystal. The fitting function is equation 6-1, that is Exponential Tail Fit Analysis:

$$\text{Fit} = \text{A} + B_1 * e^{-t/\tau_1} + B_2 * e^{-t/\tau_2} + B_3 * e^{-t/\tau_3} + B_4 * e^{-t/\tau_4} \quad (6\text{-}1)$$

where, A is the calculated background; B_1, B_2, B_3 and B_4 are the calculated pre-exponential factor; τ_1, τ_2, τ_3 and τ_4 are containing the calculated lifetime; t is the time. As figure 6-1 shown, the fluorescence lifetime of LuAG: Ce^{3+} single crystal phosphor are 57.8 ns and 556.2 ns, the former named first lifetime and the latter is called second lifetime. In the figure 6-1, the Rel% states the intensity contribution of each of the exponential components to the overall fluorescence intensity, it can be calculated by equation 6-2.

$$\text{Rel\%} = \frac{\tau_i * B_i}{\sum \tau_i * B_i} * 100\% \quad (6\text{-}2)$$

And, χ^2 is the goodness of fit (or chi-squared), the value of the χ^2: for a good fit this should be close to unity.

	Fix	Value / ns	Std. Dev / ns		Fix	Value	Std. Dev	Rel %
τ_1	☐	57.8212	0.10777	B_1	☐	14649.261	33.1284	99.42
τ_2	☐	556.1926	150.34868	B_2	☐	8.858	1.8894	0.58
τ_3	☐			B_3	☐			
τ_4	☐			B_4	☐			
				A	☐	4.370		

χ^2 : 1.160

Figure 6-1: Fitting result of the LuAG: Ce^{3+} single crystal

The fluorescence lifetime curve of the LuAG: Ce^{3+} single crystal phosphor at room temperature is shown in figure 6-2, the black line is the measured curve and the red line is fitted curve. The decay is governed by first decay time 57.8 ns which intensity contribute to the overall fluorescence intensity is 99.42%. And the second lifetime is 556.2 ns which intensity contribute to the overall fluorescence intensity is very small, just 0.58%. The fitting residuals are shown in the bottom part of figure 6-2, indicating the fit quality is perfect.

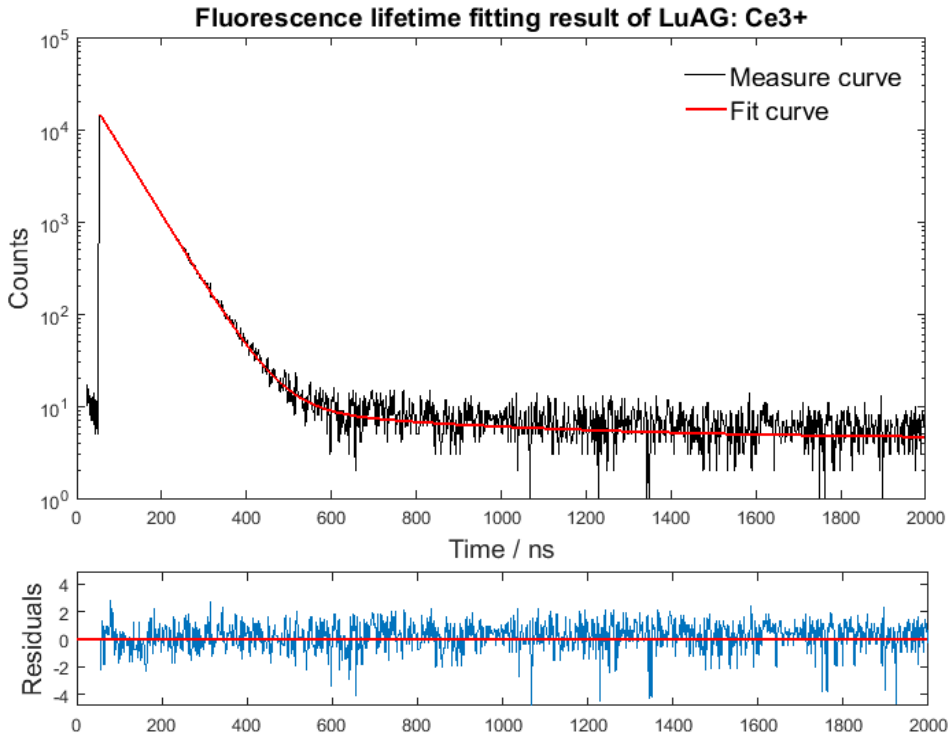

Figure 6-2: Fluorescence lifetime of the LuAG: Ce^{3+} at room temperature. Excitation wavelength, 450 nm; emission wavelength, 550 nm.

Table 6-1 shows the fluorescence lifetime of five samples, it contains the first lifetime, second lifetime and average lifetime. We can use the equation 6-3 to calculate the average lifetime.

$$\tau_{ave} = \sum \tau_i * a_i \tag{6-3}$$

where, τ_{ave} is average lifetime; τ_i is the first lifetime, second lifetime and so on; a_i is the intensity contribution of each of the lifetime to the overall fluorescence intensity. For example, the average lifetime of LuAG: Ce^{3+} is equal to 57.8*99.42%+556.2*0.58% = 60.7 ns. In the table 6-1, the intensity contribution to the overall fluorescence intensity of second lifetime of LuAG: Ce^{3+}, YAG: Ce^{3+} (wheel), YAG: Ce^{3+} (single crystal) and GDYAG: Ce^{3+} are less than 1%, which can be ignored. Only the intensity contribution

to the overall fluorescence intensity of second lifetime of GGAG: Ce^{3+} is higher and can be reached 19%.

Comparison of average lifetime of this five samples, the average lifetime of LuAG: Ce^{3+} and GGAG: Ce^{3+} are very closely around 61 ns. And the other three samples (YAG: Ce^{3+} (wheel), YAG: Ce^{3+} (single crystal) and GDYAG: Ce^{3+}) are very closely around 67 ns.

Table 6-1 Fluorescence lifetime of five samples

Samples	First lifetime		Second lifetime		Average lifetime
	Decay time	Rel%	Decay time	Rel%	
LuAG: Ce^{3+}	57.8 ns	99.42%	556.2 ns	0.58%	60.7 ns
YAG: Ce^{3+} (wheel)	64.0 ns	99.10%	303.1 ns	0.90%	66.2 ns
YAG: Ce^{3+} (single crystal)	64.4 ns	99.37%	513.1 ns	0.63%	67.2 ns
GGAG: Ce^{3+}	56.0 ns	80.75%	83.06 ns	19.25%	61.2 ns
GDYAG: Ce^{3+}	64.7 ns	99.47%	447.3 ns	0.53%	66.7 ns

6.2 Quantum efficiency

Laser emitted from laser device is consists of two different wavelengths. The strong one is around 447 nm and the weaker one is around 456 nm, the intensity of strong laser is three times than that the weaker laser. Therefore, a single wavelength laser with a wavelength of 450 nm was used in the experiments [53].

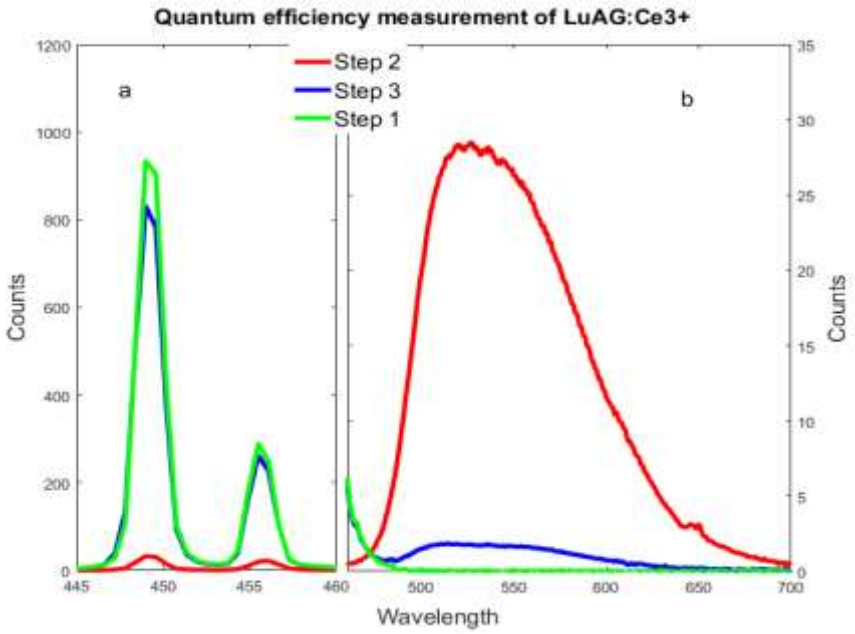

Figure 6-3: Quantum efficiency measurement of LuAG: Ce^{3+} single crystal phosphor.

The measurement process of LuAG: Ce^{3+} as an example is shown in figure 6-3. Note: there have two different vertical axes, from 0 to 1200 is for figure 6-3 (a); from 0 to 35 is for figure 6-3 (b). The green line is step 1 measure reference (excitation) result; red line is measure emission spectrum result, that include the directly and indirectly (re-excitation); blue line is measure re-excited emission spectrum result.

The quantum efficiency was measured under different power of lasers using the previously described method. We measured quantum efficiency at 1W, 2W, 3W, 4W and 5W lasers, and table 6-2 shows the measure results.

Table 6-2 Quantum efficiency measurement results

Samples	1W		2W		3W		4W		5W	
	IQE	EQE	IQE	EQE	IQE	EQE	IQE	EQE	IQE	EQE
LuAG	1.03	1.01	0.96	0.85	0.93	0.85	0.86	0.73	0.82	0.64
GDYAG	0.97	0.76	0.94	0.76	0.98	0.73	Dead	Dead	Dead	Dead
YAG (SC)	0.67	0.55	0.74	0.56	0.71	0.55	Dead	Dead	Dead	Dead
YAG(wheel)	1.09	0.92	1.04	0.87	Dead	Dead	Dead	Dead	Dead	Dead
GGAG	0.81	0.73	Dead	Dead	Dead	Dead	Dead	Dead	Dead	Dead

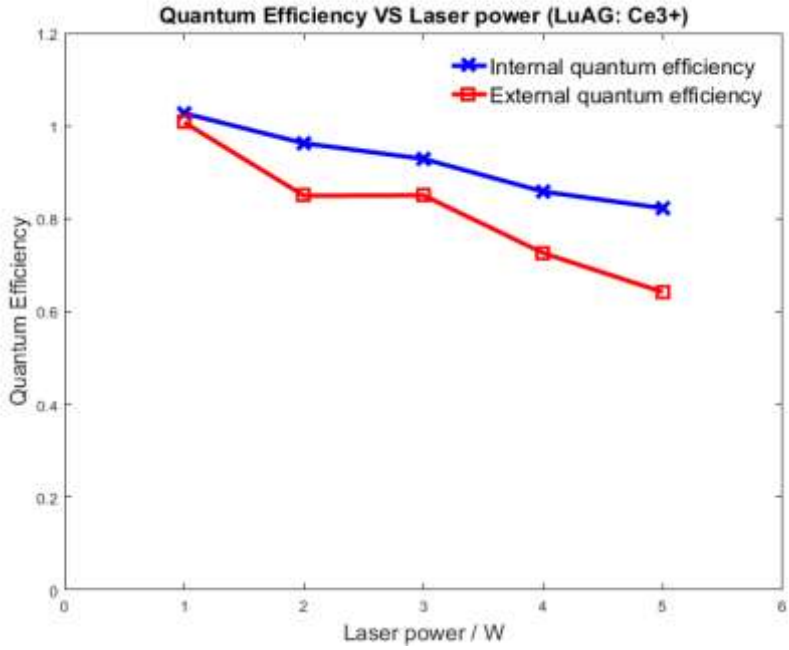

Figure 6-4: The relationship between quantum efficiency and laser power of LuAG: Ce^{3+}

Table 6-2 is shown the IQE (internal quantum efficiency) and EQE (external quantum efficiency) measurement result. YAG (SC) is short for YAG single crystal,

“Dead” means that the sample could not emit spectrum at certain powers. LuAG: Ce^{3+} single crystal can be work at 4W and 5W, GGAG: Ce^{3+} is dead at 2W, YAG wheel is dead at 3W, GDYAG: Ce^{3+} and YAG: Ce^{3+} single crystal are dead at 4W. Due to the shortcomings of the measurement system itself thus the measurement results are not very accurate and 10 present error should to consider [54]. Therefore, it can explain that the LuAG: Ce^{3+} quantum efficiency at 1W and YAG wheel internal quantum efficiency 1W, 2W are more than 1.

The relationship between quantum efficiency and laser power of LuAG: Ce^{3+} single crystal phosphor are shown in figure 6-4, indicating the quantum efficiency is decreased as the function of the increase laser power, and the external quantum efficiency is less than that of the internal quantum efficiency [55].

Chapter 7 Temperature change results and discussions

In this part, we will change the samples temperature to check the effect of luminescence with temperature. In this experimental, we use the Metal Ceramic Heater Element, 24 W (HT24S) to heating our samples, and use the FS-5 fluorescence spectrophotometer to check the Excitation and emission spectrums at different temperature.

7.1 Excitation and emission spectrums

In this experiment of temperature control, we should check two point, first one is effect of temperature on Excitation and emission spectrums; and the other one is effect of temperature on lifetime. Therefore, in this part, I will show the result of effect of temperature on Excitation and emission spectrums.

7.1.1 Single crystal LuAG: Ce^{3+}

The Excitation and emission spectrums of LuAG: Ce^{3+} at different temperature are shown in figure 7-1, where the excitation spectrum is shown in figure 7-1 (a), and the emission spectrum is shown in figure 7-1 (b). From the excitation spectrum (figure 7-1 a), we can find that when the temperature increases, the spectrum width at the two excitation peaks of LuAG: Ce^{3+} expand, and the peaks shift to shorter wavelengths; from figure 7-1 (b), we can find that there are two variations in the emission spectrum as the temperature rises: the changes in luminous wavelength (shift to longer wavelength) and luminous intensity. For the changes in luminous wavelength, when the temperature is increased from room temperature to 350 ℃, the emission peak shifts from 515 nm to 545 nm. For the changes in luminous intensity, the emission intensity increases firstly, and then it decreases [56]. The emission intensity reaches to the highest value at 100 degree, where the increment is lower than approximately one percentage.

The red shift and the changes in emission intensity can be found from figure 7-2 (a) and (b), respectively. Figure 7-2 (a) shows the CIE (Commission International de l'Éclairage) chromaticity coordinates of the emission spectrum at different temperature. The specific coordinate values are listed as follows: (0.3504, 0.5863) at 25 ℃, (0.3611,

0.5849) at 100 ℃, (0.3675, 0.5827) at 150 ℃, (0.3757, 0.5791) at 200 ℃, (0.3817, 0.5756) at 250 ℃, (0.388, 0.5715) at 300 ℃, and (0.3927, 0.5682) at 350 ℃. Figure 7-2 (b) shows the relationship between the normalized emission intensity and temperature. The red line represents the heating process and the blue line represents the cooling process. The emission intensity rises below 100 ℃

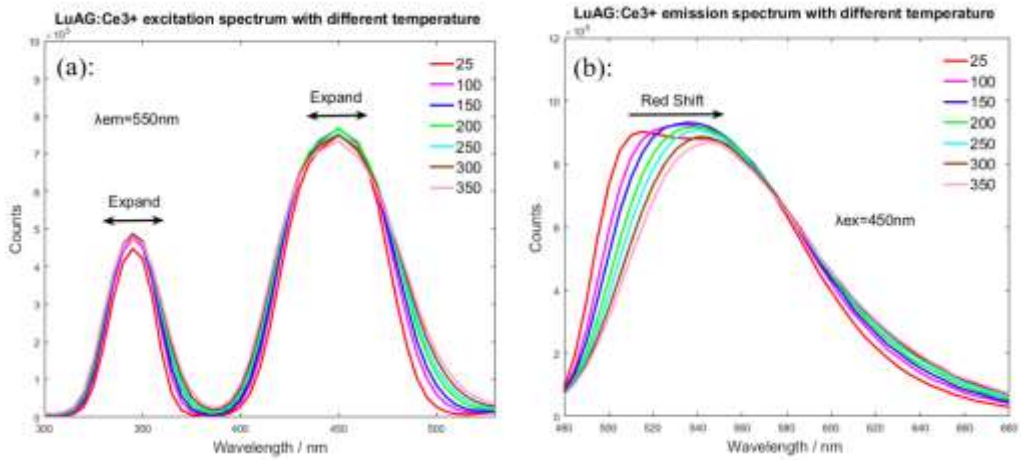

Figure 7-1: Excitation and emission spectrums of LuAG: Ce^{3+} at different temperatures

When the temperature is higher than 100 ℃, the emission intensity decreases slowly, and it decreases 6% at 350 ℃ [57]. The emission intensity of the heating process and the cooling process at same temperature is almost equal, which means that there is no hysteresis between the heating and cooling processes.

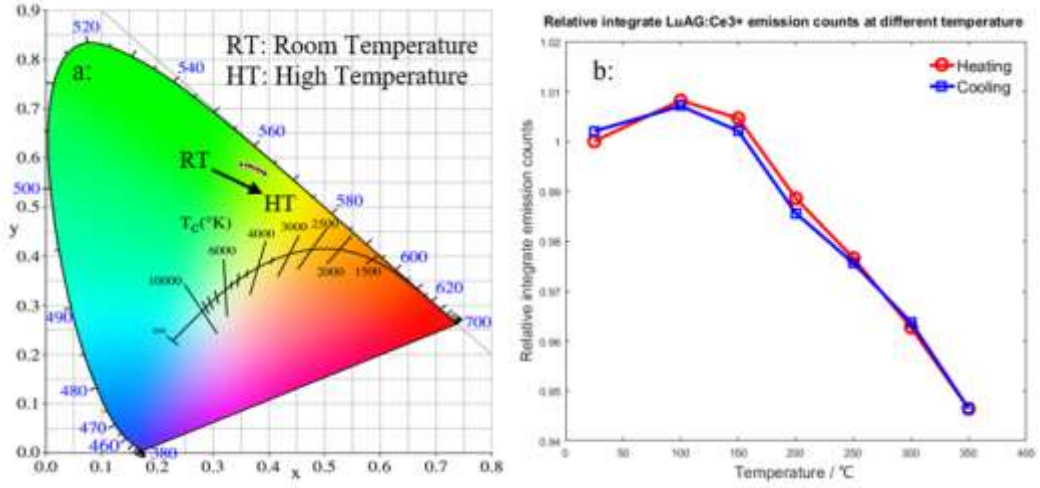

Figure 7-2: CIE chromaticity coordinates and relative emission intensity of LuAG: Ce^{3+}

7.1.2 **Single crystal GGAG: Ce^{3+}**

Excitation and emission spectrums of GGAG: Ce^{3+} are shown in figure 7-3. From figure 7-3 (a), we can find that the excitation and emission peaks of GGAG: Ce^{3+} drop rapidly with temperature increase, where when the temperature is above 200 degree centigrade, the emission peak is almost disappeared. Figure 7-3 (b) shows the normalized result, we can find that the emission peaks shift to longer wavelength (red shift) with temperature increase, where of the maximum shift is ~15 nm.

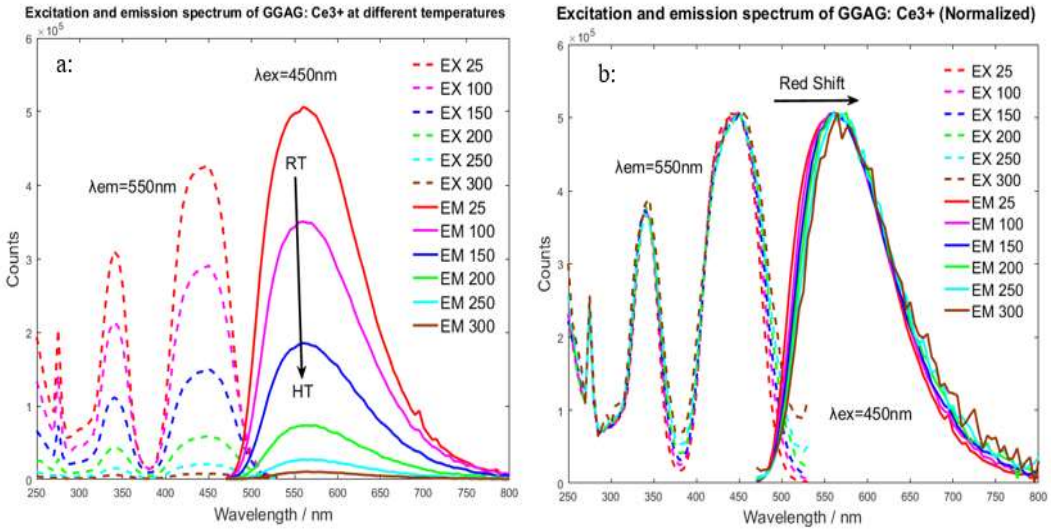

Figure 7-3: Excitation and emission spectrums of GGAG: Ce^{3+} at different temperature

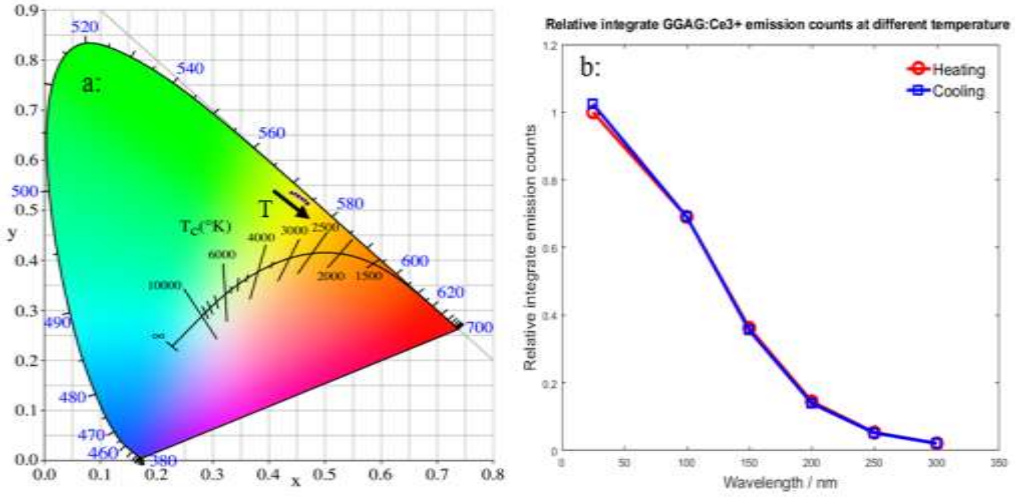

Figure 7-4: CIE chromaticity coordinates and relative emission intensity of GGAG: Ce^{3+}

Figure 7-4 shows the CIE chromaticity coordinates and the relative emission intensity of GGAG: Ce^{3+}. The variation of the output color with temperature is shown

in figure 7-4 (a), the CIE coordinate values are: (0.4418, 0.5349) at 25 ℃, (0.4481, 0.5315) at 100 ℃, (0.4535, 0.5279) at 150 ℃, (0.46, 0.523) at 200 ℃, (0.4656, 0.5181) at 250 ℃ and (0.4689, 0.5128) at 300 ℃. The relative emission intensity of GGAG: Ce^{3+} is shown in figure 7-4 (b), the red line represents the heating process and the blue line represents the cooling process. The heating process and the cooling process are almost overlapping, and we can also find that the trend of emission intensity change is monotonous decline and very fast [58].

7.1.3 **Single crystal GDYAG: Ce^{3+}**

Excitation and emission spectrums of GDYAG: Ce^{3+} at different temperature are shown in figure 7-5. From figure 7-5 (a) we can find that the excitation and emission peaks of GDYAG: Ce^{3+} decrease with temperature increase [59]. The emission spectrum at room temperature and 100 degree very good coincide, that means in the temperature range from 25 to 100 degree the emission intensity not decrease. After 100 degree, the emission intensity begins to drop. Compared with room temperature, when the temperature increased to 350 degree the emission intensity decreased to 20%.

Figure 7-5 (b) shows the normalized results of emission spectrum at different temperature, the red shift with temperature. The amount of shift approximately is 15 nm. At the red part (the wavelength from 680 nm to 800 nm), the emission intensity has a little bit increase.

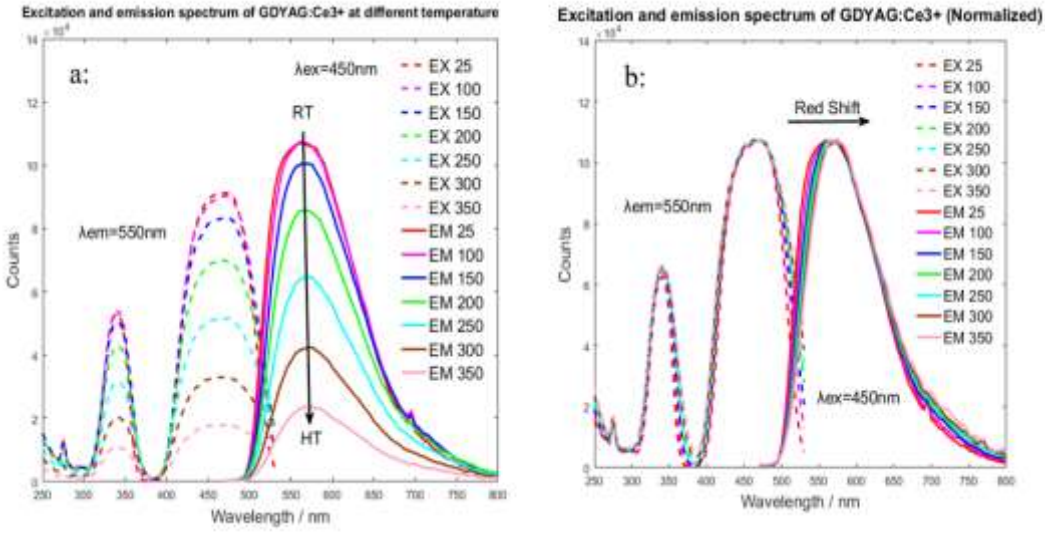

Figure 7-5: Excitation and emission spectrums of GDYAG: Ce^{3+} at different temperature

CIE chromaticity coordinates and the relative emission intensity of GDYAG: Ce^{3+} are shown in figure 7-6. The change of emission output color with temperature is shown in figure 7-6 (a), the CIE chromaticity coordinates at different temperature are: (0.4589, 0.5285) at 25 ℃, (0.4641, 0.5245) at 100 ℃, (0.4705, 0.5193) at 150 ℃, (0.4749, 0.5154) at 200 ℃, (0.479, 0.5117) at 250 ℃, (0.4823, 0.5085) at 300 ℃ and (0.4861, 0.5046) at 350 ℃. The relationship between the relative emission intensity and temperature is show on figure 7-6 (b), the red line represents the heating process and the blue line represents the cooling process [60]. The emission intensity of heating process is same as cooling process, thus there is no hysteresis phenomenon. After 150 degree, the trend of decrease is very linear.

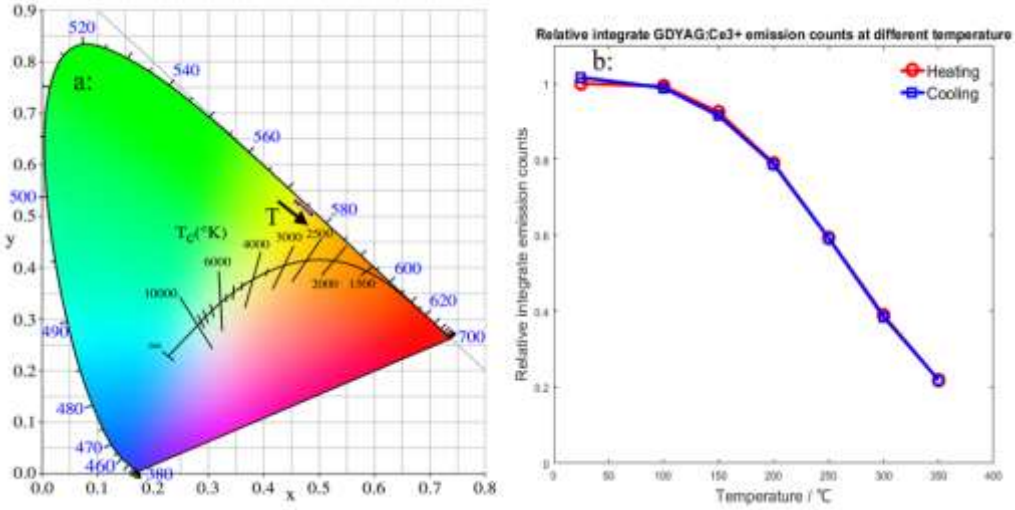

Figure 7-6: CIE chromaticity coordinates and relative emission intensity of GDYAG: Ce^{3+}

7.1.4 **Single crystal YAG: Ce^{3+}**

The excitation and emission spectrums of YAG: Ce^{3+} single crystal at different temperature are shown in figure 7-7. Form figure 7-7 (a) we can find that the excitation and emission spectrums decrease with temperature increase, the emission spectrum is not drop when the temperature increase from room temperature to 150 degree. When the temperature is above 200 degree centigrade, the emission intensity has been dropped, but the rate of drop is not very fast. When the temperature increased to 350 degree, the emission spectrum decreased to half. Figure 7-7 (b) shows the normalized results, it is good way to shows the red shift of emission spectrum. The excitation spectrum is not shift (or very small shift) with temperature increase, and the emission spectrum has 15

nm (approximately) red shift with temperature increase. At the red part (the wavelength from 680 nm to 800 nm), the emission intensity has a little bit increase [61].

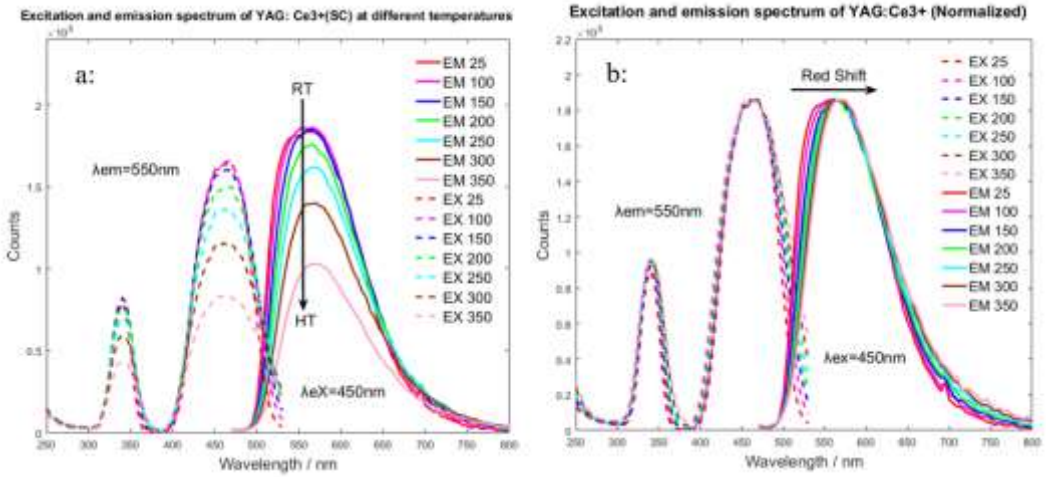

Figure 7-7: Excitation and emission spectrums of YAG: Ce^{3+} single crystal at different temperature

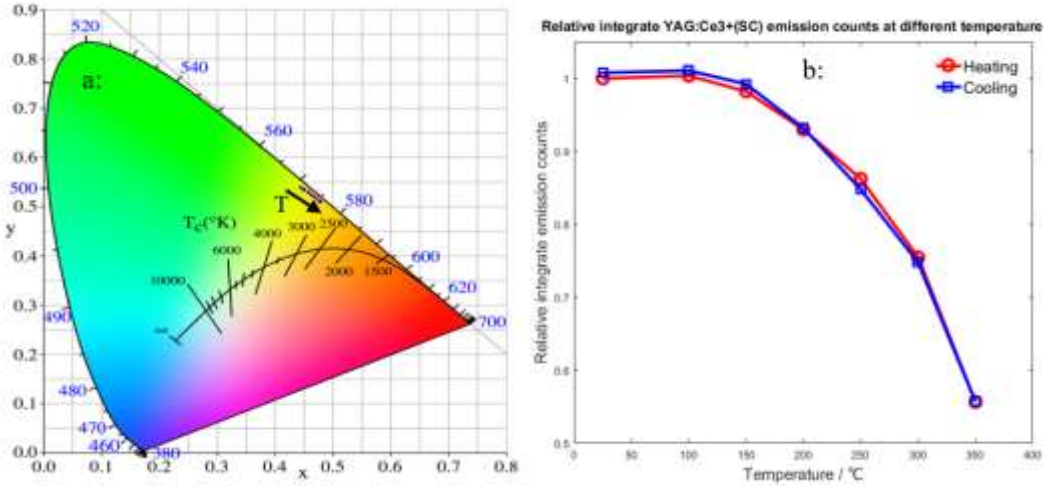

Figure 7-8: CIE chromaticity coordinates and relative emission intensity of YAG: Ce^{3+} single crystal

CIE chromaticity coordinates and the relationship between the relative emission intensity and temperature of YAG: Ce^{3+} single crystal is shown in figure 7-8. The change of emission output color with temperature is shown in figure 7-8 (a), the CIE chromaticity coordinates at different temperature are: (0.4454, 0.5383) at 25 ℃, (0.4507, 0.5346) at 100 ℃, (0.4581, 0.5289) at 150 ℃, (0.4637, 0.5243) at 200 ℃, (0.4692, 0.5195) at 250 ℃, (0.4742, 0.515) at 300 ℃ and (0.4793, 0.5101) at 350 ℃. The relationship between the relative emission intensity and temperature is shown in figure 7-8 (b), the red line represents the heating process and the blue line represents

the cooling process. After 150 degree, the rate of emission intensity drop is increase with temperature.

7.1.5 **Polycrystalline YAG: Ce^{3+}**

Figure 7-9 shows the excitation and emission spectrums of YAG: Ce^{3+} polycrystalline at different temperature. From figure 7-9 (a) we can found the emission spectrum rise and fall with temperature increase, the trend of emission spectrum can be divided into rise stage and fall stage. The rise stage is from room temperature to 150 degree, and the fall stage can be observed from 150 degree to 350 degree. The normalized of excitation and emission spectrums are shown on figure 7-9 (b), the excitation spectrum almost not change, the emission spectrum has 15nm (approximately) red shift. At the red part (the wavelength from 680 nm to 800 nm), the emission intensity has a little bit increase.

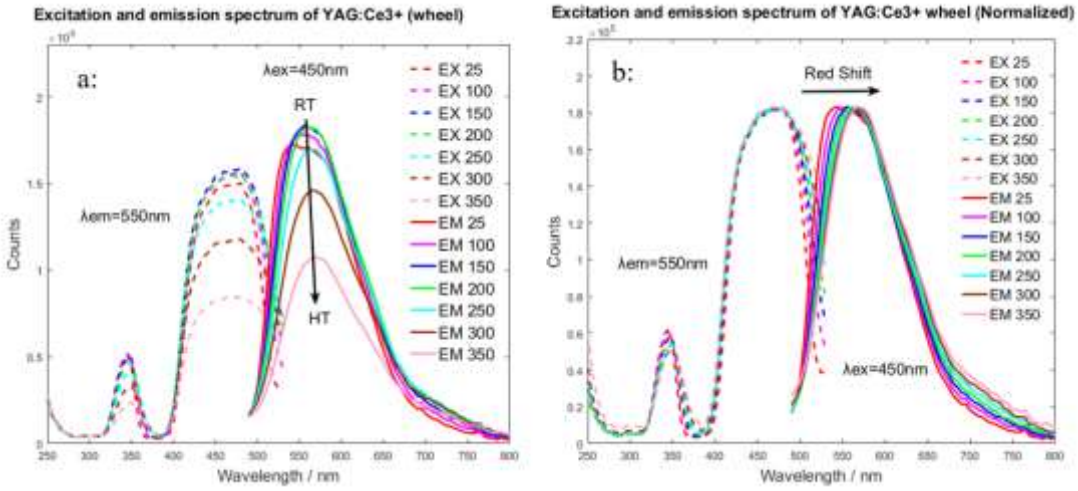

Figure 7-9: Excitation and emission spectrums of YAG: Ce^{3+} polycrystalline at different temperature

CIE chromaticity coordinates and the relationship between the relative emission intensity and temperature of YAG: Ce^{3+} polycrystalline is shown in figure 7-10. The change of emission output color with temperature is shown in figure 7-10 (a), and the CIE chromaticity coordinates at different temperature are: (0.4355, 0.5449) at 25 ℃, (0.4428, 0.5394) at 100 ℃, (0.4498, 0.5339) at 150 ℃, (0.4559, 0.5287) at 200 ℃, (0.4612, 0.5238) at 250 ℃, (0.4655, 0.5194) at 300 ℃ and (0.4682, 0.516) at 350 ℃. The relationship between the relative emission intensity and temperature is shown in figure 7-10 (b), the red line represents the heating process and the blue line represents the cooling process. At here, the emission relative emission intensity of heating process

and cooling process has a little bit different, that is error from measurement produce. After 200 degree, the rate of emission intensity drop is very fast [62].

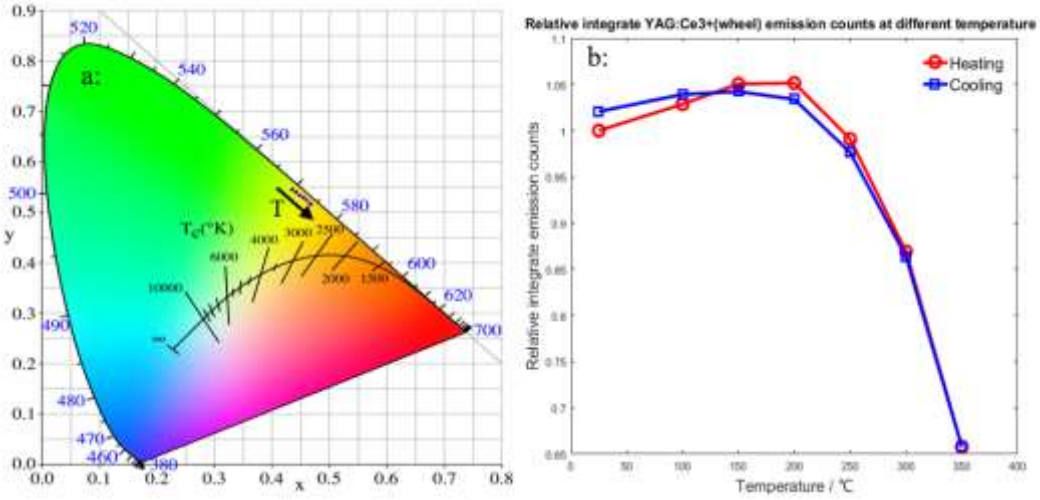

Figure 7-10: CIE chromaticity coordinates and relative emission intensity of YAG: Ce^{3+} polycrystalline

7.1.6 **Comparison the five samples**

Figure 7-11 shows the relative emission intensity for the five samples at different temperature. We can find that LuAG: Ce^{3+} single crystal has the best performance, where the change of emission intensity with temperature is smallest. Therefore, the LuAG: Ce^{3+} single crystal can work at high temperature and have the best thermal stability [63].

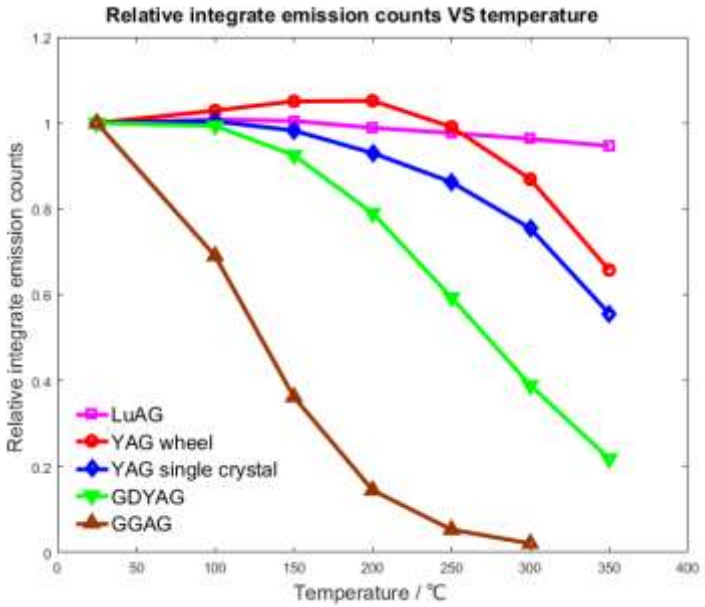

Figure 7-11: Comparison of relative emission intensity of five samples at different temperature

The thermal stability of GGAG: Ce^{3+} single crystal is worst; the thermal stability of GDYAG: Ce^{3+} single crystal is also not good, but it's better than the GGAG: Ce^{3+} single crystal. The thermal stability of YAG: Ce^{3+} is much better than GDYAG: Ce^{3+} and GGAG: Ce^{3+}, and it is worse than LuAG: Ce^{3+}. Comparison of YAG: Ce^{3+} single crystal and polycrystalline [64], the polycrystalline is better than single crystal. Only YAG: Ce^{3+} polycrystalline can be seen clearly that relative emission intensity is rise with temperature increase (from room temperature to 200 degree).

7.2 Fluorescence lifetime

When we finish the experiment of effect of temperature on Excitation and emission spectrums, we should check the effect of temperature on fluorescence lifetime. Thus, in this part, I will show the result of effect of temperature on fluorescence lifetime.

7.2.1 Single crystal LuAG: Ce^{3+}

Fluorescence lifetime measurement results of LuAG: Ce^{3+} single crystal at different temperature is shown in figure 7-12 (a), and the comparison results of relative emission intensity and fluorescence lifetime at same temperature is shown in figure 7-12 (b). In figure 7-12 (b), the red line represents the change of fluorescence lifetime with temperature, and the label is shown on the right axis; the blue line represents the trend of relative emission intensity with temperature, and the label is shown on left axis [65]. We can find that the fluorescence lifetime rises slowly with the temperature increase, which is opposite to the trend of relative emission intensity changes with temperature.

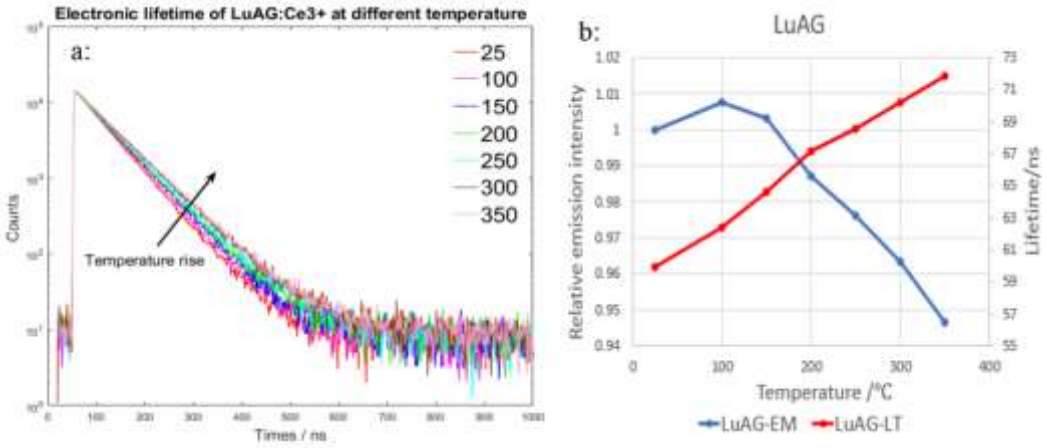

Figure 7-12: (a), Fluorescence lifetime measurement results of LuAG: Ce^{3+} single crystal at different temperature. (b), Comparison of relative emission intensity and fluorescence lifetime at same temperature.

7.2.2 **Polycrystalline YAG: Ce^{3+}**

Figure 7-13 shows the fluorescence lifetime measurement results of YAG: Ce^{3+} polycrystalline at different temperature, and comparison results of relative emission intensity and fluorescence lifetime at same temperature [66]. From figure 7-13 (b) we can found the trend of fluorescence lifetime with temperature is same as the trend of relative emission intensity change with temperature increase. Before 250 degree, the change of fluorescence lifetime not evident; after 250 degree, the fluorescence lifetime start to drop (obviously).

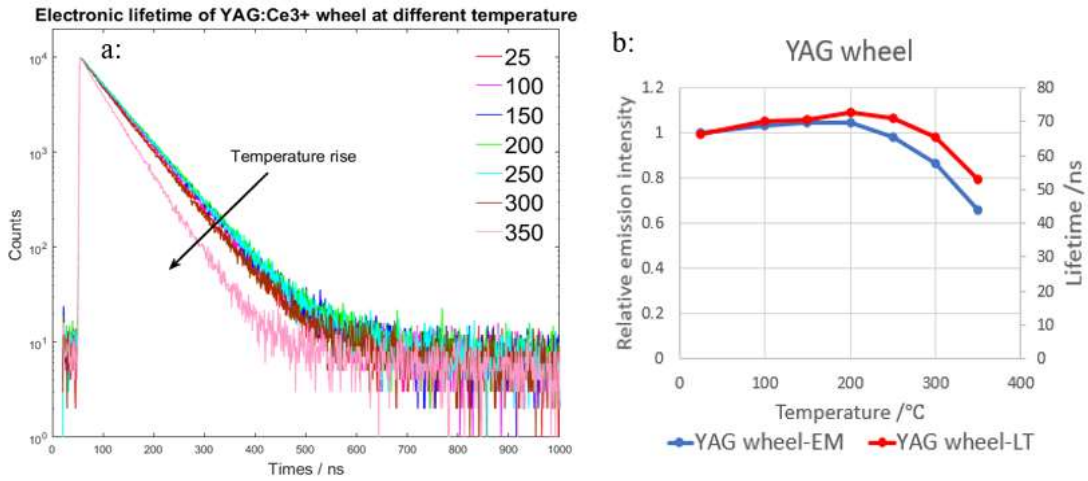

Figure 7-13: (a), Fluorescence lifetime measurement results of YAG: Ce^{3+} polycrystalline at different temperature. (b), Comparison of relative emission intensity and fluorescence lifetime at same temperature.

7.2.3 **Single crystal YAG: Ce^{3+}**

Fluorescence lifetime measurement results of YAG: Ce^{3+} single crystal at different temperature is shown in figure 7-14 (a), and the comparison results of relative emission intensity and fluorescence lifetime at same temperature is shown in figure 7-14 (b). The fluorescence lifetime of YAG: Ce^{3+} single crystal is very stable from room temperature to 300 degree, around 68 ns. When the temperature is higher than 300 degrees [67], the fluorescence lifetime of a sharp decline. The trend of fluorescence lifetime change with temperature and the trend of relative emission intensity change with temperature are generally similar [68].

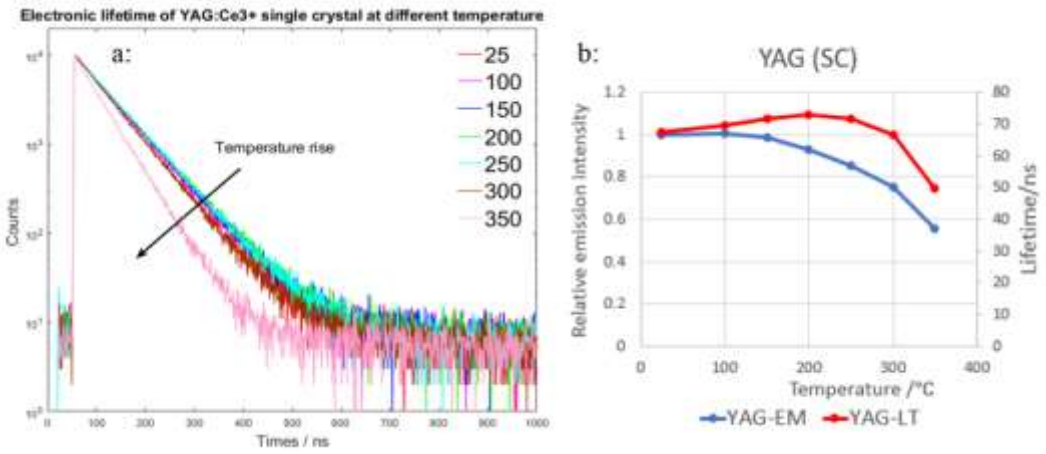

Figure 7-14: (a), Fluorescence lifetime measurement results of YAG: Ce^{3+} single crystal at different temperature. (b), Comparison of relative emission intensity and fluorescence lifetime at same temperature.

7.2.4 **Single crystal GDYAG: Ce^{3+}**

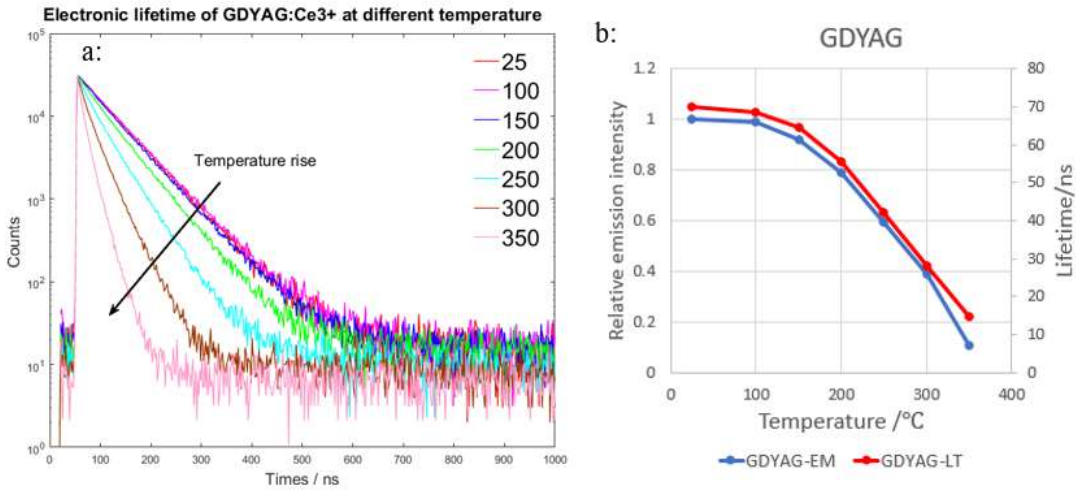

Figure 7-15: (a), Fluorescence lifetime measurement results of GDYAG: Ce^{3+} single crystal at different temperature. (b), Comparison of relative emission intensity and fluorescence lifetime at same temperature.

Figure 7-15 (a) shows the fluorescence lifetime measurement results of GDYAG: Ce^{3+} single crystal at different temperature, and figure 7-15 (b) shows the comparison results of relative emission intensity and fluorescence lifetime at same temperature [69.70]. From the graph of fluorescence lifetime measurement results, the fluorescence lifetimes at room temperature, 100 degree and 150 degree are very close. However, above the 150 degree, the fluorescence lifetime decreases linearly with increasing

temperature, the trend of fluorescence lifetime change with temperature is same as the trend of relative emission intensity change with temperature [71].

7.2.5 **Single crystal GGAG: Ce^{3+}**

Figure 7-16 (a) shows the fluorescence lifetime measurement results of GGAG: Ce^{3+} single crystal at different temperature, and figure 7-16 (b) shows the comparison results of the relative emission intensity and fluorescence lifetime at same temperature. The descent speed of the GGAG: Ce^{3+} single crystal fluorescence lifetime with temperature is very fast, that is very consistent with the trend of relative emission intensity change with temperature increase [72].

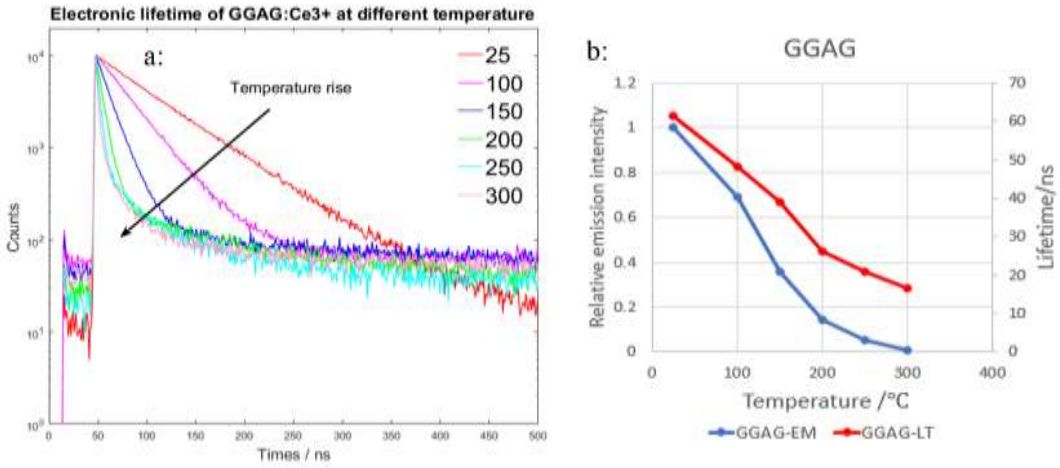

Figure 7-16: (a), Fluorescence lifetime measurement results of GGAG: Ce^{3+} single crystal at different temperature. (b), Comparison of relative emission intensity and fluorescence lifetime at same temperature.

7.2.6 **Comparison of fluorescence lifetime of the five samples at different temperatures**

Figure 7-17 shows the comparison of the fluorescence lifetime for the five samples at different temperature. We can find that the fluorescence lifetimes of the YAG: Ce^{3+} single crystal and the YAG: Ce^{3+} polycrystalline are close at same temperature [73,74]. It indicates that the fluorescence lifetime depends on the material composition and is not related to the crystal type. Because the amount of the fluorescence lifetime rise with temperature increase is not big, thus the trend of fluorescence lifetime with temperature be horizontal.

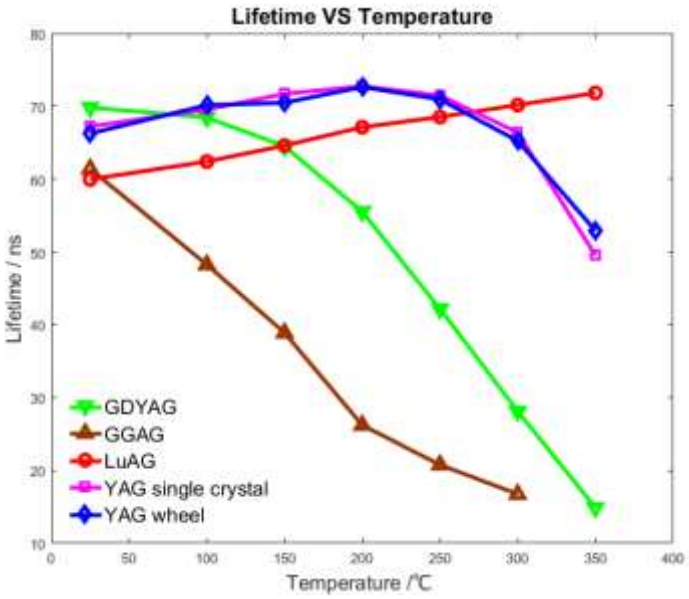

Figure 7-17: Comparison of fluorescence lifetime of five samples at different temperature

7.3 Theoritical analysis based on Mott–Seitz mechanism

In the previous two sections, I focused on the effects of temperature changes on the luminescent properties of the samples incoulding emission peak shift and thermal quenching. In this section, the reasons for these changes will be given by Mott–Seitz mechanism configurational coordinate diagram.

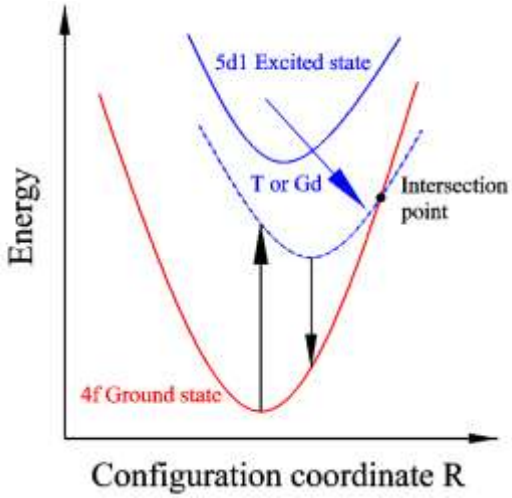

Figure 7-18: Configuration coordinate diagram of Ce^{3+} center. The influence of increased temperature and Gd element addition on the position of $5d_1$ excited state parabolas and that of conduction band is marked.

Figure 7-18 show the configuration coordinate diagram of Ce^{3+} center. The influence of temperature increase [75] is treated as the influence of Gd element addition

[76] on the position of $5d_1$ excited state. We can find that the $5d_1$ excited state position moving in the direction close to 4f ground state with the increase of the working temperature or Gd element addition in the sample. Therefore, the parabolas of $5d_1$ excited state and 4f ground state has an intersection point when the working temperature is enough to high. The meaning of the intersection point is the 5d1 excited state and 4f ground state are equal. In this case, the excitation process cannot occur, which is the reason of thermal quenching. The addition of Gd elements can exacerbate this effect, and reducing the quenching temperature.

Chapter 8 Conclusion

In this work, we have characterized Ce doped single crystals as the stationary phosphor candidates used for blue laser excited projector. The excitation and emission spectrums and the life time of the single crystal phosphor are characterized by the FS5 fluorescence spectrophotometer; the quantum efficiency is measured by the integrating sphere and the blue laser device (without heatsink). According to the measurement results, we can draw the following conclusions:

- The specific effect of temperature on quantum efficiency: when the temperature is less than a special value, the quantum efficiency increases with increasing temperature; however, when the temperature is greater than this special value, the quantum efficiency decreases with increasing temperature. This special value is called “Quenching Temperature”. Before reaching to this special value, the increase in quantum efficiency is very gentle, but when the temperature is higher than this special value, the quantum efficiency decreases very rapidly.
- The existence of Gd element reduces significantly the quenching temperature. This means that the phosphor containing the Gd element cannot be used under high power lasers.
- Compared with the polycrystalline phosphors, the quenching temperature for Ce doped single crystal phosphors is higher.

The ideal geometry and design of the Ce doped single crystals can serve as potential phosphor candidates in high-power blue diode laser driven projectors.

Bibliography

[1]:http://velvetchainsaw.com/2012/05/23/your-senses-your-raw-information-learning 06,02,2017.

[2]: Ann Holms, March 7, 2005, An Introduction to the Cathode-Ray Tube.

[3]: Ankita Tyagi, Dr. S. Chatterjee, Liquid Crystal Display: Environment & Technology, International Journal of Environmental Engineering Science and Technology Research, Vol. 1, No. 7, July 2013, PP: 110-123, ISSN: 2326-3113 (Online)

[4]: NEC Technologies Visual Systems Division, Technology White Paper Plasma Displays, May 1998.

[5]: Rıdvan KARAPINAR, Electro-optic Response of a Polymer Dispersed Liquid Crystal Film, 02.06.1997

[6]: Bernard Geffroy, Philippe le Roy, Review Organic light-emitting diode (OLED) technology: materials, devices and display technologies, 2006 Society of Chemical Industry.

[7]: Alexander A. Kuznetzov, Sergey B. Lee, Mei Zhang, Electron field emission from transparent multiwalled carbon nanotube sheets for inverted field emission displays, CARBON 48 (2010) p41 – p4 6.

[8]: Kishore V. Chellappan, Erdem Erden, and Hakan Urey, Laser-based displays: a review, 4 August 2010.

[9]: http://www.tech-faq.com/how-lcd-projectors-work.html.

[10]: Matthew S. Brennesholtz, Projection Displays Second Edition, 2008.

[11]:https://www.christiedigital.com/emea/cinema/cinema-products/digital-cinema-projectors/Christie-CP42LH-3DLP-RGB-Digital-Cinema-Laser-Projector

[12]: Tommy Penner, February 1, 2013, Display Tech: Home Projectors.

[13]: http://vdcds.com/vdc-display-systems-vdcds/

[14]: Geoffrey Morrison • Posted: Dec 30, 2012, Review: ViewSonic Pro9000 LED/Laser Hybrid Projector.

[15]: Shionoya,S.,Yen,W.,Phosphor Handbook,CRC Press,Boca Raton,(1999)

[16]: Werts, M.H.V. Science Progress,88,(2),101–131,(2005)

[17]: J. Reichman, Handbook of Optical Filters for Fluorescence Microscopy (Chroma Technology, Brattleboro, 2010).

[18]: J.S. Kim, E.S. Oh, J.C. Choi, M. Lee, J.H. Bahng, H.L. Park, T.W. Kim, Int. J. Inorg. Mater. 3, 183 (2001)

[19]: M.-G. Ko, J.-C. Park, D.-K. Kim, S.-H. Byeon, J. Lumin. 104, 215 (2003)

[20]: M. Leskela, L. Niinisto, Mater. Chem. Phys. 31, 7 (1992).

[21]: Sony's OLED display (2005), p. 1.

[22]: B. Henderson, G.F. Imbusch, Optical Spectroscopy of Inorganic Solids (Oxford University Press, Oxford, 1989), p. 645.

[23]: O.J. Rubio. J. Phys. Chem. Solids. 52(1), 101 (1991)

[24]: P. Dorenbos, (2000). "The 5d level positions of the trivalent lanthanides in inorganic compounds." J. Lumin. 91:155-176.

[25]: https://www.cnet.com/news/why-lasers-are-the-future-of-projectors/.

[26]: P. Goldberg, Luminescence of Inorganic Solids (Academy Press, New York, 1966), p. 765.

[27]: E. Nakazawa, S. Shionoya, J. Phys. Soc. Jpn. 28, 1260 (1970).

[28]: V. V. N. Ravi Kishore, K. L. Narasimhan and N. Periasamy, On the radiative lifetime, quantum yield and fluorescence decay of Alq in thin films, Phys. Chem. Chem. Phys., 2003, 5, 1386–1391.

[29]: Yanagida T, Takahashi H, Ito T, Kasama D, Enoto T, Sato M, Hirakuri S, Kokobun M, Makishima K, Yanagitani T, Yagi H, Shigeta T and Ito T 2005 IEEE Trans. Nucl. Sci. 52 1836

[30]: Ludziejewski T, Moszy´ nski M, Kapusta M, WolskiD, Klamra W and Moszy´ nska K 1997 Nucl. Instrum. Methods Phys. Res. A 398 287

[31]: Mita Y, Kobayashi T, Miyamoto Y, Ishii O and Sawanobori N 2004 Phys. Status Solidi b 241 2672.

[32]: Haranath D, Chander H, Sharma P and Singh S 2006 Appl. Phys. Lett. 89 173118

[33]: StelianArjoca, EncarnaciónGVíllora, DaisukeInomata, Temperature dependence of Ce:YAG single-crystal phosphors for high-brightness white LEDs/LDs, Mater.Res.Express2(2015)055503.

[34]: Peter A Tanner, Lianshe Fu, Lixin Ning, Bing-Ming Cheng and Mikhail G Brik: Soft synthesis and vacuum ultraviolet spectrum of YAG: Ce^{3+} nanocrystals: reassignment of $Ce3^{+}$ energy levels. J. Phys.: Condens. Matter 19 (2007) 216213 (14pp).

[35]: J Chen, T C Lu, Y Xu, A G Xu, D Q Chen, Ab initio study of a charged vacancy in yttrium aluminum garnet (Y 3 Al 5 O 12), J. Phys.: Condens. Matter 20 (2008) 325212 (6pp).

[36]: L. Xiao, X. Cheng, and J. Xu, ‘‘High-Power Nd:YAG Planar Wave-guide Laser with YAG and Al_2O_3 Claddings,’’ Opt. Commun., 281 [14] 3781–5 (2008).

[37]: Yu. Zorenko, V. Gorbenko, I. Konstankevych, A. Voloshinovskii, G. Stryganyuk, V. Mikhailin, V. Kolobanov, D. Spassky, Single-crystalline films of Ce-doped YAG and LuAG phosphors: advantages over bulk crystals analogues, Journal of Luminescence 114 (2005) 85–94.

[38]: Du Yong, Shao Chong-Yun, Dong Yong-Jun, Yang Qiu-Hong, Hua Wei, Spectrum investigation of *S*, Ce:YAG (*S*: Pr^{3+}, Eu^{3+}, Gd^{3+}) single crystals and their applications in white LEDs. Chin. Phys. B Vol. 24, No. 11 (2015) 117801.

[39]: Ji-Guang Li and Yoshio Sakka, Recent progress in advanced optical materials based on gadolinium aluminate garnet ($Gd_3Al_5O_{12}$). Sci. Technol. Adv. Mater. 16 (2015) 014902 (18pp).

[40]: Ran Huang, Sai Li, Shaolin Xue, Zhixing Jiang, Shuxian Wu, Preparation and Characterization of YAG: Ce^{3+} Phosphors by Sol-solvothermal Process. IPCBEE vol.28(2012) © (2012) IACSIT Press, Singapoore.

[41]: Lili Wang, Lin Mei, Gang He, Jiangtao Li, Lihua Xu, Preparation of Ce:YAG Glass-Ceramics with Low SiO_2. J. Am. Ceram. Soc., 94 [11] 3800–3803 (2011).

[42]: Yung-Tang Nien, Improved Photoluminescence of $Y_3Al_5O_{12}$: Ce Nanoparticles by Silica Coating. J. Am. Ceram. Soc., 93 [6] 1688–1691 (2010).

[43] Joanna M. Ogiegło, Arturas Katelnikovas, Luminescence and Luminescence Quenching in $Gd_3(Ga,Al)_5O_{12}$ Scintillators Doped with Ce^{3+}, American Chemical Society, 2013, 117, 2479−2484.

[44] Mohit Tyagi, Fang Meng, Merry Koschan, Samuel B Donnald, Effect of codoping on scintillation and optical properties of a Ce-doped $Gd_3Ga_3Al_2O_{12}$ scintillator, 31 October 2013 46 (2013) 475302.

[45] Joanna Iwanowska, Lukasz Swiderski, Tomasz Szczesniak, Performance of cerium-doped $Gd_3Al_2Ga_3O_{12}$ (GAGG:Ce) scintillator in gamma-ray spectrometry， Nuclear Instruments and Methods in Physics Research A 712 (2013) 34–40。

[46]: Kei Kamada, Takayuki Yanagida, Jan Pejchal, Martin Nikl, Takanori Endo, Kousuke Tsutsumi, Yutaka Fujimoto, Akihiro Fukabori, and Akira Yoshikawa, Crystal

Growth and Scintillation Properties of Ce Doped $Gd_3(Ga, Al)_5O_{12}$ Single Crystals, IEEE TRANSACTIONS ON NUCLEAR SCIENCE, VOL. 59, NO. 5, OCTOBER 2012.

[47]: N. J. Cherepy, S. A. Payne, B. W. Sturm, J. D. Kuntz, Z. M. Seeley, B. L. Rupert, R. D. Sanner, O. B. Drury, T. A. Hurst, S. E. Fisher, M. Groza, L.Matei, A.Burger, R.Hawrami, K.S.Shah, and L.A.Boatner, "Comparative gamma spectroscopy with SrI2(Eu), GYGAG(Ce) and bi-loaded plastic scintillators," in Proc. IEEE Nucl. Sci. Symp. Conf. Rec., 2010, pp. 1288–1291.

[48]: O. B. Drury, N. J. Cherepy, T. A. Hurst, and S. A. Payne, "Garnet scintillator-based devices for gamma-ray spectroscopy," in Proc. IEEE Nucl. Sci. Symp. Conf. Rec., 2009, vol. 1–5, pp. 1585–1587.

[49]: M. Korzhik, A. Federov, A. Annenkov, A. Borissevitch, A. Dosso- vitski, O. Missevitch, and P. Lecoq, "Development of scintillator materials for PET scanners," Nucl. Instr. Meth. A, vol. 571, pp. 122–125, Jan. 2007.

[50]: J. Glodo, W. W. Moses, W. M. Higgins, E. V. D. van Loef, P. Wong, S. E. Derenzo, M. J. Weber, and K. S. Shah, "Effects of Ce concentration on scintillation properties of LaBr3:Ce," IEEE Trans. Nucl. Sci, vol. 52, no. 5, pp. 1805–1808, May 2005.

[51]: Nikl M, Mihokova E, Mares J A, Vedda A, Martini A, Nejezchleb K and Blazek K 2000 Phys. Status Solidi b 181 R10.

[52]: Zorenko Y, Gorbenko V, Konstankevych I, Grinev B and Globus M 2002 Nucl. Instrum. Methods A 486 309.

[53]: Mares A, Beitlerova A, Nikl M, Solovieva N, D'Ambrosio C, Blazek K, Maly P, Nejezchleb K and de Notaristefani F 2004 Radiat. Meas. 38 353.

[54]: Dujardin C, Mancini C, Amans D, Ledoux G, Abler D, Auffray E, Lecoq, Perrodin D, Petrosyan A and Ovanesyan K L 2010 J. Appl. Phys. 108 013510.

[55]: Nikl M 2005 Phys. Status Solidi a 202 201

[56]: Takagi K and Fukazawa T 1983 Appl. Phys. Lett. 42 43

[57]: Wu P and Pelton A D 1992 J. Alloys Compounds 179 259

[58]: Manabe T and Egashira K 1971 Mater. Res. Bull. 6 1167

[59]: Yanagida T, Ito T, Takahashi H, Sato M, Enoto T, Kokubun M, Makishima K, Yanagitani T, Yagi H and Shigeta T 2007 Nucl. Instrum. Methods A 579 23

[60]: Cherepy N J et al 2009 IEEE Trans. Nucl. Sci. 56 873.

[61]: F. Meng, M. Koschan, S. B. Donnald, Yuntao Wu, C. L. Melcher, “Suppression of YAG phase formation in YAP:Ce pellets”, Nuclear Science Symposium and Medical Imaging Conference (NSS/MIC), 2014 IEEE.

[62]: A. T. R. Williams, S. A. Winfield and J. N. Miller, Relative fluorescence quantum yields using a computer controlled luminescence spectrometer, Analyst, 1983, 108, 1067.

[63]: S. Dhami, A. J. de Mello, G. Rumbles, S. M. Bishop, D. Phillips and A. Beeby, Phthalocyanine fluorescence at high concentration: dimers or reabsorption effect Photochem. Photobiol, 1995, 61, 341.

[64]: W. Ahn, J. H. Park, and Y. J. Kim, “Synthesis, Phase Formation and Luminescence of $(Sr,Ba)_3MgSi_2O_8$: Eu^{2+} by a Sol-Gel-Combustion Hybrid Process,” Ceram. Inter., 41S744-49 (2015).

[65]: A. A. Setlur and A. M. Srivastava, “On the Relationship between Emission Color and Ce^{3+} Concentration in Garnet Phosphors,” Opt. Mater., 29 [12] 1647-52 (2007).

[66]: Feldmann, C., Jüstel, T., Ronda, C.R. and Schmidt, P.J. (2003) Inorganic Luminescent Materials: 100 Years of Research and Application. Advanced Functional Materials, 13, 511-516.

[67]: Ivanovskikh, K.V., Ogieglo, J.M., Zych, A., Ronda, C.R. and Meijerink, A. (2012) Luminescence Temperature Quenching for Ce^{3+} and Pr^{3+} d-f Emission in YAG and LuAG. ECS Journal of Solid State Science and Technology.

[68]: Yan, B., You, J.-P., Tran, N.T. and Shi, F.G. (2013) Influence of Phosphor Configuration on Thermal Performance of High Power White LED Array. 2013 IEEE International Symposium on Advanced Packaging Materials, Irvine, 27 February 2013-1 March 2013, 274-289.

[69]: M. Nikl, J. Pejchal, E. Mihokova, J. A. Mares, H. Ogino, A. Yoshikawa, T. Fukuda, A. Vedda and C. D'Ambrosio „Antisite defect-free $Lu_3(GaAl)_5O_{12}$: Pr scintillator, Appl. Phys. Lett. 88 (2005) 141916.

[70]: M. Nikl, A. Vedda, M. Fasoli, I. Fontana, V. V. Laguta, E. Mihokova, J. Pejchal, J. Rosa, and K. Nejezchleb, “Shallow traps and radiative recombination processes in $Lu_3Al_5O_{12}$: Ce single crystal scintillator”, Physical Review B 76 (2007)195121.

[71]: L. Wen, X. Sun, Z. Xiu, S. Chen, C-T. Tsai, “Synthesis of nano crystalline yttria powder and fabrication of transparent YAG ceramics” Journal of the European Ceramic Society. Vol. 24, no. 9, pp. 2681-2688. Aug. 2004.

[72]: Chung K et al 2005 A computer program for the deconvolution of thermos luminescence glow curves Radiat. Prot. Dosim. 115 343–9.

[73]: Tyagi M, Rothfuss H, Donnald S B, Koschan M and Melcher C L 2013 Effect of Ca 2+ co-doping on the scintillation kinetics of Ce doped Gd 3 Ga 3 Al 2 O 12 IEEE Trans. Nucl. Sci. doi:10.1109/TNS.2013.2276101.

[74]: Tyagi M et al 2013 Effect of doping on the temperature dependence of Gd_2SiO_5: Ce photoluminescence IEEE Trans. Nucl. Sci. 60 973.

[75]: S Arjoca, D. Inomata, Y. Matsushita, and K. Shimamura, "Growth and optical properties of $(Y1{-}xGdx)_3Al_5O_{12}$: Ce^{3+} single crystal phosphors for high-brightness neutral white LEDs and LDs," CrystEngComm 18, 4799-4806 (2016).

[76]: K Kamada, T Yanagida, J Pejchal, "Scintillator-oriented combinatorial search in Ce-doped $(Y,Gd)_3(Ga,Al)_5O_{12}$ multicomponent garnet compounds" J. Phys. D: Appl. Phys. 44 (2011) 505104 (8pp).

Appendix

Comparative Study of Blue Laser Diode driven Ce:YAG, Ce:LuAG, Ce:GAGG, and Ce:GdYAG Single Crystal Phosphors in Application of High-Power Lightning and Display Technologies

Mustafa H. Balci[1)], Fan Chen [1)], A. Burak Cunbul[1)], Øyvind Svensen[2)], M. Nadeem Akram[1)], Xuyuan Chen[1)]
[1)] University College of Southeast Norway, Faculty of Technology, Natural Sciences and Maritime Sciences
Department of Microsystems
Campus Vestfold, +47 31 00 90 28, Xuyuan.Chen@usn.no
[2)] Barco Fredrikstad AS, Habornveien 53, 1630 Gamle Fredrikstad Norway, Oyvind.Svensen@barco.com

Abstract: Phosphor converted warm white light with high luminous efficacy and color rendering index is crucial for the future of blue diode laser driven lightning and display technologies. Particularly in projection displays where the high power (over 150 W) blue laser source is focused on the phosphor, the ideal phosphor candidate has to provide better conversion efficiency, longer lifetime (20000 hours) and lower thermal overheat. We have characterized Ce doped single crystals as stationary phosphor candidates for blue laser driven solid lighting without heatsink. The luminous properties of the single crystals are improved when compared to the commercial phosphor wheels (Ce^{3+}: $Y_3Al_5O_{12}$) and luminous efficacy over 250 lm/W was achieved. The high-power blue diode laser driven temperature increase versus quantum efficiency is discussed. The results indicate that Gd and Ga doping decreases the luminescence quenching temperature. The ideal geometry and design of these single crystals can serve as potential phosphors candidates for high-power blue diode laser driven projectors.

Key words: single crystal phosphors, Ce-doped garnets, luminescence, quantum efficiency, thermal quenching, high power blue laser excitation

1. Introduction

Laser diodes (LDs) are replacing the conventional lightning and display technologies rapidly due to their long lifetime and high conversion efficiencies. Phosphor materials excited by LDs provide high brightness and low cost solution for better color quality in display technologies. Since LDs deliver much higher light intensities than LEDs, improvement of highly efficient, and temperature stable phosphors are very important to overcome the stability and life time issues [1].

Conventional ceramic powder phosphors, embedded

in resin binders, which are used for fixing onto phosphor wheels has major stability issues as they degrade under high blue-irradiation and temperature, and the light conversion efficiency drops drastically as well as the color quality and the lifetime of the system [1, 2]. The Stokes shift and quantum efficiency (QE) losses major heat generation and due to the low thermal conductivity of resins, the heatsink or rotating speed of the wheel becomes the limiting factor. Additionally, the rotation also limits the optical design and light collection efficiency particularly in projection.

On the other hand single-crystal phosphors (SCPs) exhibit outstanding features compared to conventional ceramic powders. SCPs possess reproducible higher conversion efficiency, temperature stability, and a high irradiation resistance, with the availability of any shape [3]. SCPs already demonstrated high conversion efficiency (>90% above 200 °C) and better thermal stability [3] makes them stationary phosphor candidates for white lightning and display technologies.

Ce^{3+} ion has been widely used as an activator in the white LDs phosphor due to is optical absorption at wide light region from UV to blue light and exhibit broad emission band owing to the 5d-4f transition of Ce^{3+}. Since 5d orbital electrons are not shielded by outer 6s and 6p orbital electrons, the excitation and emission band position of Ce^{3+}-activated phosphors is strongly affected by the crystal structure of host materials [4]. Therefore, investigation of different host materials can provide the understanding of the

luminescence properties as well as the heat dissipation properties which are crucial for high power lightning and display technologies. Moreover, it is very important to investigate SCP emission as a function of temperature and Gd, Ga content. For this reason, the efficient scintillator Ce:YAG, Ce:LuAG, Ce:GAGG, and Ce:GdYAG SCPs were characterized as stationary phosphor candidates for blue laser driven solid lighting without heatsink.

2. Experimental section

2.1 Single Crystal Phosphor samples

Czochralski (CZ) grown Ce(1%):$Gd_3(Al,Ga)_5O_{12}$ (Ce:GAGG) 1 cm^2 and 0.5 mm thick polished single crystal phosphor (SCP) was purchased from FURUKAWA DENSHI Co.Ltd.(Japan). 0.3% Ce activated CZ method grown 1 cm^2 and 0.5 mm thick polished SCPs of Ce:$(Y,Gd)_3Al_5O_{12}$ (Ce:GdYAG), Ce:$Lu_3Al_3O_{12}$ (Ce:LuAG), Ce:$Y_3Al_5O_{12}$ (Ce:YAG) were provided by CRYTUR company(Czech Republic). Commercial Ce;YAG wheel (ceramic powder) was provided by BARCO Fredrikstad AS.

2.2 Experimental procedure and instruments

Above RT, samples were heated over a metallic–ceramic resistive heater (ThorLabs), and the temperature was monitored by IR camera and also thermocouple (ThorLabs). Temperature dependent photoluminescence (PL) measurements were carried out by using FS05 Edinburgh fluorospectrometer instrument, with a 150 W Xe lamp as an excitation source. PL decay measurements were carried out by using TSCPS, with a picosecond pulsed laser from Edinburgh Instruments (FS05) emission at 447 nm.

Nichia laser diodes bank array (445 nm, 34 optical W for 8 diodes) has been established by focusing the 4 collimated beam on 0.5 mm^2 (measured by CCD). The optical power out-put of the laser was checked by Laserpoint (A-300-D60-HPB) power-meter. Internal and external quantum efficiency was collected by using an integrating sphere (ThorLabs) and coupled by an optical fiber to the irradiance calibrated Avantes PL spectrometer. The color coordinates, correlated color temperature (CCT) and color rendering index (Ra) were calculated from the emission spectrum using Avantes software.

3. Main Results and discussion

In contrast to ceramics, SCPs possess minimum crystal defects providing less radiative quenching probabilities. Therefore, SCPs exhibit higher conversion efficiency at room temperature and above [3]. Fig. 1 shows the internal quantum efficiency of SCPs in comparison with commercial ceramic powder (wheel). The internal quantum efficiency of ceramic powder and Gd, Ga incorporated SCPs decreases with the temperature increase. The high temperature dependence of the fluorescence intensity of Ce:GdYAG could be attributed to the increase in the Stokes' shift, indicating a large relaxation in the excited 5d state of Ce^{3+} ions, as is observed for conventional YAG phosphors [5]. While Ce:YAG and Ce:LuAG SCPs shows even increase and stability. The internal quantum efficiency of Ce:YAG and Ce:LuAG SCPs reaches its maximum at about 250 °C. In the case of ceramic powder phosphor and Ce:GAGG SCP, a continuous decline is observed with the temperature due to defect related non-radiative recombination paths.

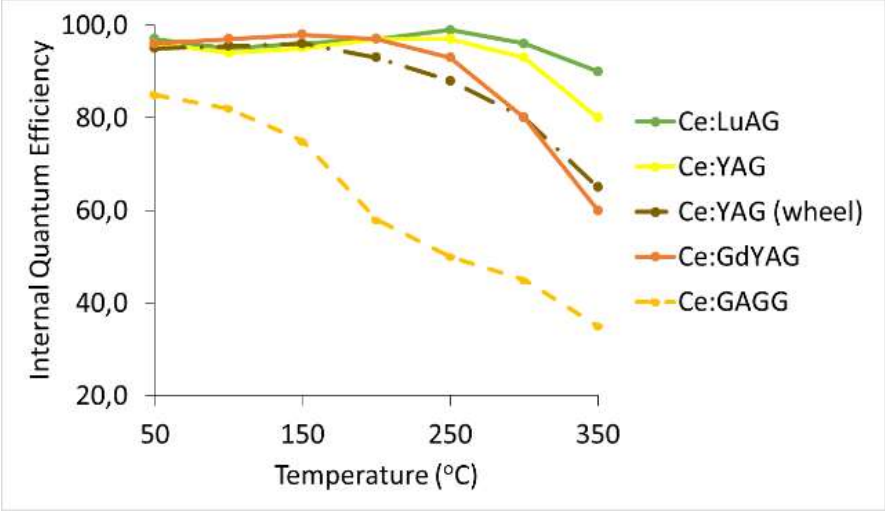

Fig. 1. Temperature dependent internal quantum efficiency of SCPs.

3.1 Fluorescence life time

In general fluorescence lifetime is related to thermal quenching [5]. The temperature dependences of fluorescence lifetime in Table 1 agrees with the internal quantum efficiency and thermal stability in Fig. 1 and 2.

Table 1. Temperature dependent fluorescence lifetime (FL) (ns) of SCPs,

Samples	FL at RT (ns)	FL at 100 °C (ns)	FL at 200 °C (ns)
Ce:LuAG	58.48	59.64	60.23
Ce:YAG(wheel)	65.58	63.25	61.24
Ce:YAG	67.43	68.53	67.43
Ce:GAGG	61.14	57.64	45.39
Ce:GdYAG	67.98	65.83	51.29

The lifetime of Ce:LuAG showed almost no change with temperature indicating the stability [5].

3.2 Thermal quenching

The quenching temperature (QT) (temperature at which the intensity and lifetime drop to half of their correlates well in both high excitation power induced temperature and fluorescence lifetime [1, 6].

It is a well-known phenomenon that substitution of Y with Gd causes lowers the luminescence quenching temperature in conventional YAG phosphors [5]. This quenching behavior could be explained by the mutual dependence on radiative and non-radiative recombination processes via Mott–Seitz mechanism [1, 6].

Temperature and quantum efficiency data directly induced by the high power laser is shown in Fig. 2. The intensity in a focused area, thus local heating induces very different QTs than constant heating the sample with low power excitation in Fig. 1.

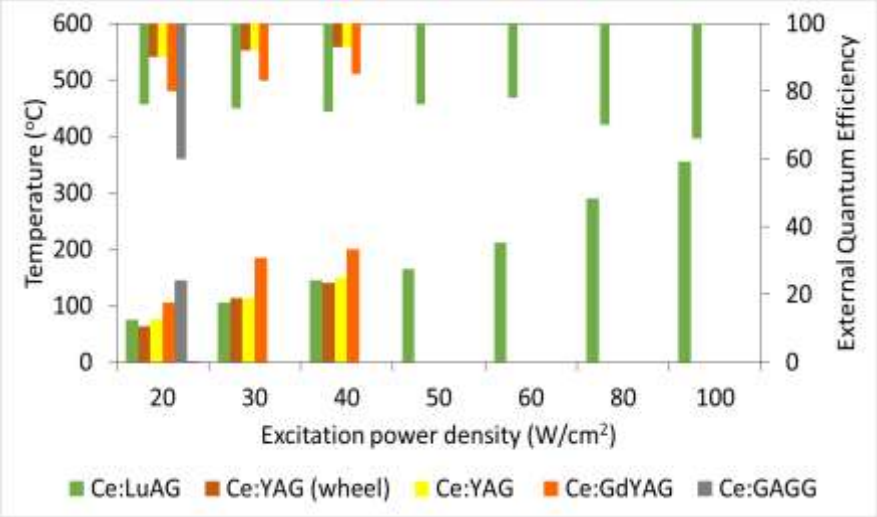

Fig. 2. Excitation power (W/cm^2) induced temperature profiles of the SCPs and corresponding external quantum efficiencies (top and right scale).

As shown in Fig. 2, Ce:LuAG is highly stable and the maximum temperature 350 °C was measured when excitation optical power 100 W/cm^2 (5W/0.5mm^2) is achieved. Ce:GAGG could not be measured above 20W/cm^2 and reached its QT very rapidly at 145 °C. CE:GdYAG and Ce:YAG were stable only up to 40W/cm^2 and their QT remained below 200 °C. The thermal management, crystal quality (defect free), and the heat conductivity of the material plays a crucial role to maintain the high conversion efficiencies.

3.3 Color management

Gd incorporation into Ce:YAG red-shifts the emission. This shift is the result of a decrease in the energy difference between the 5d and 4f centroids and an increase in the ligand field on the 5d level was also

experimentally observed in the case of Ce:GdYAG ceramics [7]. 3500 - 6500 K white correlated color temperatures and color rendering index of 80 can be reached together with a blue light LD (445 nm) (Fig. 3) whereas 5300 - 6500 K color rendering indices around 70 is achieved with Ce:YAG.

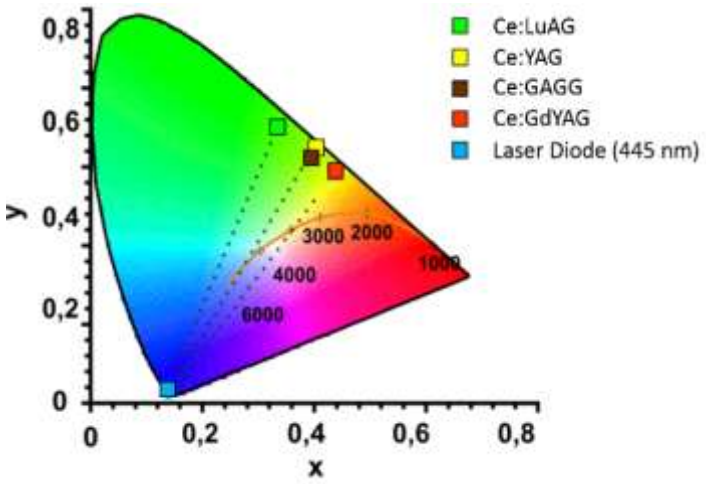

Fig. 3. Color coordinates of Ce doped single crystals in CIE 193 chromaticity diagram.

Therefore, Ce:GdYAG SCPs could be a promising candidate for high-brightness neutral white sources. Although Ce:GdYAG is an attractive candidate for neutral white lighting due to warmer and wider color gamut possibilities, QT in Fig. 1 and 2 limits their application particularly for high power LD. Moreover, lower QT causes spectrum shifts which are the major concerns in color stability [7, 8].

4. Conclusions

We have demonstrated real time measurements of the SCPs under high power densities. It is found that Ce:LuAG SCP is the most efficient and temperature stable phosphor at high power excitation densities up to 100W/cm^2. Although the color quality is improved with Gd and Ga incorporation into host material, the thermal quenching temperature and stability has decreased.

Acknowledgement

Norwegian research council for the financial support, University College of Southeast Norway (USN), and NorFab are acknowledged for the lab facilities. PhD candidate Svein Arne J. Hansen (BARCO) is acknowledged for providing high power laser set-up.

References

[1] S Arjoca, E. Víllora, D. Inomata, K. Aoki, Y. Sugahara and K. Shimamura, "Temperature dependence of Ce: YAG single-crystal phosphors for high-brightness white LEDs/LDs," Mater. Res. Express **2**, 055503, (2015).

[2] Y. Shimizu and K. Bandou, "Development of White LED light source," Rare Earth **40**, 150-151 (2002).

[3] E. G. Villora, K. Shimamura, D. Inomata and K. Iizuka, "Single-crystal phosphors for high-brightness white lighting," SPIE Newsroom, (2016).

[4] W. M. Yen, S. Shionoya and H. Yamamoto, Phosphor Handbook, (CRC Press, Boca Raton, FL, 2007).

[5] S. Fujita and S. Tanabe, "Thermal Quenching of Ce^{3+}:$Y_3Al_5O_{12}$ Glass-Ceramic Phosphor," Jpn. J. Appl. Phys. **48**, 120210 (2009).

[6] S Arjoca, D. Inomata, Y. Matsushitaa, and K. Shimamura, "Growth and optical properties of $(Y_{1-x}Gd_x)_3Al_5O_{12}$:Ce single crystal phosphors for high-brightness neutral white LEDs and LDs," CrystEngComm **18**, 4799-4806 (2016).

[7] L. Chen, X. Chen, F. Liu, H. Chen, H. Wang, E. Zhao, Y. Jiang, T-S. Chan, C-H. Wang, W. Zhang, Y. Wang, and S. Chen, "Charge deformation and orbital hybridization: intrinsic mechanisms on tunable

chromaticity of $Y_3Al_5O_{12}:Ce^{3+}$ luminescence by doping Gd^{3+} for warm white LEDs," Scientific Reports **5**, 11514 (2015).

[8] L. Chen, C-C. Lin, C-W. Yeh, and R-S. Liu, "Light Converting Inorganic Phosphors for White Light-Emitting Diodes," Materials **3**, 2172-2195 (2010).